DETECTING WHITE LAYER IN HARD TURNED COMPONENTS USING NON-DESTRUCTIVE METHODS

A Thesis

Presented to

The Academic Faculty

By

Ian S. Harrison

In Partial Fulfillment

Of the Requirements for the Degree

Master of Science in Mechanical Engineering

Georgia Institute of Technology

December 17, 2004

DETECTING WHITE LAYER IN HARD TURNED

COMPONENTS USING NON-DESTRUCTIVE METHODS

Approved:

Dr. Thomas R. Kurfess, Chairman
School of Mechanical Engineering
Georgia Institute of Technology

Dr. Steven Y. Liang
School of Mechanical Engineering
Georgia Institute of Technology

Dr. Shreyes N. Melkote
School of Mechanical Engineering
Georgia Institute of Technology

Date approved: January 9, 2004

DEDICATION

This work is dedicated to my family.

ACKNOWLEDGEMENT

This work would not have been possible without the assistance and support that the author received from several generous people. This project would not have been possible without the instrumental support from each of the committee members, especially my advisor Dr. Kurfess.4 The other members of the PMRC group were also very supportive, thank you especially to Steven Sheffield and Sangil Han for their assistance with equipment in the PMRC lab and general advice about the project. Other members of the Georgia Tech community also donated their instrumentation to this project. Dr. Preet Singh and Pablo Conde donated lab space for the electrochemical tests and assisted with experiments. Dr. Hamid Garmestani donated the use of an x-ray diffractometer for the residual stress experiments.

The author would also like to acknowledge support from industry. Kennametal donated the CBN cutting inserts, and advice on the hard turning process. Ed Oles from Kennametal inspired the electrochemical tests in this work. The Timken Company donated the 52100 steel bars used in the experiments. American Stress Technologies repaired and calibrated the Barkhausen sensor, and independently tested some of the samples. This project was funded through the Advanced Technology Project of NIST.

TABLE OF CONTENTS

LIST OF TABLES

LIST OF FIGURES

LIST OF SYMBOLS

(Symbols are listed in the order of appearance)

Symbol	Definition
MRR	Material Removal Rate
D_{avg}	Average part diameter during turning
d	Depth of cut
f	Feed rate
N	Spindle speed during turning
T	Machining time
l	Length of a machining pass
α	Rake angle
ϕ	Shear plane angle
V	Cutting speed
n, C, x, y	Constants in Taylor's tool life equation
C_p	Cost of production, per part
C_m	Materials cost
C_s	Setup cost
C_l	Material handling cost
C_t	Tooling cost
T_p	Time to produce a part
T_l	Material handling time

T_m	Machining time
T_c	Tool change time
N_p	Number of parts produced per cutting tool
σ_{ij}	Stress at a point in a part cross section
n_j	Normal vector
σ_n	Real stress
σ_a	Applied stress
σ_r	Residual stress
d	Interplanar spacing in a crystal lattice
θ	X-ray beam incidence angle
n	An integer used in Bragg's law
λ	X-ray wavelength
R_o	Polarization resistance
E	Potential difference
i	current density
B	Tafel constant
b_a	Anodic Tafel slope
b_c	Cathodic Tafel slope
CR	Corrosion rate
d	Density of a corroding substance
EW	Equivalent weight of a corroding substance
I	Electrical current

V	Voltage
R	Electrical resistance
Z	Electrical impedance
ω	Angular frequency
ϕ	Phase angle
R_s	Solution resistance
R_p	Polarization resistance
j	Square root of –1
D	Barkhausen signal intensity
$f1, f2$	Spectrum frequency limits of Barkhausen signal
x	Penetration depth
HV	Vicker's hardness
F	Indentation force
θ	Angle between the faces of a hardness indenter
d	Length of a diagonal of an indentation
ε	Strain
Φ	Specimen rotation angle for x-ray diffraction
Ψ	Specimen tilt angle for x-ray diffraction
SS	Sum of squares
$X, Y, Z, \theta, \phi, \sigma$	Point location and orientation

SUMMARY

Hard turning is a machining process where a single point cutting tool removes material harder than 45 HRC from a rotating workpiece. Due to the advent of polycrystalline cubic boron nitride (PCBN) cutting tools and improved machine tool designs, hard turning is an attractive alternative to grinding for steel parts within the range of 58-68 HRC, such as bearings. There is reluctance in industry to adopt hard turning because of a defect called 'white layer.' White layer is a hard, 1-5 μm deep layer on the surface of the specimen that resists etching and therefore appears white on a micrograph. When aggressive cutting parameters are used, even using a new tool, white layer is expected. If more conservative parameters are selected, one does not expect white layer. There is some debate if white layer actually decreases the strength or fatigue life of a part, but nevertheless it is not well understood and therefore is avoided.

This research examines the use of two different non-destructive evaluation (NDE) sensors to detect white layer in hard turned components. The first, called a Barkhausen sensor, is an NDE instrument that works by applying a magnetic field to a ferromagnetic metal and observing the induced electrical field. The amplitude of the signal produced by the induced electrical field is affected by the hardness of the material and surface residual stresses.

This work also examines the electrochemical properties of white layer defects using electrochemical impedance spectroscopy. White layer has traditionally been identified by etching the material with a nitric acid solution. This suggests that the corrosion properties of white layer are different than the bulk material. This idea is verified by measuring the electrochemical potential of surfaces with white layer and comparing to surfaces without any. Further corrosion tests using the electrochemical impedance spectroscopy method indicate that parts with white layer have a higher corrosion rate.

The goal of this study is to determine if it is possible to infer white layer thickness reliably using either the Barkhausen sensor or electrochemical impedance spectroscopy

(EIS). The general procedure is to use typical process parameters and a high-CBN content tool to examine a process that does not initially produce white layer. As the tool wears, the likelihood for white layer to form increases. Measurements from both sensors are compared with direct observation of the microstructure in order to determine if either sensor can reliably detect the presence of white layer.

CHAPTER 1

INTRODUCTION AND PROBLEM STATEMENT

This project is part of a wider effort to understand and optimize a new machining process, hard turning, so that it is more appealing to industry. Hard turning involves machining exceptionally hard steels on a lathe using a single point cutting tool. This process is very similar to conventional turning, although the machine and cutting tool must be designed to withstand the greater forces and higher temperatures involved.

One of the advantages of hard turning is that it is capable of high enough material removal rates to be used for roughing, but it is also capable of achieving tolerances and surface texture requirements that would allow it to replace finishing processes. In many cases, it is comparable to finish grinding for both technical and economic reasons. The potential to eliminate the costs associated with additional finishing processes is appealing to industry. However, before this can be achieved, there must be a better understanding of the quality of the finished parts that this process produces. In particular, a surface condition known as 'white layer' is troubling to many manufacturers because its properties and the mechanism for its formation are not well understood.

Since white layer may occur unexpectedly, and because the current method for detecting it is destructive, a manufacturer cannot confidently determine if a hard turned part has the condition. Therefore, additional finishing processes must be used to remove material from any parts that might have white layer, effectively removing a potential benefit of hard turning. If a reliable, non-destructive technique for detecting white layer could be found, then hard turning might be more applicable as a finishing process. This project examines the use of two different non-destructive methods: a Barkhausen sensor and electrochemical impedance spectroscopy, to examine if either can successfully detect white layer in hard turned parts.

Problem Statement

Current methods for detecting white layer are not suitable for industry. The most reliable laboratory method for detecting white layer involves examining a cross section of the finished workpiece under a microscope. The cross section is first polished and etched so that the grain structure is visible on a micrograph. This technique is time consuming, labor intensive, and most importantly, it destroys the workpiece. Therefore, this method is unacceptable for production parts.

Another approach is to predict white layer formation using a model of the hard turning process. To be useful with respect to the white layer problem, the model must be both reliable and accurate enough to replace inspection techniques. Methods to predict white layer formation are under development, but are not yet robust enough to be adopted by industry. (Chou and Evans, 1999)

Therefore, if hard turning is to be adopted as a finishing process and white layer is considered undesirable in hard turned parts, then it is necessary to find a nondestructive technique for identifying it. This research examines the use of two types of non-destructive sensors, one called a Barkhausen sensor and the other using electrochemical impedance spectroscopy, to detect white layer defects in parts machined by hard turning.

The Barkhausen sensor is a relatively new non-destructive evaluation (NDE) device that works by applying a magnetic field to a ferromagnetic metal and observing the induced electrical field. The Barkhausen sensor can take measurements quickly and without contacting the workpiece and it is known to be sensitive to several factors that are correlated with white layer. This research addresses the accuracy and reliability of white layer thickness measurement using the Barkhausen sensor.

Electrochemical methods are also considered as a potential means for detecting white layer. Since the current method for detecting white layer, etching, is a chemical process, this suggests that the electrochemical properties of white layer may be distinct from a machined surface without white layer. A sodium hydroxide solution used for the

experiments since it is less reactive than nital acid, and therefore could be considered a non-destructive test in most circumstances.

To gather data, several types of steel are heat treated to several different hardness values and then turned on the Hardinge lathe. The feed, cutting speed, depth of cut, and cutting tool used in the process are also varied so that a wide range of materials and machining conditions can be examined. After machining, the microstructure on the surface of the parts is examined for white layer using the traditional technique of chemical etching. The white layer measurements are compared with the output from the Barkhausen sensor and the electrochemical tests to see if either method is effective at recognizing white layer. The micro-indentation hardness and residual stress of some of the parts are examined to gain insight into the results. Additionally, observational data are gathered during the cutting process including the force on the cutting tool.

Research Objectives

The primary objective of this project is to determine if either the Barkhausen sensor or electrochemical impedance spectroscopy methods are effective at detecting white layer non-destructively. If there is a correlation between white layer thickness and the measurements from either sensor, then this implies that the sensor is responsive to white layer.

Since there are different methods of white layer formation, it is important to know if the sensor is effective for detecting white layer created from different mechanisms. Therefore the Barkhausen sensor is tested on samples that have been machined from three different bearing steels, and both sensors are tested using parts machined from a variety of machine parameters that might be encountered in industry. These experiments also collect additional data about the hard turning process, which can be used to calibrate and test new methods for white layer modeling.

The measurements obtained from the Barkhausen sensor are supplemented by additional information about the surface integrity of the parts. Since the Barkhausen sensor is

known to be affected by both residual stress and hardness, these properties are compared with the Barkhausen measurements and white layer thickness to see if changing residual stress masks the effect of harder white layer.

Electrochemical impedance spectroscopy (EIS) measurements are supported with additional tests of the electrochemical properties of the parts: steady state open-circuit potential, and linear polarization resistance. These additional tests add confidence to the EIS results and reveal important information about the corrosion properties of white layer. Three conditions are tested in this experiment: a sample of fully annealed material, one with no white layer, and one with white layer. It is believed that the potential of a sample with white layer is distinct from one without any white layer present. This may be a reasonable proposition since white layer appears white on a micrograph because it is more resistant to oxidation during etching.

Finally, the applicability of the Barkhausen sensor and electrochemical methods to industry is discussed. In the past, it has been difficult to transfer machine sensors from the laboratory to industry. Some suggestions are proposed for applying the results from the two sensors in an industrial environment.

CHAPTER 2

BACKGROUND

Machining is material removal process, accounting for about $300 billion in labor and overhead each year in the United States. (Kalpakjian and Schmid, 2002) During machining, chips of the material are scraped off using a cutting tool. The chips are discarded and a finished workpiece remains. It is one of the most important and most accurate manufacturing processes, capable of producing surfaces to typical tolerances of 25 microns. With the advent of NC technology and its application to machining, machine tool are now capable of interpolating across several axes to produce complex 3D surfaces. (Tlusty, 2000)

Typical materials for machining are metals and plastics, although other materials may be suitable for machining to varying degrees. In machining, stock is removed using one of the following methods: cutting operations such as milling, abrasive processes such as grinding, or advanced machining operations such as electric discharge machining. Often machining is used as a finishing process used to improve the quality of surfaces that were originally made using another process, such as casting. For example, an automobile crankshaft might be forged to approximate its final shape, and then its critical surfaces are ground to achieve greater tolerance and surface finish requirements. Machining is also used to correct warpage in surfaces that have deformed after hardening or tempering. (Yankee, 1979)

Turning is a machining process used to create rotationally symmetric parts on a lathe using a single point cutting tool. The stock material is fixtured to a rotating axis and a cutting tool is passed across its surface to produce the finished part. A lathe can also be used for other machining operations such as drilling, boring or reaming. (Lindberg, 1968)

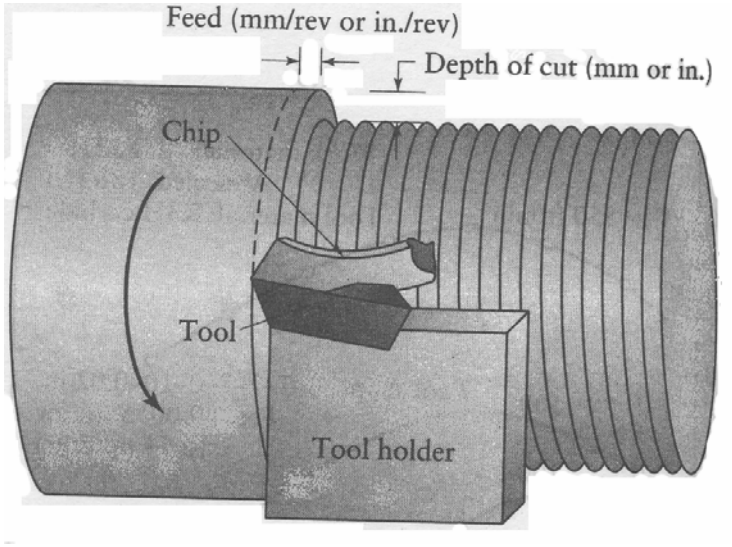

Figure 1: Definitions associated with turning (Kalpakjian and Schmid, 2002)

Figure 1 shows the typical definitions associated with turning. The axial direction is typically denoted as the z-axis, the radial direction is typically defined as the x-axis. The speed of the tool in the direction of its travel is termed the feed of the cut. The tangential velocity of the tool relative to the workpiece is simply called its speed. The depth of cut is the distance that the tool cuts into the workpiece in the radial direction. The material removal rate is the volume of workpiece material removed per unit time, and it is calculated as (Tlusty, 2000):

$$MRR = \pi D_{avg} dfN \tag{1}$$

The time to machine a workpiece of length, l, is (Tlusty, 2000):

$$T = \frac{l}{fN} \tag{2}$$

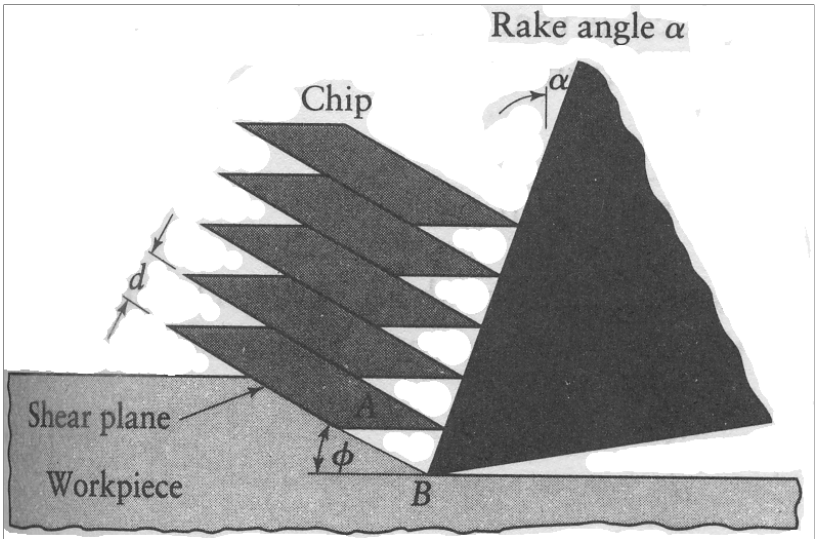

Figure 2: Chip formation in turning. (Kalpakjian and Schmid, 2002)

During turning, material is removed from the rotating workpiece as a single chip. Depending on the machining parameters, the chip may be a single, continuous strand, or it may break into discontinuous pieces. The material impinges on the cutting tool and a force is exerted between them. As the spindle continues to rotate, the force increases until the material yields and separates from the workpiece. In most cases the chip forms a saw toothed profile, as see in Figure 2. This shows that cutting is a discontinuous process and that the force between the chip and the tool is not constant. Instead, the force builds up until it is great enough to cause the workpiece material to yield, and then the force briefly relaxes. (Kalpakjian and Schmid, 2002)

In most cases, turning operations can be approximated using an orthogonal machining model. This model assumes that chip formation can be reduced to 2 dimensions. A diagram of the forces between the cutting tool and chip are shown in Figure 3. In hard turning, the rake angle, α, is usually negative to increase the strength of the tool. This means that radial force, F_t, acts to push the cutting tool and workpiece apart. (Ramesh, 2002)

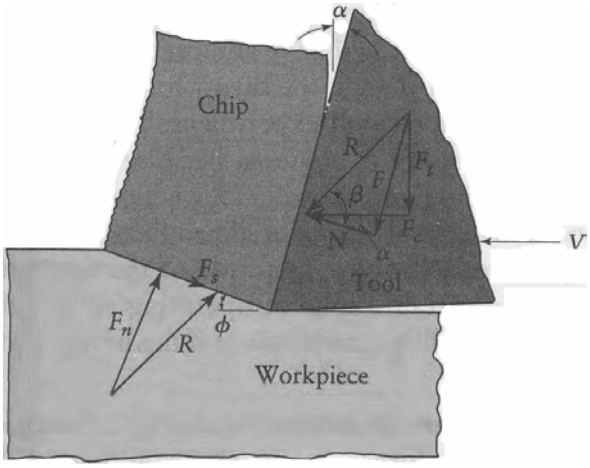

Figure 3: Forces between the tool and the chip. (Kalpakjian and Schmid, 2002)

Most of the deformation of the material is localized to the shear zone, resulting in high temperatures emanating from this area. The shear zone is a planar region that extends at an angle from the tip of the tool to the depth of cut. There are several models that describe this phenomenon, depending on the cutting speed and the combination of materials in the workpiece and cutting tool. In most situations, about 10% of the heat generated goes into the workpiece, 10% of the heat goes into the cutting tool, and the rest enters the chip. (Kalpakjian and Schmid, 2002)

Despite advances in materials science, the life of a cutting tool is limited. Cutting tool mass is lost to adhesion, abrasion, diffusion and catastrophic tool failure. Adhesion occurs when the insert and workpiece material are forced into contact at high temperature and pressure. In this case, the two materials briefly form a chemical bond and then are broken apart due to mechanical forces, ripping material from the tool. Abrasive wear occurs when a locally hard area of the workpiece, possibly an inclusion, scrapes material from the tool. Diffusion wear is especially dominant at high temperatures and when the workpiece and tool material have chemical affinity. A concentration gradient exists between the workpiece and the tool because they are made of different materials. The random motion of molecules may allow them to cross the tool-workpiece interface to areas where they are in lower concentration. This alters the composition of the tool and makes it weaker. Catastrophic tool failure occurs if excessive force is applied to the tool,

causing macroscopic pieces to break away. The likelihood for catastrophic failure increases after the other types of wear weaken the tool. Thermal shocks may cause cracking that decreases the structural integrity of the tool. (Kalpakjian and Schmid, 2002)

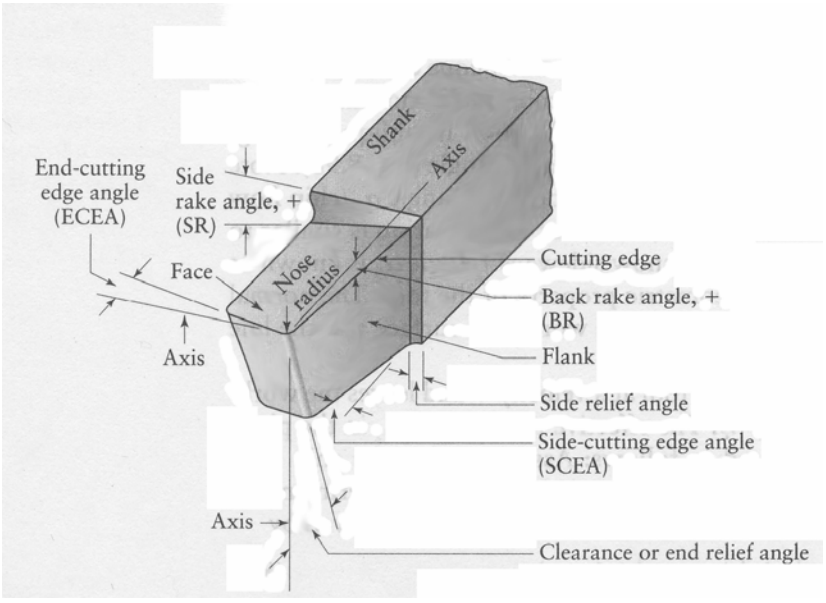

Figure 4: Cutting tool terms. (Kalpakjian and Schmid, 2002)

The terms for describing the geometry of a cutting tool are shown in Figure 4, and the primary regions of tool wear are shown in Figure 5. As the tool moves across the machined surface of the part, its flank face rubs against the workpiece—this creates the flank wear region. Flank wear is primarily caused by adhesion and abrasion, and flank wear rate increases with temperature. The width of the flank wear region is equal to the depth of cut, and flank wear may be pronounced at the depth-of-cut line. The amount of flank wear is typically described by the average length (in the direction parallel to the tool path). Crater wear occurs where the chip impacts the tool and is deflected away. As crater wear progresses, a bowl shape develops on the face of the tool. The primary factors affecting crater wear are the temperature and the chemistry of the tool and workpiece. (Tlusty, 2000)

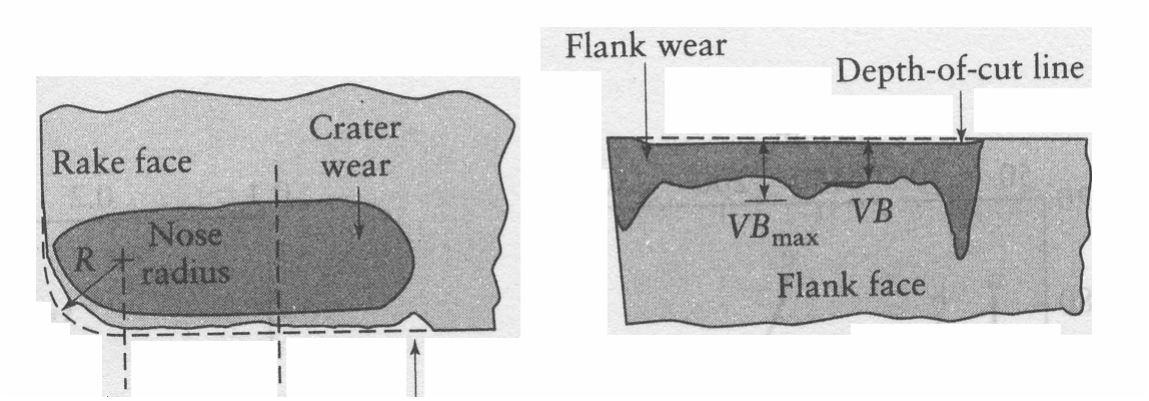

Figure 5: The regions of wear on a cutting tool. (Kalpakjian and Schmid, 2002)

Typically, as a tool wears it becomes sharper but weaker. The crater basin and the flank wear form a sharp edge that easily breaks off due to catastrophic wear. Eventually the tool becomes so worn that it can no longer produce parts that are within specifications and the worn tool must be replaced with a fresh one. (Dawson, 1999) Prior to catastrophic failure, tool life for cutting most steels has been shown to obey an empirical relationship known as Taylor's tool life equation:

$$VT^n = C \tag{3}$$

This equation reflects the fact that cutting speed has a dominant effect on the tool life—as speed increases, the tool life decreases. The constants C and n must be determined experimentally for each material and machining process. The feed rate and depth of also affect tool life, but to a lesser degree than the speed. For a more complete understanding between these factors, equation (3) is modified to include these other factors. It is interesting to note that the material removal rate may be increased by decreasing the speed and increasing the depth of cut or feed rate. (Grover, 1996)

$$VT^n d^x f^y = C \tag{4}$$

The costs associated with machining a part include: purchasing the materials, setup and handling costs, and the costs of labor required to fixture the fresh tool in the machine. The sum of these costs is the total cost of machining per part:

$$C_p = C_m + C_s + C_l + C_t \tag{5}$$

Each of the terms in this equation can be affected by the decision to grind or hard turn a part. For example, the tooling cost, C_t, may be lower for hard turning if a small lot of parts with complex geometries are to be machined. If the same parts were to be machined by grinding, an expensive, custom grinding wheel might have to be purchased.

The presence of white layer primarily affects the setup cost, C_s, and the material handling cost, C_l. If the part has to undergo another finishing step after hard turning in order to remove white layer, then this adds the cost of another setup. Additionally, material handling costs increase if the part must be inspected for white layer.

The time to produce a part is given by:

$$T_p = T_l + T_m + \frac{T_c}{N_p} \tag{6}$$

This time may be increased if the part must be inspected for white layer, or if another finishing process is used to remove the white layer. (Kalpakjian and Schmid, 2002)

Hard Turning

Hard turning is similar to conventional turning, but it involves cutting workpiece material that is harder than 45 HRC. Usually hard turned parts have a hardness of 58-68 HRC. Greater consideration must be given to the process parameters since harder materials, and therefore higher localized pressures and temperatures, are involved. (Sheehy, 1997)

Background

A wide variety of metals can be machined using hard turning methods. Examples of hard turning workpiece materials include: Steel alloys, Bearing steels, Hot and cold work tool steels, High speed steels, Die Steels, Case hardened steels, Waspoloy, Stellite and other aerospace alloys, Nitrited irons and hard chrome coatings, Heat treatable powered metallurgy. (Boggio, 1996) It is important that the metal be hardened to a narrow hardness range (a range of about 2 HRC) and that the heat treating depth is constant, in order to reduce cyclic loads on the cutting tool. An improperly hardened part may reduce the life of the cutting tool and surface cracks may form when it is turned. (Sheehy, 1997)

Only a few known materials have the extreme properties necessary to cut hardened metals at a satisfactory speed. The cutting tools used for hard turning must be strong enough to withstand the high forces involved and their chemical composition must resist diffusing into the workpiece at the high temperatures at the tool-chip interface. Most importantly, the cutting tool must be harder than the workpiece material at the temperatures the tool experiences during machining. Most of the advances in cutting tool materials have been in creating materials that retain their hardness at high temperatures. (Tlusty, 2000)

As a prerequisite to adoption by industry, suitable tools must have low tool cost to tool life ratio, in order to minimize the total part cost. It is interesting to note that diamond, the hardest known material, meets the mechanical requirements for hard turning. However, it is not used for machining ferrous metals because diamond, a form of carbon, diffuses easily into iron and therefore expensive diamond tools have a short tool life when machining iron. Typical tool materials for hard turning include cubic boron nitride (CBN), ceramic, or cermet tools. (Dawson, 1999)

CBN is the hardest material besides diamond and has been shown cost effective for certain hard turning applications. CBN inserts began to increase in popularity after General Electric discovered that combining CBN with a titanium nitride binder may

increase its tool life by five times. (Boggio, 1996) In most inserts, polycrystalline cubic boron nitride is sintered to a carbide substrate. The CBN is an excellent choice for cutting hardened steels because its hardness improves edge strength and it is chemically inert to ferrous metals. (Boggio, 1996; Kennametal, 2004) Another advantage of CBN is its wear properties—it is very wear resistant, and it wears predictably, which is easy to compensate for in NC machines. (Boggio, 1996)

In practice, most cutting tool manufacturers offer two grades of CBN tools with either a low or high CBN content. High-CBN content inserts are hard, but it is also quite brittle. For example, one manufacturer's high-CBN insert has a Knoop hardness of 28 GPa but a transverse rupture strength of 0.9 GPa. (Chou, Evans et al., 2003) For applications when cutting edge strength is critical, such as roughing operations, interrupted cuts, or turning especially hard materials, high CBN content inserts are used. When improved wear resistance is desired, low-CBN content inserts are used. Inserts with low-CBN content typically are not as hard, but have better strength than their high-CBN counterparts. For example, one brand of low-CBN insert has a Knoop hardness of 25 GPa, and a transverse rupture strength of 1.0 GPa.

No tool material is the best in all situations. Ceramic tools are the least expensive of the tools commonly used to machine hardened steel, but they have poor fracture toughness and therefore conservative machining parameters must be used. (Schneider, 1999) Ceramic tools also perform poorly when exposed to thermal or mechanical shocks, and therefore they are not an acceptable choice when coolant is used or if there is an interrupted cut. (Schneider, 1999) On the opposite end of the spectrum, high-CBN content cutting tools, such as Kennametal's KD120 line of inserts, are the strongest cutting material and perform well for deep roughing cuts or interrupted cuts. However, high-CBN tools are the most expensive and tend to wear the quickest. Low-CBN content tools, such as Kennametal's KD050, fit somewhere in the middle, they are tougher than ceramic tools, but last longer than high-CBN content tools. Although diamond is the hardest known material, it is not a good cutting material for steel since carbon diffuses

easily into iron and therefore diamond tools wear quickly when cutting steel. (Boggio, 1996)

It is also important the machines and tools used in hard turning be exceptionally rigid. The large forces involved tends to deflect the tool, reducing its life and decreasing the part's accuracy. The cutting insert must have little overhang when fixtured in the tool holder. The toolholder itself must be short so that the insert is as close as possible to the turret to minimize a cantilever beam effect. The workpiece must be fixtured securely in the spindle, and as close as possible to the spindle bearings. Chatter may be avoided by damping systems in the machine. (Sheehy, 1997)

Importance

In many situations, hard turning is a favorable alternative to grinding when machining rotationally symmetric parts. Hard turning is a more flexible process, and therefore has an advantage when manufacturing small batches or custom parts. To create a complex surface using grinding, it is typically necessary to use a specially shaped grinding wheel that matches the desired surface. A different grinding wheel is necessary for each complex surface, and each wheel can cost a lot. Using an NC lathe, the tool position can be controlled to follow the desired shape. It is simple to adjust the NC program for different dimensions or different shapes entirely. (Sheehy, 1997)

Hard turning and conventional turning can often be performed on the same machine. When machining a hardened part, this eliminates the need to re-fixture the part or the need to move it to additional machining cells. This is another driver that reduces the machining time for hard turning versus grinding. In addition, grinding centers are considerably more expensive than lathes. Therefore, hard turning requires less startup capital than grinding. Hard turning may not require cutting fluid, and the chips produced are larger than from grinding, meaning that the process is more environmentally friendly. (Sheehy, 1997)

Recent advances in cutting materials and machine design have made hard turning more appealing to industry, because hard turning is now capable of achieving dimensional accuracy and surface finishes. When hard turning, it is reasonable to expect surface finishes of 0.003 mm (0.00011") and a dimension tolerance of 0.005mm (0.00020”). (Boggio, 1996) In many cases this means that turning may be used as a finishing operation, eliminating the need for additional finishing processes such as grinding. In some cases however, especially when hard turning compliant parts, the roundness of compliant parts may be the biggest limitation. (Dawson, 1999)

Hard turning is a more energy efficient process than grinding, meaning that less energy is lost to heat and redundant work. Since less heat needs to be dissipated from the workpiece, cutting fluid is not typically needed. This eliminates the need to store and dispose of environmentally hazardous cutting fluids mixed with grinding sludge. However, hard turning requires higher temperatures and pressures than grinding because the force is localized at the cutting point—this makes it difficult to turn long slender pieces that might deflect. The ability to rough and finish machine a part in a single setup reduces setup time and material handling costs. (Sheehy, 1997)

Current Issues

In order for hard turning to be a viable alternative to grinding, it is critical that process parameters are selected to suit the operation. Process parameters in hard turning have a more narrow range of acceptable values than in convential turning, and failure to properly optimize may lead to a combination of poor tool life, poor surface finish, unacceptable dimensional accuracy, or the onset of chatter.

There is reluctance in industry to adopt hard turning because of a surface condition called white layer. There is some debate if white layer actually decreases the strength or fatigue life of a part, but nonetheless it is not well understood and therefore is avoided. (Abrao and Aspinwall, 1996; Smith, 2001; Akcan, Shah et al., 2002) White layer’s properties and the conditions that cause it to form are discussed in greater detail in the next section.

However, due to the many factors that affect white layer formation, it is currently difficult to predict exactly when it forms or how severe the condition are. Research to improve the predicition of white layer is on-going. (Chou and Evans, 1999)

The properties of white layer, and the conditions that cause it to form are similar to a defect in ground parts called grinding burn. Both grinding burn and white layer are the result of aggressive process parameters, either high machining speed or aggressive feed rate. Grinding burn is more likely to occur if the grinding wheel is worn; redressing the wheel reduces the chance of grinding burn. Similarly, white layer is more likely to occur if the tool is worn; changing to a fresh tool may eliminate white layer. Grinding burn tends to penetrate deeper into the surface of the part than white layer, grinding burn is typically 5 to 10 times as thick as white layer. This may be because in turning, the tool is only briefly in contact with an area of the part, while in grinding, the wheel stays in contact with the entire surface, allowing more time for heat to diffuse into it. (Dawson and Kurfess, 2001)

It was mentioned earlier that an advantage of hard turning is that the cutting tools can be bought "off-the-shelf" and they are much cheaper than a single grinding wheel. However, the cutting inserts used for hard turning are currently many times more expensive than the inserts typically used in conventional turning. If care is not taken to optimize the process parameters to increase the tool life, the cost of these expensive materials may make the cost of hard turning prohibitive. If the batch size is large, and process parameters are not optimized to increase the tool life, the cutting tools for hard turning may wear quickly and end up costing more than the grinding wheel. Much of the current research is aimed at optimizing process parameters in hard turning to improve tool life. (Boggio, 1996)

White Layer

White layer is a micro-structural condition where the grain structure of a metal is extremely refined. This condition may occur on the machined surface of hard turned parts, especially when aggressive machining parameters are applied or a worn cutting

tool is used. In industry, when white layer exists, it is typically less than 2 μm thick and is removed by another finishing process, such as superfinishing. (Dawson, 1999) It would be advantageous if the Barkhausen sensor could be used to detect when excessive tool wear results in white layer so that this extra step could be eliminated.

The typical method for observing white layer in the laboratory involves chemically etching a cross-section of a sample in order to visually accentuate the microstructure. When a specimen is etched and then observed with an optical microscope, white layer appears white. If observed under a scanning electron microscope, it appears featureless. (Chou and Evans, 1999) White layer is usually accompanied by a 'dark layer' underneath it, although dark layer may appear without white layer. As the name implies, dark layer appears darker than the bulk material after etching. (Akcan, Shah et al., 2002) Images of parts with and without white layer are shown in Figure 6.

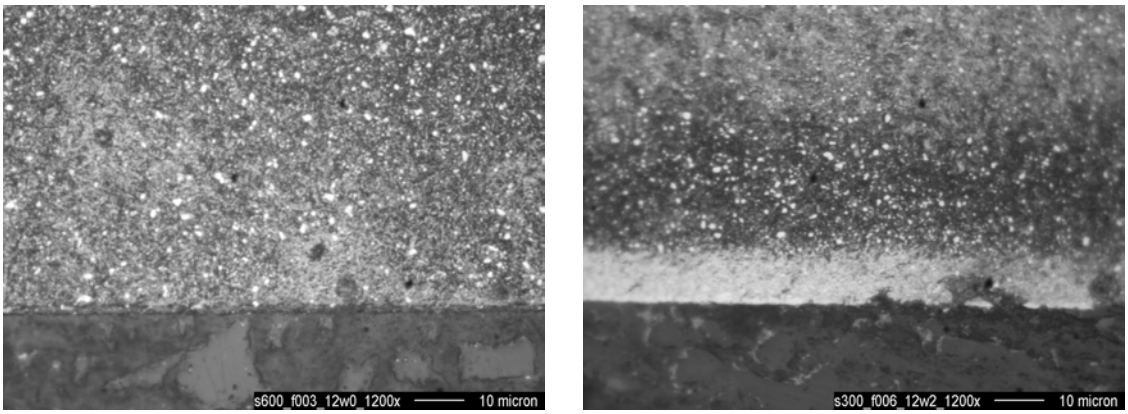

(a) (b)

Figure 6: A sample without white layer (a), and a sample with white layer (b).

Properties

White layer occurs on the surface of steel and may be up to 10 μm thick. The dark layer underneath it may be two or three times thicker. (Ramesh, 2002) The transition between white and dark layer is usually abrupt, and occurs within a transition zone less than 1 μm in depth. (Akcan, Shah et al., 2002)

Observation of white layers using a scanning electron microscope and an optical microscope suggest that it has a nanocrystalline structure due to large strain deformation and dynamic recrystallization. It has been proposed that the white layer does not have visible grain boundaries because the grains are small enough that they scatter light—not necessarily because it is resistant to chemical attack. (Akcan, Shah et al., 2002)

White layer hardness has been measured to be significantly greater than the martensite in the bulk of the material. (Akcan, Shah et al., 2002) Using nano-indentation hardness measurements, the hardness was found to be approximately 12.85 GPa, compared o about 10.70 GPa for the bulk material. The grain size has been measured between 30-500nm. (Akcan, Shah et al., 2002)

Formation

Although this study is primarily concerned with white layers on the surface of hard turned parts, similar microstructures, also termed white layers have, been observed as a result of other processes. For example, the surface of a sample that has been electro-discharge machined also has a white layer. White layer has also been observed on surfaces that experience wear, such as on the surface of railroad tracks or a pin-on-disk test. (Griffiths, 1984)

White layer is sometimes referred to as untempered martensite, and dark layer is referred to as over tempered martensite, because of their similar properties to heat treatment defects. (Abrao and Aspinwall, 1996) The similarity to heat treatment effects is supported

by models that use heat effects as the primary cause of white layer formation. (Chou and Evans, 1999)

In turning, when aggressive cutting parameters are used, even using a new tool, white layer accompanied by tensile stress is expected. This is an unacceptable condition that is typically undesirable. If less aggressive parameters are used with a new tool, one expects no white layer and a compressive residual stress. As the tool wears however, these desirable characteristics diminish and a white layer develops. White layers may form at either low or high cutting speeds. At low speeds it forms due to grain refinement, at high speeds it forms due to rapid heating and quenching. (Akcan, Shah et al., 2002; Ramesh, 2002)

Residual Stress

Another important aspect of the surface integrity of a hard turned part is its residual stress. Latent stresses between different areas within a solid body are known as residual stresses. These stresses may develop due to heat-treatment, manufacturing, cold work, or other processes. (Bhadeshia, 2002) For example, as a metal cools below its melting point, residual stresses may develop as one area solidifies more quickly than other areas. The real stress is the sum of the residual stress and the stresses from any forces applied externally to the part. This relation is stated as:

$$\int_A \left(\sigma_{ij} \bullet n_j\right) dA = 0 \tag{7}$$

It is well documented that compressive residual stresses on the surface of a part have beneficial effects on the fatigue life (Zhu, Tao et al., 1998), crack propagation (Moshier and Hillberry, 1999), and stress corrosion of materials (Toribio, 1998), whereas tensile residual stress reduces the material's performance. While a specimen is in equilibrium, the integral of the stress normal to any cross-section is equal to zero, as stated in Equation (8). (Lu and Society for Experimental Mechanics (U.S.), 1996) Therefore, if the surface of a part has tensile residual stress, this is balanced by compressive stress inside the part.

$$\sigma_n = \sigma_a + \sigma_r \tag{8}$$

As seen in Figure 7, compressive stress acts to close cracks that form, while tensile stress applies additional stress to the crack. Since crack formation is believed to be the primary cause of fatigue failure, it is common for manufacturing specifications to call for compressive residual stresses. (Moshier and Hillberry, 1999) To achieve this specification, the residual stress may be altered by adjusting the manufacturing process parameters, or by addition additional manufacturing operations, such as shot peening. (Torres and Voorwald, 2002) Compressive residual stress on the surface of hard turned parts is critical for prolonging their service life, and (Mittal and Liu, 1998) described a procedure for determining the optimum process parameters to achieve compressive residual stress.

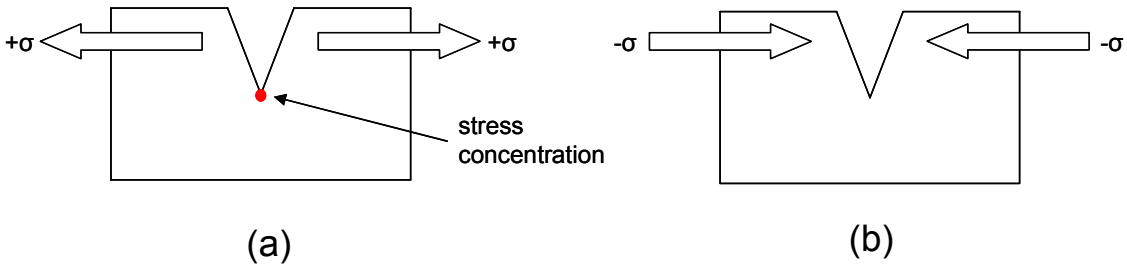

Figure 7: Effect of (a) tensile, and (b) compressive stresses on cracks.

X-ray diffraction is a widely used technique for determining residual stress. It is a non-destructive, non-contact method that is effective as measuring stress in materials with a crystalline grain structure. (Rudd, 2002) Due to the wavelength of x-rays (about 1 Å) the periodic spacing of atoms within a crystal acts as a diffraction grating. When a monochromatic x-ray beam is directed at an angle to the surface of a crystal, some of the beam is reflected by atoms at and slightly below the surface. (Halliday, Resnick et al., 1997) This situation is shown in Figure 8.

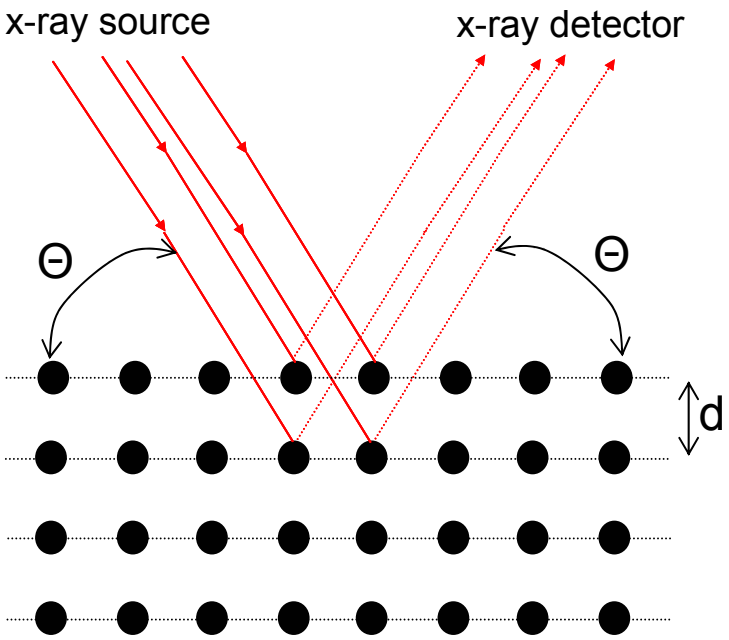

Figure 8: X-ray beam reflection.

The reflected beam is observed to peak in intensity when Bragg's law is satisfied:

$$2d \sin\theta = n\lambda \tag{9}$$

If a detector is positioned to record the intensity of the reflected beam, then the interplanar spacing, *d,* can be determined. (Lu and Society for Experimental Mechanics (U.S.), 1996) Although a polycrystalline material, such as steel, is composed of many randomly oriented crystals, for usual experimental conditions a sufficient number of these (1 to 5% of the irradiated volume) are suitably positioned on the surface so that a peak can be observed. (Lu and Society for Experimental Mechanics (U.S.), 1996) For an iron sample and typical x-ray intensities, most of the reflected beam is diffracted from atoms less than 5 μm deep into the surface. (Prevey, 1986)

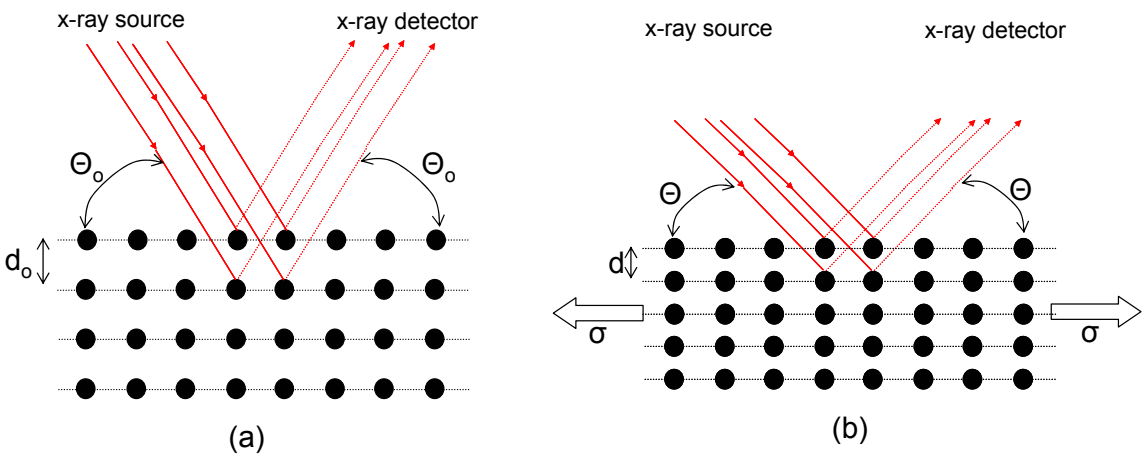

Figure 9: Effect of stress on the peak intensity angle. Sample (a) is undeformed, sample (b) is stressed.

When a sample is stressed, it deforms, and the lattice spacing changes, as shown in Figure 9. If the properties of the material are well known, then the residual stress can be inferred from the lattice spacing. X-ray diffraction is capable of measuring lattice spacing to approximately 1 part in 10^5. Therefore, for an alloy with an elastic modulus of 60 GPa, the stress could be measured to an accuracy of approximately 1 MPa. (Brandon and Kaplan, 1999)

Barkhausen Effect

The Barkhausen effect was discovered by the German physicist Heinrich Georg Barkhausen in 1919 as part of his work in acoustics and magnetism. It is one of four microscopic effects that occur in the interaction between stress and a time-varying magnetic field within a ferromagnetic material—the other effects are magneto-acoustic emission, magneto-mechanical emission, and the Kaiser effect. (Gupta, Zhang et al., 1997) In the 1970s, the Tiitto's applied Barkhausen effect to develop a non-destructive evaluation (NDE) sensor for testing the integrity of metals. (Tiitto, 1978) Since then, the Barkhausen sensors have been used in a variety of NDE applications, including: measuring the uniaxial or biaxial stress state of a metal, measuring plastic deformation, determining fatigue life, and detecting defects such as grinding burn.

Physics Background

In a ferromagnetic material such as iron or cobalt, the spins of the electrons in one atom are able to influence the spin of electrons in adjacent molecules due to exchange coupling. The result is that groups of 10^9-10^{12} atoms form, with each of the group's atom's magnetic dipole moments pointing in the same direction. These clusters of atoms are called Weiss domains and the boundaries between them are Bloch walls. In a demagnetized sample, the magnetic dipole of each of the magnetic domains points in a random direction and there is no net magnetic field. A sample can be demagnetized if it is heated above its Curie temperature and then cooled, or if it experiences mechanical shocks. (Halliday, Resnick et al., 1997; Lewin, Spring 2002)

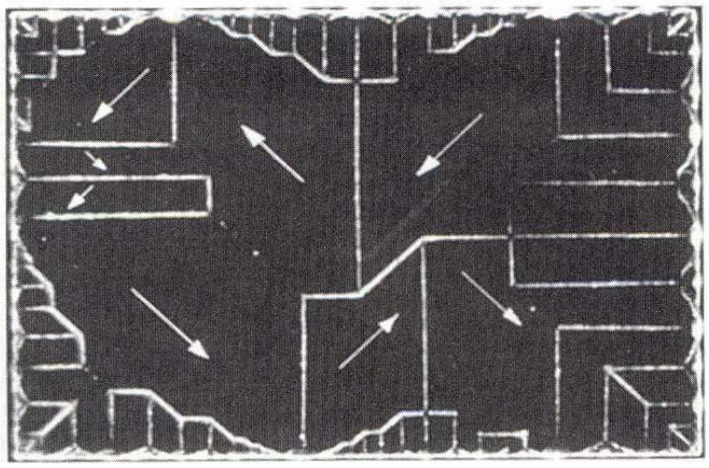

Figure 10: Magnetic domain walls in a ferromagnetic material

An external magnetic field can align the magnetic dipole moments of these domains. When a ferromagnetic sample is placed in an external magnetic field, it enhances the strength of that field because (i) domains aligned with the external field grow to include more atoms and (ii) domains that are not aligned flip direction. When the external field is removed, some of these changes linger and the sample now has a net magnetic field. (Tiitto, 1978; Tiitto, 1987)

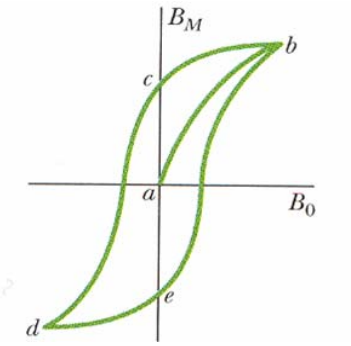

Figure 11: The hysteresis curve

The response of a ferromagnetic material to an external field is summarized by the hysteresis curve shown in Figure 11. In the figure, B_o is the external magnetic field, and B_M is the field resulting from the ferromagnetic material. (The figure is not to scale since the strength of B_M is typically thousands of times stronger than B_o) The curve starts at point *a*. When a demagnetized sample is exposed to an external magnetic field, its own field increases along curve *ab*. As the strength of the external field increases, all of the domains are aligned and we reach saturation—the strength of B_M cannot be increased beyond saturation. From point *b*, if the external field is reduced to 0 the result is that curve *bc* is traversed to point *c*. The diagram shows that the sample is now magnetized in the same direction as the external field. If the direction of the external field is switched, then curve *cd* is followed to point *d*. If the direction of the field is switched again, curve *deb* is traversed back to point *b*. (Halliday, Resnick et al., 1997) If an alternating external magnetic field is applied to a sample, so that the hysteresis curve is followed as a loop, then the magnetic domains repeatedly switch directions. The changing magnetic field in each of the domains creates a tiny, but detectable, electrical pulse in a coil of wire. The collection of all these pulses is known as Barkhausen noise. (Tiitto, 1978)

Factors Affecting the Barkhausen Response

There are several aspects of the Barkhausen sensor that can be analyzed, most common are the root mean square (RMS) of the signal, the maximum noise amplitude, the noise

envelope, or the power spectrum. (Rautioaho, Karjalainen et al., 1988; Krause, Pulfer et al., 1996; Gupta, Zhang et al., 1997) The root mean square of the Barkhausen Noise Amplitude (BNA) is the most commonly used parameter, and its units are often referred to as MP (magnetoelastic parameter). Many different factors, including hardness and residual stress, affect the shape of the hysteresis curve and therefore the BNA. The Barkhausen sensor uses an electromagnet to create a changing magnetic field and uses another coil of wire to detect the electrical pulses. If the domain walls can move freely, the sample quickly magnetizes to saturation and the hysteresis curve is tall and thing. If the domain walls are pinned, then the hysteresis curve is short and fat. (Tiitto, 1978; Tiitto, 1987; Halliday, Resnick et al., 1997; Lewin, Spring 2002)

Both the amplitude of the noise signal and its pulse height distribution are known to change when the stress on a sample changes. However, it is typical to only measure the change in amplitude since this is easier and usually more accurate. (Jagadish, Clapham et al., 1990) The power spectrum of the Barkhausen noise approximately ranges from the magnetizing frequency to 250 kHz. (American Stress Technologies, 1999)

Some of the factors that are known to be correlated with BNA are described below:

Control factors

- Sensor frequency—Varies the frequency of the AC voltage applied to the magnetizing coil, which determines the penetration depth. The sensor is sensitive to greater depths if a lower frequency is used. High frequencies induce eddy currents that damp the signal. This Barkhausen sensor has three settings: 3-15kHz, 20-70kHz, or 70-200kHz. (American Stress Technologies, 1999)

- Sensor magnitude—The sensor's MAGN setting varies the amount of electrical current passing through the magnetizing coil, and therefore the strength of the external magnetic field. The field should be strong enough that the hysteresis loop is relatively large, but not so strong that it saturates the sample. (American Stress Technologies, 1999)

- Material—Different materials react differently to an applied magnetic field. As the part material changes, so does its hardness, grain size, magnetic permeability, and electrical conductivity. (American Stress Technologies, 1999; Totten, Howes et al., 2002)

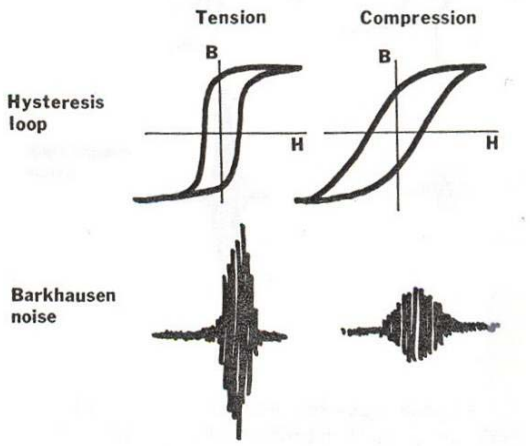

Figure 12: Effect of residual stress on BNA. (Fix, Tiitto et al., 1990)

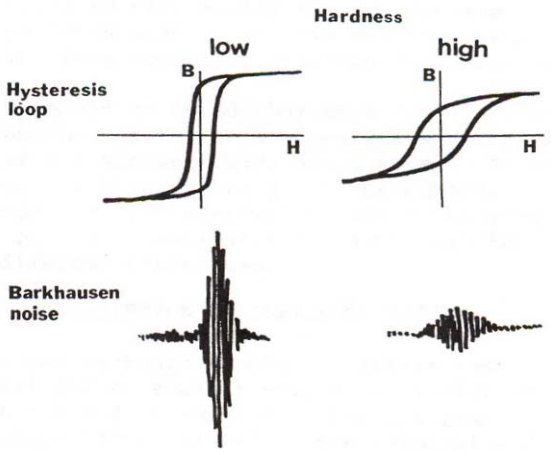

Figure 13: Effect of hardness on BNA. (Fix, Tiitto et al., 1990)

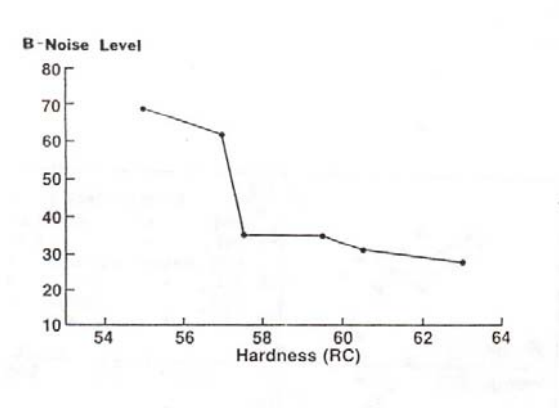

Figure 14: Effect of hardness on BNA. (Fix, Tiitto et al., 1990)

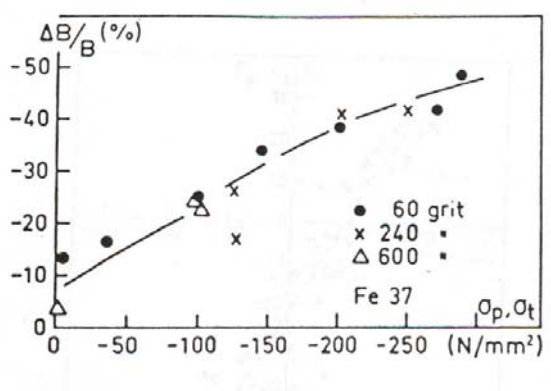

Figure 15: Effect of residual stress on BNA. (Fix, Tiitto et al., 1990)

Noise factors

- Cyclic strain and plastic deformation—No cyclic strain of the part. Plastic deformation although it is a necessary consequence of machining, is considered insignificant because it is approximately the same for each of the parts. (Totten, Howes et al., 2002)

- Texture/Surface finish—The surface finish is usually neglected, because it is similar enough for each of the parts to be considered approximately the same. (Totten, Howes et al., 2002)

- Grain size—Grain boundaries may impede the movement of domain walls, and therefore change the shape of the hysterisis curve. The Barkhausen effect is also responsive to the location, size, and type of carbide precipitates. (Gatelier-Rothea, Chicois et al., 1998) Typically this is assumed to be aliased with other factors, especially the material type and hardness. (Totten, Howes et al., 2002) However, for these experiments, it should be noted that white layer generated at higher speeds is coarser than that generated at lower speeds. (Ramesh, 2002)

- Chemical composition— At high machining speeds, the chemical composition has been shown to be the same as the bulk material, most likely because the carbon does not have time to diffuse. In contrast, at lower machining speeds significant cementite presence was found in white layers. These differences are explained by the occurrence of phase transformation at higher machining speeds. (Ramesh, 2002)

- Cutting temperature—Higher machining speeds cause greater thermal loads on the workpiece surface. This alters some of the primary properties that affect the Barkhausen response, especially the grain size and possibly the chemical composition. (Ramesh, 2002)

- Inclusions—Inclusions affect the sensor response because they have different properties than the bulk material. Inclusions may affect the overall permeability, hysteresis loss, and coercivity of the material. (Parakka and Jiles, 1997)

Sensors in Manufacturing

Associated with industry's consistent need to reduce manufacturing costs and improve accuracy, are the ideas of producing the first part correctly and producing zero defects. These concepts are also strongly linked with the move towards just-in-time manufacturing, which requires high quality and flexible processes. In many cases, especially when parts are made in small batches, it is vital that every part be machined correctly on the first attempt. If can be accomplished, then the overall setup time can be greatly reduced. Similarly, if all of the parts can be machined to high quality, then there is less scrap, less inspection time, and less wasted machining time.

During the past few decades, two different approaches have attacked these issues to reduce costs for industry. The first is to gain a better deterministic understanding of the machining process. This leads to improved models that can better predict how the tool

and workpiece interact during machining. In general, this approach can be challenging due to the complexity of the machining process.

Another approach is to integrate in-process sensors with the machine tool that can evaluate the workpiece condition to optimize the machining parameters. One or more sensors detect essential properties of the workpiece and this information is input to a control loop that adjusts machine parameters such as the speed, feed, cycle time, etc. When properly designed, these control systems maximize performance so that desirable parts are manufactured at a high production rate. (Liang, Hecker et al., 2002)

There are several different workpiece properties that have been successfully controlled using in-process sensing. Kiran, et al. (1998) have used vision systems for on-line measurement of surface texture. Shunsheruddin and Kim (1985) have used reflected light to infer the surface roughness and to detect grinding burn during machining. Delio, et al. (1992) detected and controlled chatter by analyzing the spectral density of audio signals.

Although in-process sensors have been shown to be effective at improving quality within the laboratory, industry has been slow to adopt these innovations. Industrial environments impose many demands that prevent accurate sensing: chips, coolant, machine vibration, high temperatures, and other factors. The software that interprets the sensor data must properly address the non-linearity of the machining process and of the sensor. (Liang, Hecker et al., 2002)

Barkhausen sensor applications

The Barkhausen sensor has several advantages that make it appealing as an in-process gage. Most importantly, it is capable of taking rapid, non-destructive measurements on ferromagnetic materials. Off-line, the sensor is usually used by simply touching the probe to the workpiece. It can also be used for measuring rotating workpieces, also long as the sensor is held at a constant distance from the surface. Several groups have had success

using the Barkhausen sensor to measure a variety of material properties, both in-process and off-line. (Tiitto, 1987)

Moorthy et al. showed that the amplitude and frequency of the Barkhausen sensor could be used to detect heat-treatment defects in case-carburized EN36 steel. The peak of the Barkhausen signal was found to be correlated with the hardness of the part at 100μm deep. A statistically significant difference was found between the peak of the signal and whether the part was over-tempered, un-tempered, or correctly tempered. (Moorthy, Shaw et al., 2003)

Lindgren and Lepisto used a novel Barkhausen sensor design to continuously monitor fatigue in a low-carbon steel and in a high-strength alloy steel. Their sensor had no magnetizing coil, relying on the fact that the Barkhausen effect can be created by an alternating stress field (an alternating magnetic field is typically used.) Barkhausen amplitude peaked as crack nucleation began in both materials.

In many cases it was used to detect grinding burn, a defect that often limits the material removal rate of the grinding wheel. It has already been shown that the sensor is affected by residual stress and hardness, and these factors are often associated with part quality. Members of a leading manufacturer of Barkhausen sensors, designed a system to quickly test the ground surfaces of a camshaft for grinding burn. (Fix, Tiitto et al., 1990) In this study, high tensile stresses and lower hardness were associated with grinding burn, and therefore the Barkhausen sensor was effective at determining defective parts. As a next step, the Barkhausen sensor was used to optimize a grinding process to reduce residual stress and prevent grinding burn, and to determine when to dress the grinding wheel. The BNA signal steadily increased as parts were made, from ~32 MP to ~42 MP (magneto-elastic parameter). When the BNA neared the rejection limit, 45 MP, the wheel was dressed and the BNA dropped to its original value, ~32 MP. (Fix, Tiitto et al., 1990)

Although grinding burn and white layer are similar in some ways, grinding burn is typically deeper, usually extending to 75μm. (Fix, Tiitto et al., 1990) Since the penetration depth of the Barkhausen sensor used in this study is between 20 – 200 μm,

this suggests that grinding burn is easier to detect than white layer because grinding burn affects a greater percentage of the sensor's penetration depth. Hard turned parts are more difficult to analyze because of the wide range of residual stress profiles that may result. If the residual stress varies a great deal during a cutting insert's life, it may be difficult to distinguish this from the effects of white layer.

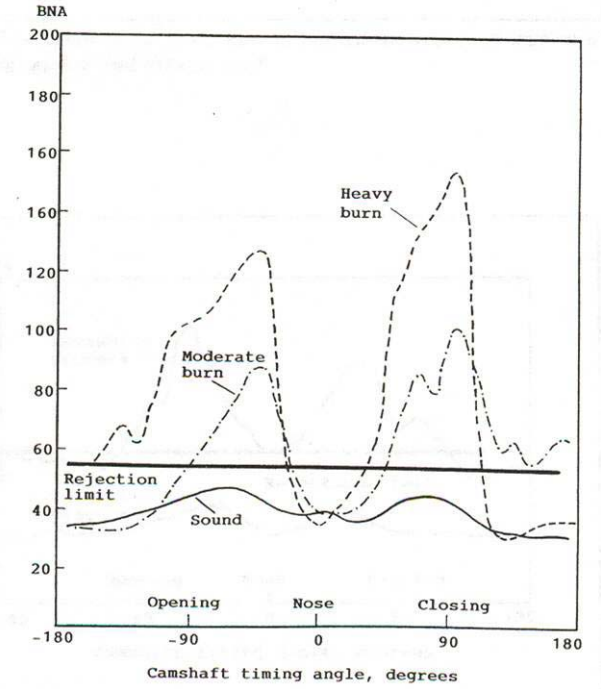

Figure 16: In-process monitoring of grinding using the Barkhausen sensor. (Fix, Tiitto et al., 1990)

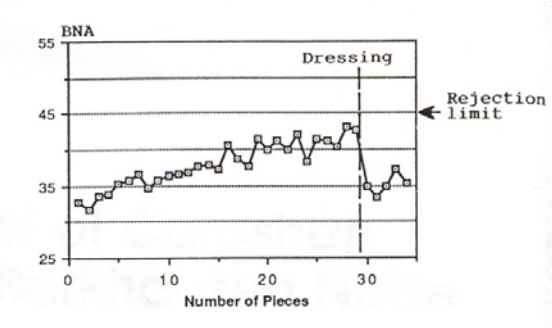

Figure 17: Using BNA to determine when to re-dress a grinding wheel. (Fix, Tiitto et al., 1990)

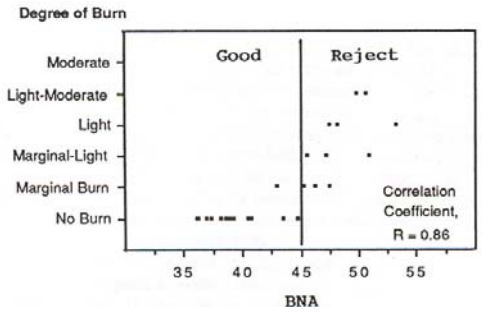

Figure 18: Using BNA to search for defective parts. (Fix, Tiitto et al., 1990)

Electrochemical Methods

Another method for detecting white layer that is considered in this study involves examining the electrochemical properties of the samples when they are immersed in an aqueous solution.

Metals are thermodynamically unstable, meaning that their atoms eventually undergo reduction and go to a lower energy state. Some metals are relatively stable and this process may take a very long time, others are relatively unstable and the transformation

occurs quickly. A metal that corrodes slowly is described as passive. A chemical reaction where a molecule loses electrons is a reduction reaction; in an oxidation reaction the molecule gains electrons. Corrosion is a chemical reaction where the atoms in a metal lose their electrons and escape into the surrounding environment as ions. This reduction reaction is balanced by an oxidation reaction that occurs elsewhere in the system.

The temperature and pH of the environment, the properties of the metal and the reaction products, and other factors all affect the corrosion process. Small changes in these factors can greatly affect the speed and mechanisms of corrosion. (Baboian, 1995) The truest method of corrosion testing is observing the part over time while it is in service, or in a controlled environment that closely resembles the in-service conditions. However, this is necessarily a time consuming method and may not lead to a deeper understanding.

Since corrosion is fundamentally an electrochemical process, it is natural to look at it from this perspective for further insight. Several different techniques have been developed to investigate the electrochemical phenomenon that occurs during corrosion. These techniques have been aided by implementing microelectronics, which can achieve higher frequencies and greater precision than devices of the past. (Revie, Uhlig et al., 2000)

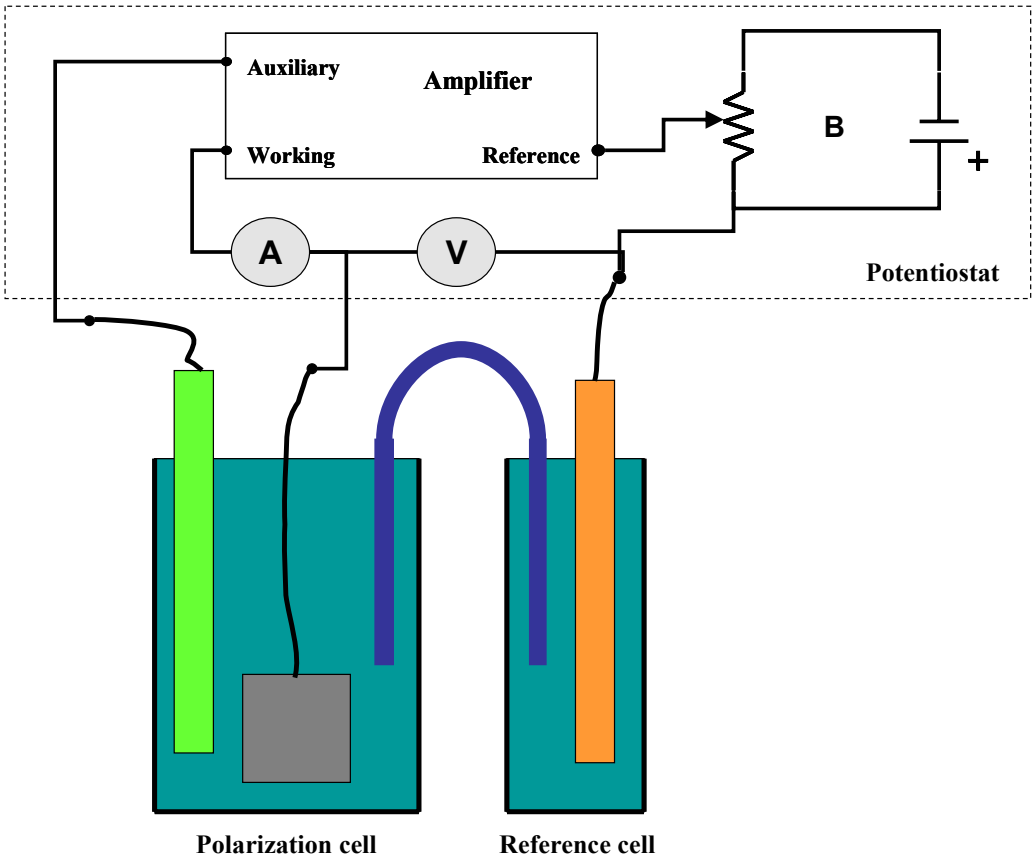

Figure 19: Potentiostat schematic

A popular device for electrochemical corrosion testing is the potentiostat. The device is setup as seen in Figure 19, and a schematic of its basic internal circuitry is shown in Figure 20. The potentiostat, especially when it can be precisely controlled by a digital computer, is a versatile tool that controls the potential that is applied to three different electrodes that are immersed in an aqueous solution and records the resulting current. The reference electrode is a material that has a known potential, for example a saturated calomel electrode, and it is used as a standard for potential measurements. The working electrode is the sample of interest. A controller in the potentiostat controls the potential difference between these two electrodes. A desired potential difference, V_2, can be applied between the reference electrode and the working electrode by setting the adjustable power supply, B. The actual potential difference is measured as V_1 and the difference, $V_e = V_2 - V_1$, is fed to an amplifier. The amplifier is connected to a counter

electrode, usually platinum, which quickly drives the system to the correct potential. (Baboian, 1995)

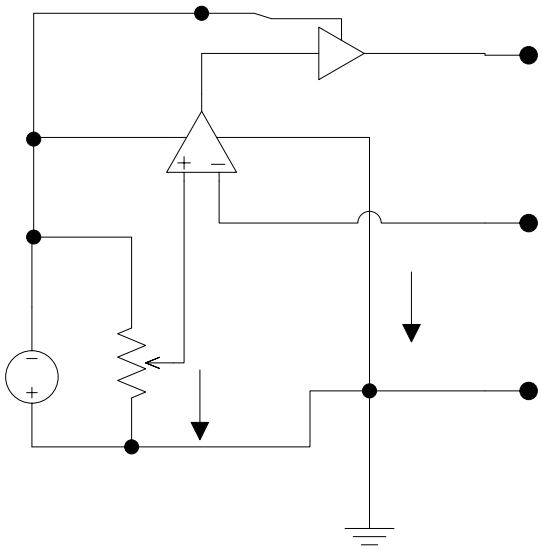

Figure 20: Circuit diagram for a potentiostat

Electrochemical Potential

When a metal is placed in a solution, there is a potential at the metal-solution interface. This potential cannot be measured by itself, in absolute terms, and therefore the potential difference is measured between a sample and a known reference. For accurate measurements, the reference electrode must maintain a constant potential for small current drains. Typical reference electrodes are calomel (mercurous chloride) or Ag/AgCl.

The potential of two dissimilar metals is different, and when they are brought into contact galvanic corrosion occurs. Atoms from the more active metal enter solution, leaving electrons and a net negative charge on this electrode. These electrons flow to the other, more noble, electrode and draw positive ions from the solution. This process is the basis for chemical batteries. Electrons may also flow within a single electrode, between areas

that have potentials that are relatively high or low. This explains how a piece of steel corrodes if it is left in a salt water bath.

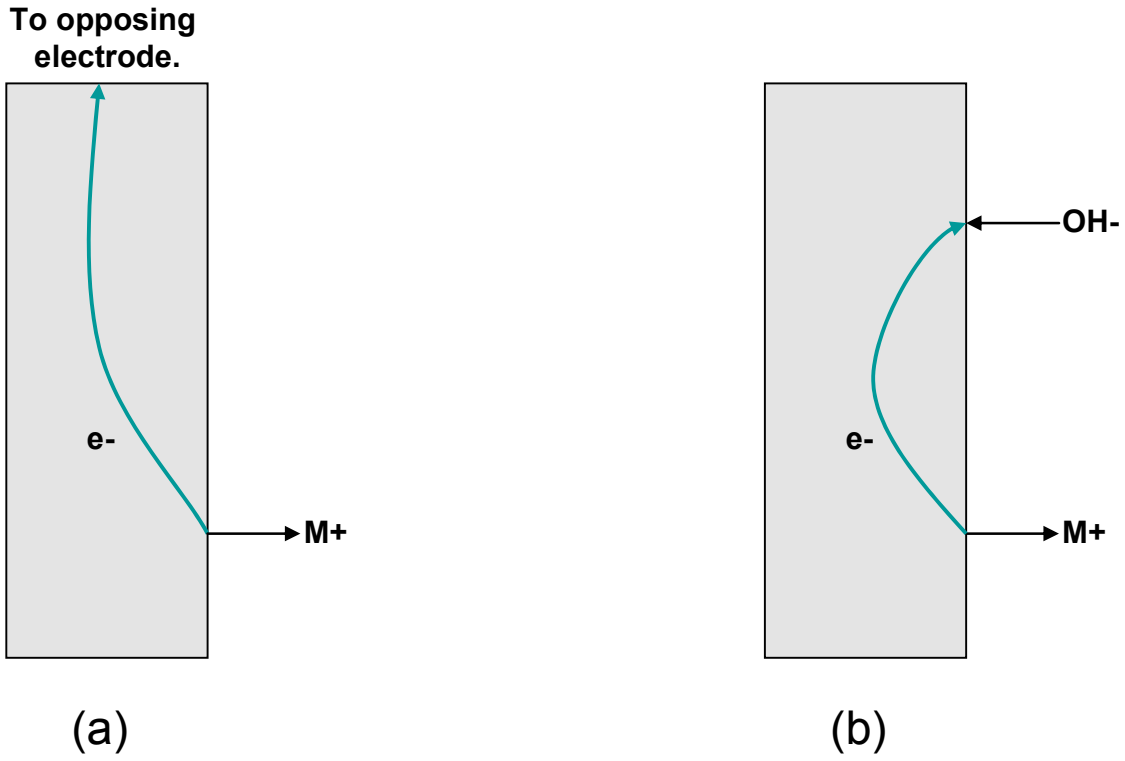

Figure 21: Different corrosion reactions. (a) Electrons flow to an opposing electrode, (b) electrons flow within the electrode.

The open circuit potential is the voltage difference between the reference electrode and the working electrode. In practice this potential is measured with a high impedance voltmeter, but a trickle of electrons flow through the voltmeter so that galvanic corrosion dominates. The potential of the reference electrode is known and can be used to convert the measurement to a standard scale for comparison to other metals. Open circuit potential is an important starting point for electrochemical tests, but it cannot alone determine the corrosion rate.

Linear Polarization Resistance

Often it is not practical to determine the corrosion rate by measuring the mass loss. Linear polarization resistance is a well established application of the potentiostat and is used for determining the instantaneous corrosion rate. This is often a good predictor of how quickly a material corrodes in service.

The difference between the potential measured across a metal-solution interface and its corrosion potential, is expressed at the polarization, ΔE. When the polarization is not zero, the metal is not in equilibrium with its ions in solution. Polarization resistance, R_p, is defined as the slope of the potential versus current-density curve at the corrosion potential. The polarization resistance has been shown to be related to the current density by the equation:

$$R_p = \lim_{\Delta E \to 0} \frac{\Delta E}{\Delta i} = \frac{B}{i_{corr}} \tag{10}$$

The constant B is determined experimentally from the data, using the anodic, b_a, and cathodic, b_c, Tafel slopes:

$$B = \frac{b_a b_c}{2.3 \bullet (b_a + b_c)} \tag{11}$$

Using Faraday's law, corrosion rate is related to current density by the formula:

$$CR = \frac{0.0129 \bullet i_{corr} \bullet EW}{d} \tag{12}$$

where the corrosion rate, CR, is given in mils (0.001 in) per year.

Electrochemical Impedance Spectroscopy

The electrochemical impedance spectroscopy (EIS) method, also called the AC impedance method, has been shown to be good at describing the corrosion process at the interface between a metal and an aqueous solution. It has found several applications as an NDE technique. Ogawa et al. (Ogawa, Minkov et al., 1999) used impedance spectroscopy to evaluate the integrity of thermal barrier coatings on gas turbine blades.

This procedure assumes that the metal-solution interface can be modeled using some combination of simple system elements. By perturbing the system at different frequencies, one can estimate the values of the elements in the model. The model determined from EIS tests also provides another method for estimating the corrosion rate. A diagram of this setup is shown in Figure 19.

In simple terms, a resistor is a circuit element that dissipates power. When a constant or direct current (DC) is applied to a resistor, Ohm's law describes how the current through the resistor is related to the voltage drop across it:

$$I = \frac{V}{R} \tag{13}$$

Impedance is the equivalent of resistance for circuits where an alternating current (AC) is applied. Impedance is the DC resistance (of resistors) plus the reactance (of capacitors, inductors and other elements). In the generalized form of Ohm's law, impedance replaces resistance, and it becomes:

$$\begin{aligned} I &= \frac{V}{Z} \\ Z &= Z(\omega) \end{aligned} \tag{14}$$

In this case, the voltage, current, and impedance are described as complex numbers. Furthermore, the impedance is a function of the frequency of the input electrical signal.

$$
\begin{aligned}
|Z| &= \sqrt{\left(\mathrm{Re}(Z)\right)^2 + \left(\mathrm{Im}(Z)\right)^2} \qquad (magnitude) \\
\angle Z = \phi &= \tan^{-1}\left(\frac{\mathrm{Im}(Z)}{\mathrm{Re}(Z)}\right) \qquad (phase) \\
\mathrm{Re}(Z) &= |Z|\cos\phi \\
\mathrm{Im}(Z) &= |Z|\sin\phi
\end{aligned}
\tag{15}
$$

Resistors and capacitors are linear devices. This important property means that in a circuit containing only these elements, the current and voltage have the same frequency. For a given frequency, the impedance is defined by two parameters: phase angle and magnitude. These quantities can be calculated using equations (15). The magnitude is the ratio of the amplitude of the current divided by the amplitude of the voltage. The phase angle is proportional to the time shift between peak current and peak voltage. The relationship between frequency, phase angle, and magnitude for a given circuit is typically displayed as a Bode plot or a Nyquist plot (polar plot). (Horowitz and Hill, 1989)

A potentiostat is used to control the potential across the working electrode and to measure the current through it. Using Ohm's law equation (14), the potential, *V*, is interpreted as the input to a dynamic system and the impedance, *Z*, is a transfer function. The model of the system is identified by determining its frequency response.

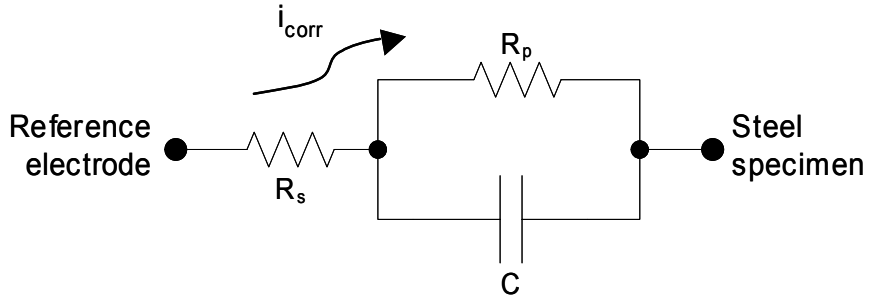

Figure 22: Randles cell circuit model for EIS tests

A number of different circuits have been shown to be effective at modeling different corrosion processes. One of the most commonly used circuits is the Randles cell, shown in Figure 22. It is a relatively simple model that assumes the flow of electrons during corrosion can be modeled as the simple network of a capacitor and two resistors. The resistor R_p is the polarization resistance and is interpreted as the resistance for an atom of the metal to lose its electrons and become an ion. The resistor R_s is the solution resistance and it a combination of all the other resistances in the system, including the resistance of the ion to cross the metal-solution interface. The capacitance, C, is primarily due to the separation of charge at the metal-solution interface.

Table 1 : The impedance of simple circuit elements.

Element	Impedance
Resistor	Z(jω) = R
Capacitor	Z(jω) = 1 / (jωC)
Inductor	Z(jω) = jωL

Another advantage of linear devices is that it is straightforward to determine their combined response. The impedance of individual circuit elements is given in Table 1. The combined response of the elements in Figure 22 is given by:

$$Z(j\omega) = R_s + \frac{R_p}{1 + R_p j\omega C} \tag{16}$$

The model parameters R_p, R_s, and C can be determined by either fitting this equation to the experimental data, or by graphical inspection of the Bode and Nyquist plots of the data. The Nyquist and Bode plots of the model in Figure 22 are shown in Figure 23. (Baboian, 1995)

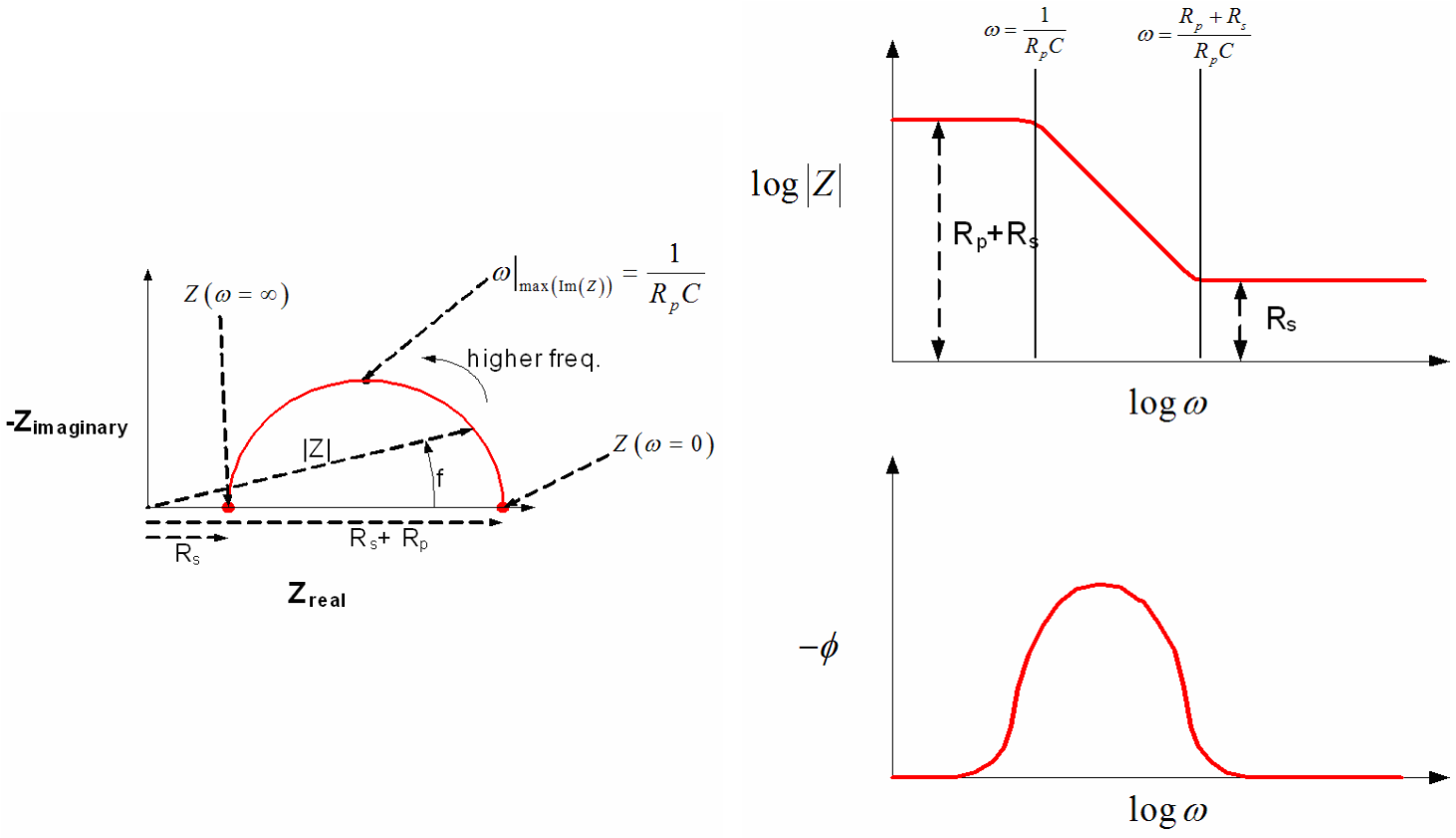

(a) (b)

Figure 23: Nyquist plot (a) and Bode plot (b) for the circuit in Figure 15. (Baboian, 1995)

The potentiometer is used to apply an oscillating voltage to the working electrode about a set potential. The magnitude of the oscillation is small to prevent disturbing the properties of the system, and its frequency is stepped through of range of about 0.001 to 100,000Hz. For each frequency, the current through the working electrode is measured as a response to the input voltage. The parameters of the model are then fit to the experimental data. For example, if the model in Figure 22 is used, it is easy to see that:

$$\begin{aligned} \lim_{\omega \to 0} Z(\omega) &= R_s + R_p \\ \lim_{\omega \to \infty} Z(\omega) &= R_s \end{aligned} \tag{17}$$

Once the parameters of the impedance model are determined, Ohm's law is used to find the current density, i_{corr}. The corrosion rate is found using Faraday's law, equation (12).

The EIS method has several advantages. One advantage of EIS is that it allows the solution resistance to be separated from the polarization resistance. This is especially important for cases with high solution resistance. The integrity of an experimental setup can be confirmed by verifying that the solution resistance is similar for each trial. Another advantage of EIS is that the shape of the Nyquist curve provides qualitative insight into the corrosion process. The shape can be used to identify the corrosion mechanism and the high frequency measurements add confidence that the low frequency measurements are correct. (Cottis, Turgoose et al., 1999)

CHAPTER 3

EQUIPMENT AND INSTRUMENTATION

This section describes the particular devices used for the experiments in this study.

Barkhausen Sensor

The Barkhausen sensor used in the experiments was manufactured by American Stress Technologies. It is a Stresscan model 500C. The sensor consists of a central unit and a handheld probe. The central until contains the circuitry for energizing the probe and for amplifying the signal. It contains a microprocessor the controls the sensors operation and analyzes the signal. The central unit has a RS-232 output port for logging data to a PC and a BNC output for connecting an oscilloscope to observe the raw magnetoelastic signal. The central unit also has a sensor port that is capable of connecting a variety of different probes to the central unit. The handheld probe that was used is designed for experimental use on medium sized parts. It contains two wire coils, one for inducing a magnetic field, and one for measuring the induced Barkhausen noise.

The Stresscan has two adjustable parameters. The MAGN setting varies the current passing through the magnetizing coil of the probe, this changes the shape of the hysteresis curve. If the MAGN setting to high, the sample reaches magnetic saturation; if it is too low, the signal is difficult to observe. The Stresscan also has a frequency setting which varies the frequency that the magnetizing coil changes polarity. At higher frequencies, the applied magnetic field creates eddy currents in the sample which damp its intensity; at lower frequencies the magnetic signal can penetrate deeper into the sample. The Stresscan has three settings: 3-15 kHz corresponding to a nominal measurement depth of 0.20mm, 20-70 kHz corresponding to a depth of 0.07mm, or 70-200 kHz corresponding to a depth of 0.02mm. The decrease in Barkhausen signal

intensity, *D(x)*, with increasing depth into the material, *x*, for a spectrum of frequencies between f_1 and f_2 is described as (American Stress Technologies, 1999):

$$D(x) = \frac{\int_{f_1}^{f_2} g(f) \exp\left[-Ax_n\sqrt{f}\right] df}{\int_{f_1}^{f_2} g(f) df} \tag{18}$$

Figure 24: Photo of the Stresscan 600C (American Stress Technologies, 1999)

Potentiostat

A PCI4/300 potentiostat by Gamry Instruments was used for all of the electrochemical tests in this project. All of the potentiostat's circuitry is implemented on a single circuit board that is connected to the PCI slot of a digital computer. Seven input/output lines are accessible from the card that are connected to sense or control different elements of the electrochemical cell. The control lines are capable of outputting between 3 nA - 300 mA of current through a range of ±11 V. Using software included with the instrument, the sensor is capable of several different electrochemical tests. For this project, it was used to measure open-circuit voltage, and to perform linear polarization and electrochemical impedance spectroscopy experiments. Other relevant specifications of this instrument are listed in Table 2:

Table 2 : Gamry PCI4/300 specifications.

Compliance Voltage	±20 V
Max. Output Current	±300 mA
Max. Applied Potential	±11 V
Current Ranges	9 ranges: 3 nA – 300 mA
Rise Time	2 μsec
Noise and Ripple	<20uV rms
EIS Frequency Range	10 μHz-300 kHz
Input Impedance	$>10^{12}$ Ω

Cutting Tools

All of the cutting tools in these experiments were CBN inserts from Kennametal. Two different grades were tested: KD050, a low-CBN content tool, and KD120, a high CBN content tool. Each of the inserts is designated by an index number, which are listed in Table 3 with explanations. These inserts were clamped in a Kennametal tool holder, DCLNR-124B.

Table 3: Explanation of the index number for the inserts.

High-CBN content insert	Low-CBN content insert	
C	C	80^o rhombus shape
N	N	0^o relief angle
G	G	Dimensional tolerance
A	A	Insert mounting type
4	4	Insert size
3	3	4.76 mm thick
2	2	0.8 mm nose radius
T	T	Negative land
KD120	KD050	Material grade

Edge preparation has a critical effect on the tool life. A tool with poor edge preparation may chip and fail quickly. (Thiele and Melkote, 1999) The three basic types of edge preparation are shown in Figure 25.

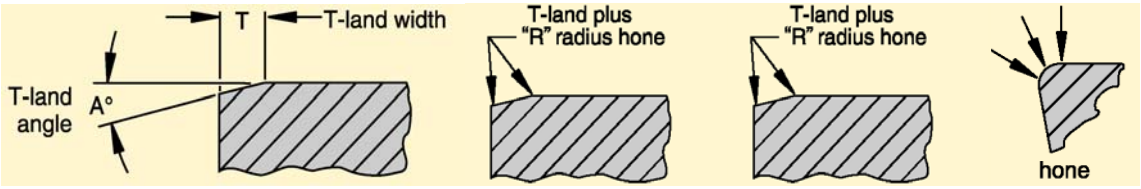

Figure 25: Various types of edge preparation. (Kennametal, 2004)

Steels

A common application of hard turning is producing the critical surfaces on the inner and outer races of a ball-bearing. For example, hard turning might be used to finish turn the surface of a ball-bearing race in order to correct warpage and out-of-roundness that occur after heat treatment. Therefore, in an effort to simulate industrial practices, typical bearing steels and hard turning machining parameters were used in these experiments.

Table 4: Chemical composition of bearing steels.

Element	52100	1070	1053
Carbon	0.93-1.05	0.65-0.75	0.48-0.55
Manganese	0.25-0.45	0.80-1.10	0.60-0.90
Phosporous (max)	0.025	0.025	0.025
Sulfur (max)	0.015	0.015	0.025
Silicon	0.15-0.35	0.15-0.35	0.15-0.35
Chromium	1.35-1.60	0.20	…
Nickel (max)	0.25	0.25	…
Copper (max)	0.30	0.30	0.30
Molybdenum	0.10	0.10	…
Aluminum (max)	0.050	0.050	0.050
Oxygen (max)	0.0015	0.0015	0.0020

AISI 52100 steel was chosen for testing since it is the most common grade used in ball bearings. This grade is a high carbon content alloy steel and its chemical composition is

given in Table 4. 52100 is commonly referred to as an 'alloy steel' because it contains significant amounts of chromium as an alloying element.

AISI 1053 and AISI 1070 were also used in the Barkhausen experiments. Both are also common grades for ball bearings and both are listed as acceptable grades for ball bearings according to ASTM A29-98 and A866-01. AISI 1053 is considered a medium carbon steel and AISI 1070 is a high carbon content steel.

Micro-indentation Hardness Tester

Micro-indentation hardness measurements were obtained using a Buehler Micromet 2104 hardness tester. It was used to verify the hardness of materials after heat treatment, and to measure the hardness on the machined surfaces of samples. This device is capable of both Knoop and Vickers indentations, and has 10X and 40X objectives for observing and measuring the indentation size. The indentation force and dwell time can be configured by the operator.

A Vickers indentation was used for all of the experiments, using a load of 2000 gf applied for 14 seconds. The Vickers indenter is a pyrimid shape with a square base, and its faces are at an angle of 22^{o} from the base. The hardness was calculated as:

$$HV = 0.102\frac{2F\sin\left(\theta/2\right)}{d^2} \tag{19}$$

The results were then converted to the Rockwell C (HRC) scale, since this commonly used for comparing hardened steels. The device was calibrated using a sample of known hardness before each set of measurements.

Zygo White Light Interferometer

Cutting tool wear was verified using a Zygo NewView 200 white light interferometer. This device is capable of determining topography by measuring the three-dimensional coordinates of points on a surface. The vertical position (z-direction) of a point is measured using interferometry. A light source from inside the instrument creates a beam of light that is divided into two parts. Half of the beam is shined onto the surface and then is reflected back onto a solid-state camera. Each pixel of the camera absorbs light from a small area on the surface. The other half of the beam bounces off a reference surface internal to the instrument, and then converges with the rest of the light on the camera. If the two beams are in phase when they converge on a camera pixel, the camera sees a bright spot; if they are out of phase, the pixel is dark. The phase shift between the beam halves is determined by the distance that the light had to travel to the sample surface. Therefore the brightness of a pixel is determined by the height of a small area on the sample that the light reflected off. The planar, x and y directions, are determined by the field of view of the camera—each pixel represents a small portion of the field of view.

The NewView 200 can record the coordinates of many points on the surface of the object. It has a camera with 640 x 480 pixels and can measure up to 100 μm in the vertical direction with a resolution of 0.1 nm. For this project, the cloud of points was exported to Matlab for analysis and comparison with a model of a fresh tool.

Force Dynamometer and Charge Amplifier

Cutting force data was collected using a Kislter 9257B piezoelectric dynamometer. This device is designed to have high rigidity and is typically used for measuring forces in milling or turning. It is capable of recording forces in all three orthogonal directions, within a range of –1100 to 1100 N. The charge signal from the dynamometer was converted by a Kistler 5010 charge amplifier into a high-level voltage output. The voltage data was recorded and analyzed in a National Instruments PCI 6036E data acquistion card, controlled by Labview software.

CHAPTER 4

EXPERIMENTAL PROCEDURES

This section describes the procedures that were used to determine the ability of the Barkhausen sensor to detect white layer in hard turned components. The traditional method of mounting and etching the specimen was used as a reference for the Barkhausen sensor measurements.

Overview

The goal of these experiments is to determine if the Barkhausen sensor can detect white layer over a broad range of machining conditions. If it is, it is also important to verify that the sensor is robust to changes in the cutting parameters or materials used. A range of materials, cutting tools and machining conditions typically found in industry were examined. A half factorial design was used, which varied four factors: the workpiece material, the CBN content of the cutting tool, the cutting speed, and the feed rate. The design of the experiment is shown in Table 5. The actual machining parameters for each level is shown in Table 6.

Three types of steels were tested, each is a popular choice for bearing applications. The speed and the feed rate of the turning operation were also varied, since they are known to affect the development of white layer. At high speeds and low feed rates, grain refinement in white layer is believed to be caused by quenching. There is rapid heating in and around the shear zone as the tool cuts the part, and then quenching as the heat quickly dissipates into the bulk of the material. At low speeds and high feed rates, the grain refinement is thought to be caused primarily by the severe plastic deformation that occurs during machining. Both the speed factor and the feed rate factor were tested at two levels, near the extremes of what might be encountered in industry, so that both of the mechanisms of white layer formation could be tested. The combination of a low speed

and low feedrate were not tested, since this results in a material removal rate that is too low to be practical in industry. The last factor that is varied is the type of cutting insert. Two different types of inserts were tested: a high CBN content tool and a low CBN content tool. All of the inserts in these experiments were prepared with a 20^{o} by 100 – 150 μm (0.004 - 0.006") land length by a 12 – 25 μm (0.0005 - 0.001") radius hone on the cutting edge.

Table 5: Experimental design matrix for the Barkhausen experiments.

	Speed	**Feed**	**CBN content**	**Steel grade**
1 replication	-	+	-	1
1 replication	+	-	+	1
1 replication	+	+	+	1
1 replication	-	+	+	2
1 replication	+	-	+	2
1 replication	+	+	-	2
1 replication	-	+	-	3
1 replication	+	-	-	3
1 replication	+	+	+	3

Table 6: Cutting parameters for each condition.

	Speed m/min (SFM)	**Feed mm/rev (in/rev)**	**CBN content**	**Steel grade**
1 replication	91.44 (300)	0.1524 (0.006)	KD050	52100
1 replication	182.88 (600)	0.0762 (0.003)	KD120	52100
1 replication	182.88 (600)	0.1524 (0.006)	KD120	52100
1 replication	91.44 (300)	0.1524 (0.006)	KD120	1050
1 replication	182.88 (600)	0.0762 (0.003)	KD120	1050
1 replication	182.88 (600)	0.1524 (0.006)	KD050	1050
1 replication	91.44 (300)	0.1524 (0.006)	KD050	1070
1 replication	182.88 (600)	0.0762 (0.003)	KD050	1070
1 replication	182.88 (600)	0.1524 (0.006)	KD120	1070

Specimen Preparation

Three grades of steel were tested in the Barkhausens experiments, only 52100 was tested in the electrochemical experiments. Each steel type was delivered as long bars that were cut into several smaller bars and then hardened as a single batch. Therefore, there was assumed to be little variation in the chemistry and hardness between the small bars or within a single bar.

The dimensions of the stock material are shown in Figure 26 and Figure 27. The 52100 tubing was received in the hardened condition in lengths approximately 50 cm long. The tubing had and outer diameter of 41.3 mm (1.625 in) and an inner diameter of 25.4 mm (1 in). The tubing was cut into 510 mm (20 in) lengths before heat treatment. Both the 1053 and 1070 stock were solid bars, 48.46 mm (1.908”) in diameter and approximately 196.9 mm (7.75”) long.

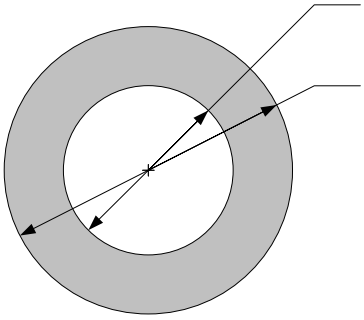

Figure 26: Cross-section dimensions of 52100 tube

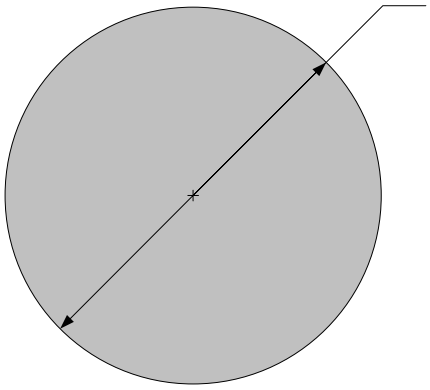

Figure 27: Cross-section dimensions of 1053 and 1070 bar.

The 52100 steel was induction hardened to about 62 HRC. To reduce hardness fluctuations and to ensure high hardness throughout the part, tube stock was used. This allowed heat flow on both the inner and outer surfaces of the tube during the heat treatment and resulted in a more consistent hardness through the cross-section than could be achieved using bar stock. Since the 1070 and 1053 stock were in bars instead of tubes,

the hardness was not as consistent from the outer diameter to the center as it was with the 52100.

Upon delivery the hardness of the material was tested using both a standard hardness tester and the micro-indentation hardness tester. An example of the micro-indentation hardness measurements are shown in Table 7. Three measurements were taken at different locations on the outer surface of the tube. Typically when testing a curved surface the result is multiplied by a correction factor. For all of the bars used in these experiments, the radius of curvature was large enough that this correction faction was essentially 1, resulting in no effect. Hardness was also measured across the cross-section of the bars. Table 7 shows measurements that were taken on a tube of 52100, at several locations from the outer diameter to the inner diameter.

Table 7: Example of the micro-indentation test to verify the hardness of a tube of 52100.

		Meas. #1 [HRC]	Meas. #2 [HRC]
Outer diameter surface:	Test #1	51.1	52.3
	Test #2	53.3	55.4
	Test #3	48.9	48.5

	Distance [mm]	Meas. #1 [HRC]	Meas. #2 [HRC]
Cross-section:	0	57.3	57.7
	2.5	60.6	59.5
	3.8	60.9	61.6
	5.1	57.7	56.6
	7.6	59.7	60.8

The 52100 tube was found to be hardened within the range 49HRC to 55HRC and the hardness varied only slightly with depth, indicating that the heat treatment affected the entire tube. Although the hardness was below its specified value of 60-62HRC, the experiments initially proceeded using this material. When turning this material with a high CBN content tool, it was quickly apparent that the tool life was shorter than expected from previous experimental data. The only known discrepancy between the machining conditions for the two data sets, was that the previous data was collected from 52100 steel that was hardened to the full 60-62HRC. Therefore, the 52100 tube was

returned for a second heat treatment to increase the hardness to the desired range, but further tests showed that this did not significantly change the tool life and correct the discrepancy. Although the tool life issue was not resolved, it was concluded that it did not have a significant effect on the issues that were being examined. The important end result is that the 52100 that was machined for the experiments in this study had a hardness of 49-55HRC.

The hardness of the 1053 and 1070 steel bars was also verified and confirmed to be in the expected range of 60-62HRC. Since this material was in bar form, it was more difficult to through harden. However, the hardness across the cross section of the 1053 and 1070 bars was measured, and it was found that for both types of steel the desired hardness was developed past the machining depth.

All machining was performed with a Hardinge Conquest T42 Super Precision lathe, using a Hardinge/GE Fanuc 18-T controller. Before machining the sample parts for the experiments, the outer surface was turned for a few clean up passes with a used CBN tool. As a result of heat treatment, all of the bars had a black scale on their surface from oxides and other impurities in the furnace. The clean up passes removed these scales and also reduced warpage and out-of-roundess error caused by an altered residual stress state after heat treatment.

Each type of steel was machined in the same manner, by repeating a canned turning cycle to reduce the outer diameter of the part and to wear the cutting tool. For each sample part, a random bar was selected and the part was turned from the material at the end of that bar. Then the part was cut off from the bar using the wire EDM, labeled and stored. More information about the machining of the sample parts is described in the next section, ‘Inducing Tool Wear.’ After machining, the specimens were stored in individual containers. They were coated with a rust inhibitor for preservation for later tests.

Inducing Tool Wear

Tool wear is known to affect aspects of surface integrity, such as changing the residual stress profile, which have an indirect effect on BNA. For any machining process, including hard turning, the cutting tool wears down as it is used. Although a machinist cannot directly control it, the cutting edge geometry continually changes as the wear progresses. Since cutting edge geometry has been shown to affect the cutting temperature and cutting forces in hard machining (Ozel, 2003), the surface integrity also changes depending on the condition of the tool.

Relevant to this study, it has been reported that tool wear contributes to white layer formation. In other words, for a given set of machining parameters, a worn tool may produce white layer while a fresh tool might not. (Akcan, Shah et al., 2002) The changing surface integrity, especially the hardness and residual stress state, should in turn affect the BNA. An important property of white layer is that is harder than the bulk material (Akcan, Shah et al., 2002), and the Barkhausen sensor should detect this. However, in most cases, the Barkhausen sensor has been shown to be effective at detecting differences in hardness as long as other material properties, especially residual stress, are held constant. (Moorthy, Shaw et al., 2003)

Unfortunately, it is impractical to vary white layer depth, while keeping other surface integrity factors relatively constant. For example, it is difficult to create two parts that have the same residual stress profile, but different white layer depths. Instead, tool wear was used to vary the white layer depth. Sets of sample parts were turned with the same machining parameters, but at different intervals of the cutting tool life. The advantage of this is that each set had some specimens with white layer, but each part in a set had similar surface texture because it was machined at the same speed, feedrate, and depth of cut.

This has the added benefit of this method is that it is similar to how the Barkhausen sensor might be used during in-process inspection in industry. For example, a Barkhausen sensor could be mounted in a lathe to measure BNA as parts are turned. With each pass

the tool would become more worn and, therefore, more likely to produce white layer. Once the BNA, as measured by the Barkhausen sensor, exceeds a threshold, the insert would be replaced with a fresh one.

In order to have an idea of how the Barkhausen sensor might perform at different intervals of the insert's life, eight sample parts are made for each machining condition using a single insert. For each of the experimental trials, the material is observed at eight equal increments of the tool life. The first part represented the surface generated by a fresh tool and it was created with a fresh insert by only making one or two passes. This part is then cut from the stock using the wire EDM. The total volume that the insert can remove, estimated from the tool life, is divided by seven to calculate the number of passes needed for the remaining seven parts. Therefore the final surface on each part represents the surface generated at an interval of the total tool life. In other words, the same tool is used to make 25.4 mm (1") long passes until it has removed 14% of the material that it can remove in its life. After this, the sample is removed from the stock for observation. This observation represents 14% of the total tool wear. This process is continued until the tool has reached its estimated tool life and then it is assumed to be fully worn.

The machined part samples for this experiment are created by simply using a canned turning cycle to remove material from the outer diameter of the stock. The speed and feed rate are set by the experimental design. The radial cutting depth is set to 50.8 μm (0.002") for comparison to the previous student's work; this depth is consistent with a finish hard turning cycle. For each machining condition, the length was adjusted so that the diameter was not reduced excessively. For example, if the tool life for a particular condition was relatively long, then the machining passes were lengthened so that more material was removed in each pass.

To avoid the need to constantly observe the tool wear during the machining operation, the tool wear is estimated from data collected by a previous student. Tool life estimates for the same machining conditions using 52100 steel are obtained from a previous student's

data. (Dawson, 1999) According to Dawson's thesis, he decided that a tool failed if: (1) edge fracture or (2) greater than 200 μm of flank wear. 200 μm of flank wear was selected as a criterion because most inserts fractured after 150-200 μm of flank wear. The total tool life for a particular speed, feed rate, and depth of cut is essentially the volume of material that can be removed by the insert before one of the tool failure criteria is reached. The same tool life estimates were used for turning the 1053 and 1070 steels, since these materials are relatively similar.

Polishing, Mounting, and Nital Etching

Once a specimen is turned on the Hardinge lathe, and then cut from the stock material using the EDM, it can be mounted for observation under the optical microscope. The typical procedure for mounting, polishing and etching was followed.

To examine the microstructure of the surface of a part for white layer, a thin slice of metal is cut from the surface using the wire EDM. If necessary, this slice is cut again to make a pie wedge shape that can fit inside the chamber of the mounting press. The surface was sliced approximately parallel to the tool path so that when the surface is viewed, it is flat instead of having feed marks.

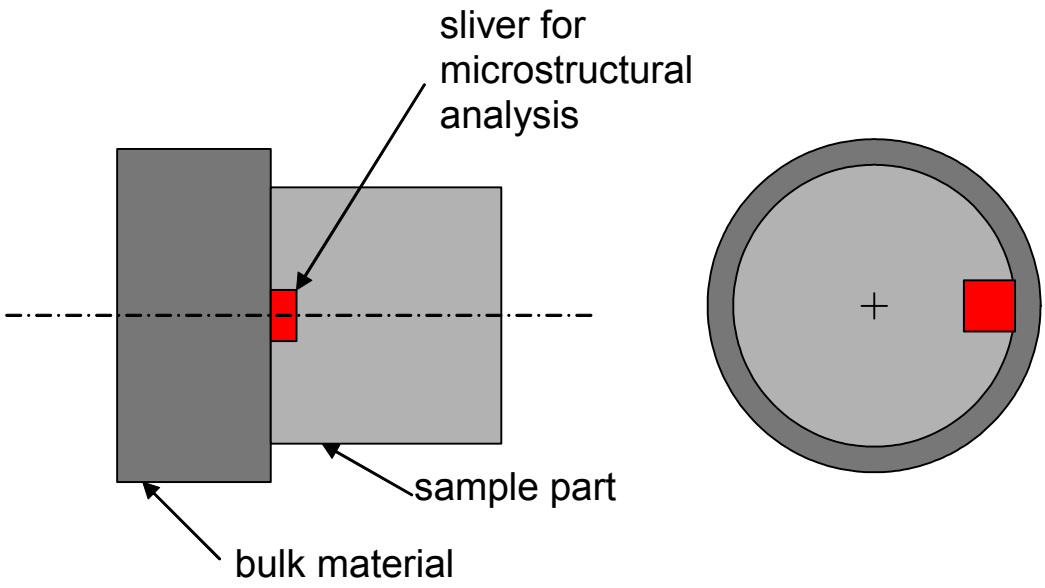

Figure 28: Location of sliver used in microstructural analysis

To preserve and fixture it for further observation, the specimen wedge was mounted in a thermoforming epoxy molding compound. Epomet G powder from Buehler was chosen as the mounting compound because it is designed to retain the edge of the specimen. The edge was especially important in this case because that is where white layer appears. The epoxy and the specimen were placed in a compression molding press and heated for 10 minutes under about 70 kPa of pressure. The heat was then removed, and the epoxy was allowed to cool under pressure until it hardened and secured the wedge.

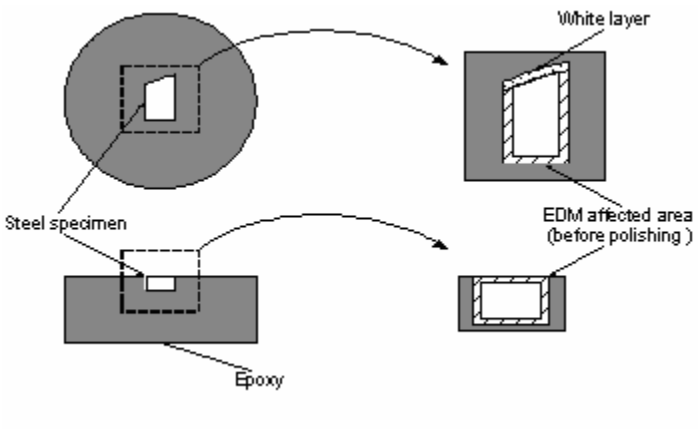

Figure 29: Epoxy disc used for microstructural analysis.

The epoxy solidified into a disc, as shown in Figure 29, with the steel specimen mounted on the top face. Since the sliver was cut from the part, each side of it was affected to a small depth by the electrical sparks from the wire EDM. Careful polishing ensured that the material affected by the EDM was removed, revealing only the microstructure of interest. Next, the epoxy disc was ground flat using Buehler Carbimet 240 grit and then 320 grit paper. Finally the discs were polished using Buehler MetaDi monocrystalline diamond slurry with progressively finer grit: 9 μm, then 3 μm and last 1 μm.

After grinding and polishing, the epoxy disc was placed in a nital solution for several seconds to etch the sample. The nital solution consisted of 2% nitric acid mixed with ethanol. This solution selectively reacts with steel—softer areas and grain react more quickly, turning them a dark grey and exposing the microstructure. Etching is a delicate process because the sample must remain in the etching solution long enough to color the bulk material but not long enough to darken the white layer. The EDM'ed edges were used as a guide in the etching process since they typically have a white layer. If white layer is not observed on the EDM'ed edges, then the sample had either been over-etched or under-etched. If a sample is not properly etched, it was re-polished to expose a fresh layer of the microstructure.

White Layer Detection

After nital etching, the specimen's microstructure can be more easily observed under an optical microscope. The microscope that is used has a digital camera attachment that is capable of taking and storing micrographs, and the pictures are then transferred to a PC for analysis. For each sample, a micrograph of the machined surface was obtained at 1200x magnification.

Since the white layer depth is not constant across the surface, five measurements were gathered for each sample and the result was averaged. To do this, the micrographs are viewed using Adobe Photoshop, and the white layer depth is measured in pixels. The pixels are scaled using a calibrated mark that appeared in each micrograph. Due to pixilation of the computer screen, the pixel-resolution of this method was approximately 0.04 m.

Barkhausen measurement

Several external factors can affect the Barkhausen sensor and introduce noise to the measurements, which make it more difficult to discern the effect of white layer. Some of these external factors are intrinsic to the Barkhausen effect and are described in the background. Other factors, such as the angle of the probe tip, are particular to the design of the specific sensor that was used. When possible, the effect of these factors was minimized to improve the precision of the measurements.

Since the Barkhausen sensor measures a changing magnetic field, it is sensitive to electromagnetic noise from the surrounding environment. For all of the measurements, the sensor must be taken to a location that is relatively isolated from electrical devices. In a production environment, the sensor should be shielded from the fields generated by these devices.

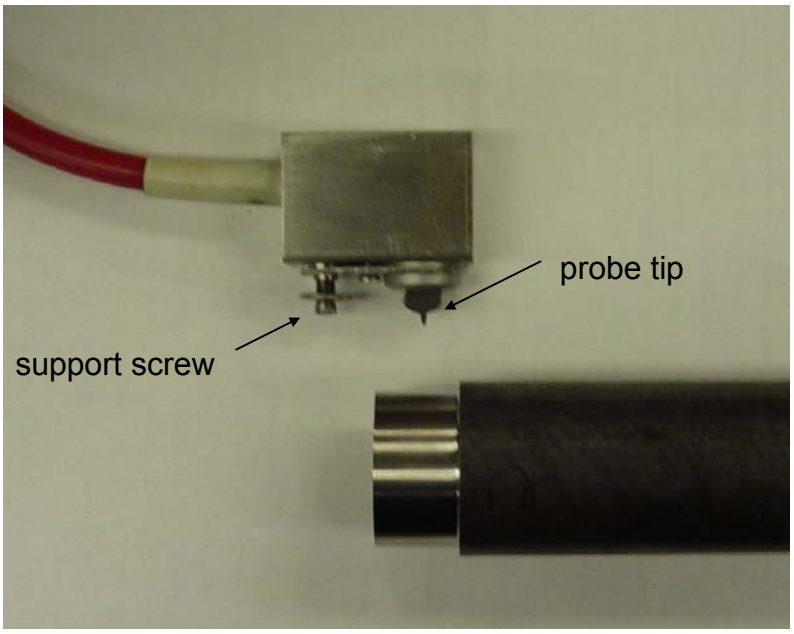

Figure 30: Photo of Barkhausen hand-held probe.

During the measurements, the probe tip must remain in contact with the surface of the specimen. To prevent dirt and residue from affecting the measurement, the surface was first washed with soap and water, and then with acetone to clean it. Additionally, because the magnetic field emitted by the probe is directional, it is important to maintain a constant angle between the probe tip and the part for all of the measurements. During some trial measurements, if the angle between the probe and the part surface is varied, the measurement can change by 20% or more. For all of the measurements, the body of the probe was aligned with the axis of the part. The photo in Figure 30 shows the hand-held probe correctly aligned with a part. (For actual measurements, the probe was in contact with the surface of the part, and the part was cut from the stock.) Although the sensor was designed to be hand-held, it is difficult to keep the probe tip perpendicular to the surface if the adjustable support screw is not resting on a level surface. If the tip is even a few degrees from perpendicular, the measurement may vary by 10-20%. To prevent this, a support block the same height as the part was placed under the support screw to fix the tip angle and to hold the probe in contact with the specimen, as seen in Figure 31.

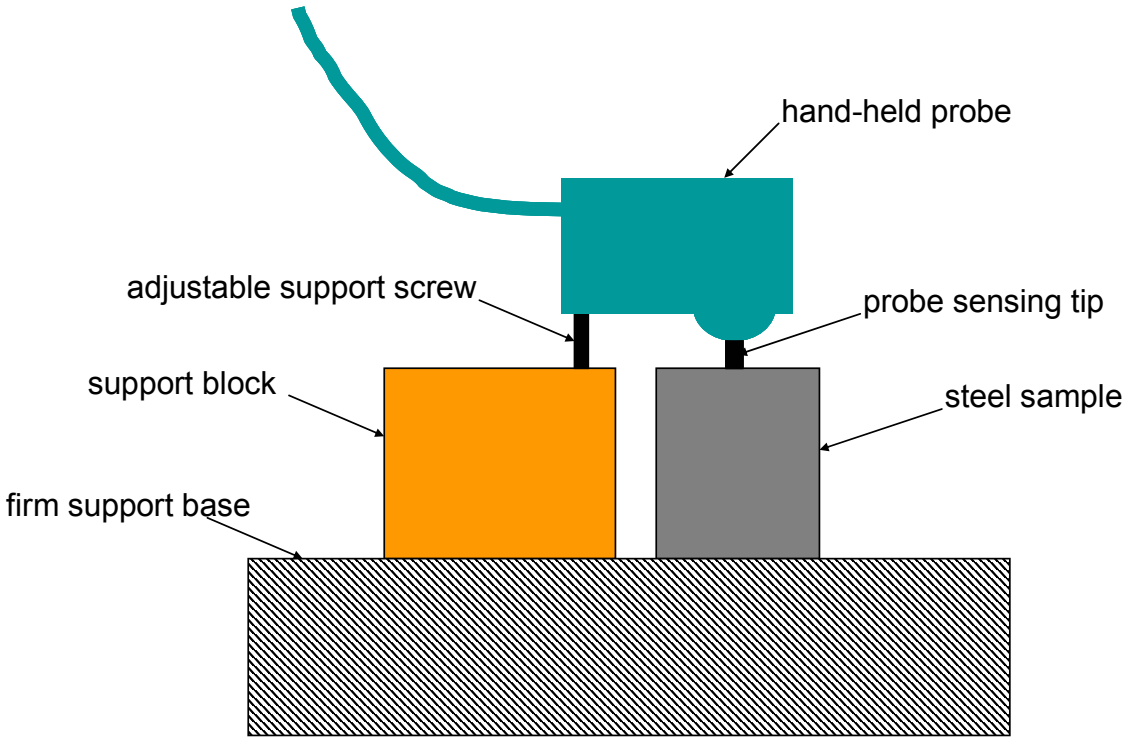

Figure 31: Diagram showing how the hand-held probe was supported.

The output from the Barkhausen sensor is described as 'noise' because it oscillates unpredictably. For most measurements, the Barkhausen noise amplitude oscillates and never settles at an equilibrium value. The effect of random noise factors was reduced by averaging several measurements. To account for the variation of the signal over time, the output from the sensor was sent to a PC that recorded data for 5 seconds and averaged the result. Then, to address measurement variation over the surface the part, this 5 second average measurement was collected at five different locations on the surface.

Residual Stress Measurement

Residual stress measurements were obtained on the machined surface of two sets of 52100 steel parts that had previously been measured with the Barkhausen sensor. To examine different mechanisms of white layer formation, one of the selected sets had been machined at high speed, and the other had been machined at low speed.

All of the measurements were obtained using a Panalytical X'Pert Pro MRD, which is equipped with a four-axis goniometer. The angle of incidence is denoted by Θ, the specimen rotation angle is Φ, and the specimen tilt angle is Ψ.

The stress tensor was calculated from the residual stress measurements using the $\sin^2 \Psi$ technique. (Prevey, 1986) Plane-stress is assumed for this calculation, so the stress perpendicular to the surface is $\sigma_3 = 0$. The undeformed interplanar spacing, d_o, is known from published results. The actual interplanar spacing, d, is calculated using x-ray diffraction measurements and Bragg's law. The actual interplanar spacing at some values of Φ and Ψ is $d_{\Phi\Psi}$. The strain in this direction is given by:

$$\left(\varepsilon_{33}\right)_{\Phi\Psi} = \frac{d_{\Phi\Psi} + d_o}{d_o} \tag{20}$$

The measured strain can be transformed into the strain normal to the sample surface, ε_{kl}, using a coordinate transformation. This gives the fundamental equation for x-ray stress analysis (Thiele, 1998):

$$\begin{aligned}\left(\varepsilon_{33}\right)_{\Phi\Psi} &= \frac{d_{\Phi\Psi} - d_o}{d_o} \\ &= \varepsilon_{11}\cos^2\Phi\sin^2\Psi + \varepsilon_{12}\sin 2\Phi\sin^2\Psi \\ &\quad + \varepsilon_{22}\sin^2\Phi\sin^2\Psi + \varepsilon_{33}\cos^2\Psi \\ &\quad + \varepsilon_{13}\cos\Phi\sin 2\Psi + \varepsilon_{23}\sin\Phi\sin 2\Psi\end{aligned} \tag{21}$$

This equation involves six unknown strain quantities, and therefore the lattice spacing, $d_{\Phi\Psi}$, must be measured for at least six combinations of Φ and Ψ. To improve accuracy, more combinations are typically used, and the strains are calculated from a linear regression. (Berruti and Gola, 2003) All of the samples measured for this study were measured using three Φ angles and seven Ψ angles, for a total of 21 combinations.

To improve the accuracy of x-ray measurements, peaks occurring at angles greater than $\Theta = 120^o$ should be considered. From previous studies, undeformed 52100 is known to

have a strong martensite peak at 156°. (Thiele, 1998) To analyze the shift in this peak, each measurement scanned the sample from Θ = 150° to Θ = 160°.

Electrochemical Experimental Procedure

Electrochemical tests are performed on two blocks of samples to examine different modes of white layer formation. One block is machined at high speed and the other is machined at a lower speed. Within each block, some of the samples are machined and then fully annealed, some are machined and do not have white layer, and some were machined and have a continuous white layer.

Table 8: Number of replications for electrochemical tests

	annealed	no white layer	white layer
machined at high speed	2	3	3
machined at low speed	2	3	3

The specimens are machined from 52100 tube, hardened to 60-62HRC, on the Hardinge lathe using a high-CBN, KD120 insert by Kennametal. The same material and the same insert geometry are used as in the Barkhausen experiments. The outer diameter of each sample after machining is approximately 38 mm (1.5") and the length is about 19 mm (0.75"). After machining, the parts were cut from the stock using an EDM. Half of the samples are machined at high speed: 182.88 m/min, 0.0762 mm/rev, and a radial depth of 0.0508 mm. The other half are machined at low speed: 91.44 m/min, 0.1524 mm/rev, and a radial depth of 0.0508 mm. The samples with no white layer and the annealed samples are machined with a new insert. The samples with white layer are machined with an insert that is within a few passes of the end of its estimated tool life. For the samples with white layer, its thickness was measured to range between 2.5 to 11 μm thick, with most samples having a white layer approximately 7 μm thick.

The samples are first washed with soap and water, dried, and then cleaned with acetone. This removes any dirt or oil that might contaminate the surface of the metal. This is

especially important for the annealed samples, which have some soot on the surface from the heat treatment process that occurred after machining. To connect the specimen to the potentiometer, a steel wire is spot welded to the inner diameter of the tube. Then the wire, the inner surface of the tube, and the EDM'ed surfaces are covered with a plastic coating to prevent them from exposure to the solution. Only an area of about 22 cm^2 on the machined surface is left exposed to the solution.

Three types of electrochemical tests are performed: open-circuit potential, electrochemical impedance spectroscopy, and linear polarization resistance. Each of the tests are performed with the aid of the PCI4/300 potentiostat, using a Ag/AgCl reference electrode and a platinum counter electrode. The working electrode is a machined specimen. The sample is fully immersed in a 1M solution of NaOH at room temperature and separated from the reference electrode by a KCl salt bridge.

Careful control is maintained over the experimental setup, since it is sensitive to changes in temperature, pH, residues on the surface of the samples, and other factors. Each part is tested in a fresh bath of NaOH solution. The NaOH solution is prepared as a single batch several hours in advance of the experiments so that the temperature, pH, and solution concentration for each test is the same. Each part is cleaned and dried before testing. The electrodes were maintained in the same physical location for each of the tests.

The first test measures the steady state open-circuit potential of the part against the reference electrode. The potential was measured with a voltmeter after the system has achieved equilibrium 20 minutes later.

CHAPTER 5

EXPERIMENT RESULTS

Tool wear verification

When machining the sample parts, it was assumed that the tool life was estimated approximately by the data collected by a previous student. This assumption was verified by visual observation of the cutting tool and measuring the actual tool wear for some representative cases. Tool wear was measured both using the traditional method of measuring the length of the flank wear zone using a microscope, and by quantifying the volumetric tool wear using data points scanned using a white light interferometer. (Dawson and Kurfess, 2000; Dawson and Kurfess, 2002)

In general, the micrographs showed that the tool wear progressed more quickly than expected when machining 52100 steel, and more slowly than expected when machining 1053 and 1070 steel. The tool life was much shorter than expected when machining 52100 steel using a high-CBN content tool. In this case, the tool failed catastrophically in approximately half of its expected tool life. Although the tool life was not estimated exactly, most machining conditions produced some parts with white layer and some without, which was the desired result.

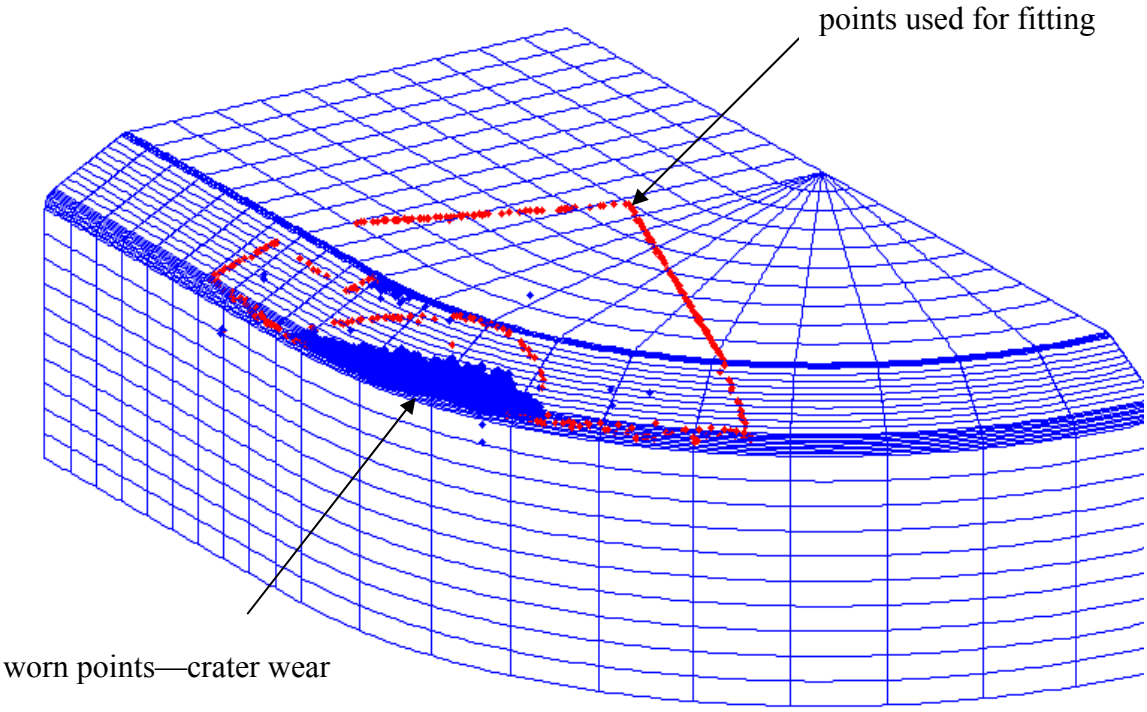

Figure 32: 3D plot showing points collected from the face of a cutting tool.

The volumetric loss of material from the cutting tool was quantified using data collected from a white light interferometer. An area of about 0.25 mm^2 was scanned on both the face and the flank side of the tool to observe flank and crater wear. Volumetric loss was calculated by integrating the difference between the point cloud gathered from the worn tool and a collection of 3D parametric surfaces representing a fresh tool. The parametric surfaces for the fresh tool were dimensioned from the geometry of the insert, and they formed a nice match with a point cloud collected from an actual fresh tool.

The point cloud was oriented to match the model by minimizing the sum of squares distance between each point and the model:

$$\min_{X,Y,Z,\theta,\phi,\sigma} SS = \sum_{i=1}^{n} \left(P_{actual}(x,y,z) - P_{model}(x,y,z) \right)^2 \qquad (22)$$

To minimized computation time, only the points on the edge of the point cloud were used for the orientation. In Figure 32, a wire mesh model of a fresh tool is shown in blue and the points on the edge of the cloud are shown in red. The sum of squares was minimized by both translating the point cloud by *X, Y,* and *Z*, and by rotating it by θ, φ, and σ.

An initial fit of the model was made by using all of the edge points. This was imperfect however, because it included the worn points which are not near the model. The worn points were identified as more that one standard deviation from the model. The worn points are displayed in red in Figure 33, and the unworn points are shown in green. A second, more accurate fit, used only the unworn edge points. Next, holes in the point cloud, such as the one to the left of the crater wear in Figure 33 were filled by a linear interpolation with adjacent points. Finally, the distance between the worn points and the model surface was used to numerically integrate the volumetric loss. The results confirmed the observations from the micrographs.

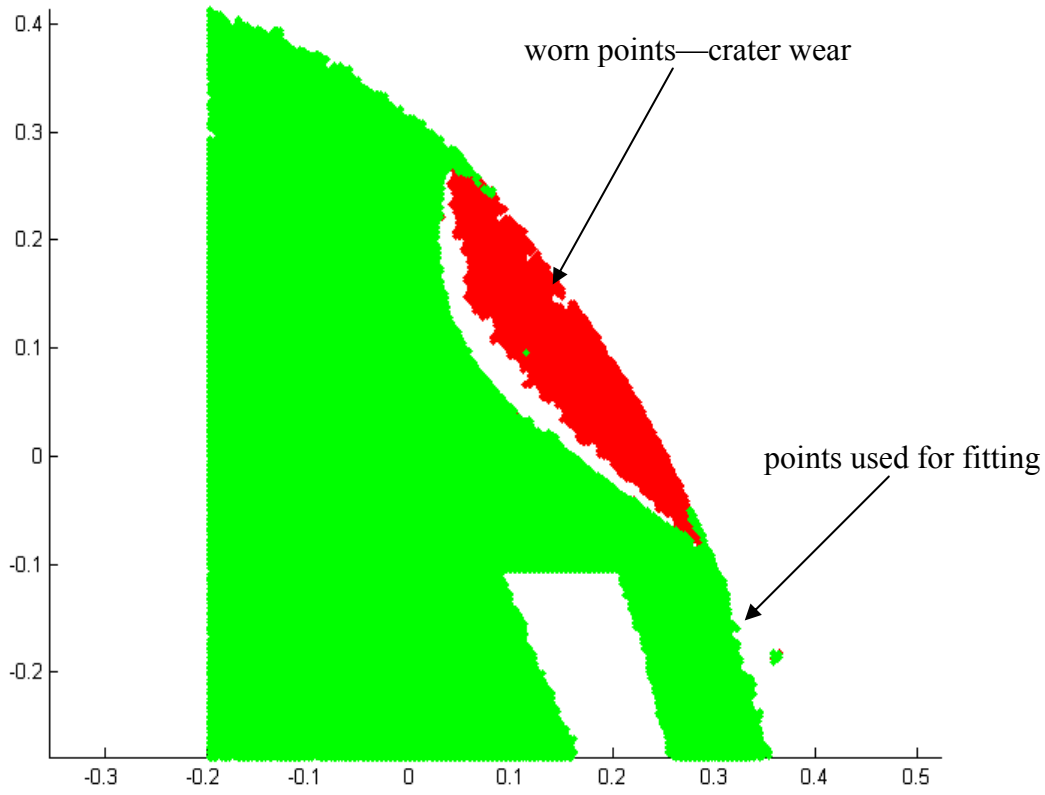

Figure 33: 2D plot of the same insert, showing a top view.

Cutting force measurements

During the machining, the cutting tool was connected to a dynamometer that was capable of recording the cutting force in all three axes.

For each machined part, the force on the cutting tool was measured using a three-axis dynamometer. This data provided insight into the cutting process. Usually the force on the tool quickly increased as the tool first entered the workpiece, then remained steady during the cut, and finally peaked at the end of the cut. The radial force was usually the largest component, followed by the tangential force component. As expected, the axial force (in a direction parallel to the tool path) was the smallest.

With a fresh tool, the tangential and radial forces were approximately equal in magnitude. As the tool became more worn, these forces both increased in magnitude, but the radial

force increased more quickly. Figure 34 shows the cutting force on a fresh insert, when machining at 182.88 m/min (600 sfm) and a feed rate of 0.0762 mm/rev (0.003 ipr). Figure 35 shows the same insert, under the same machining conditions, after it has reached the end of its tool life. The magnitude of the force on the worn insert is approximately twice that of the fresh insert. In some cases, the dynamometer recorded wildly oscillating forces, which is a good indication of chatter, and so that part was discarded. A Matlab program was used to select the flat region of the cutting force, to determine the average force on the tool. The results are shown in the Appendix.

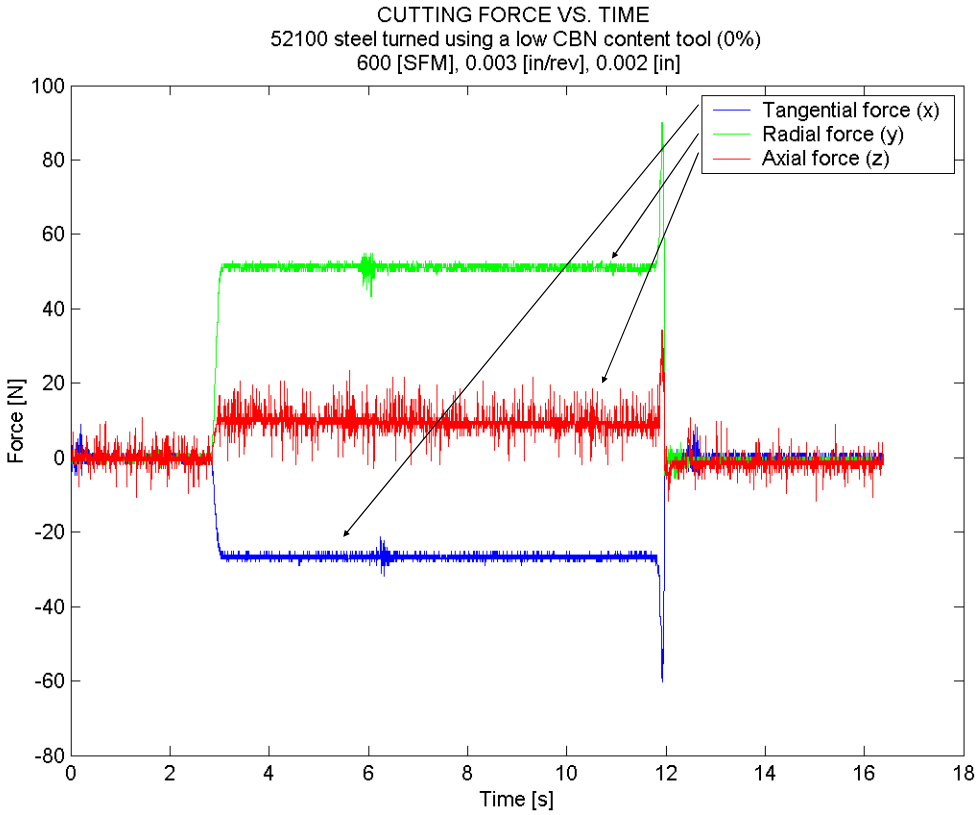

Figure 34: Example of cutting force data gathered from a new cutting tool.

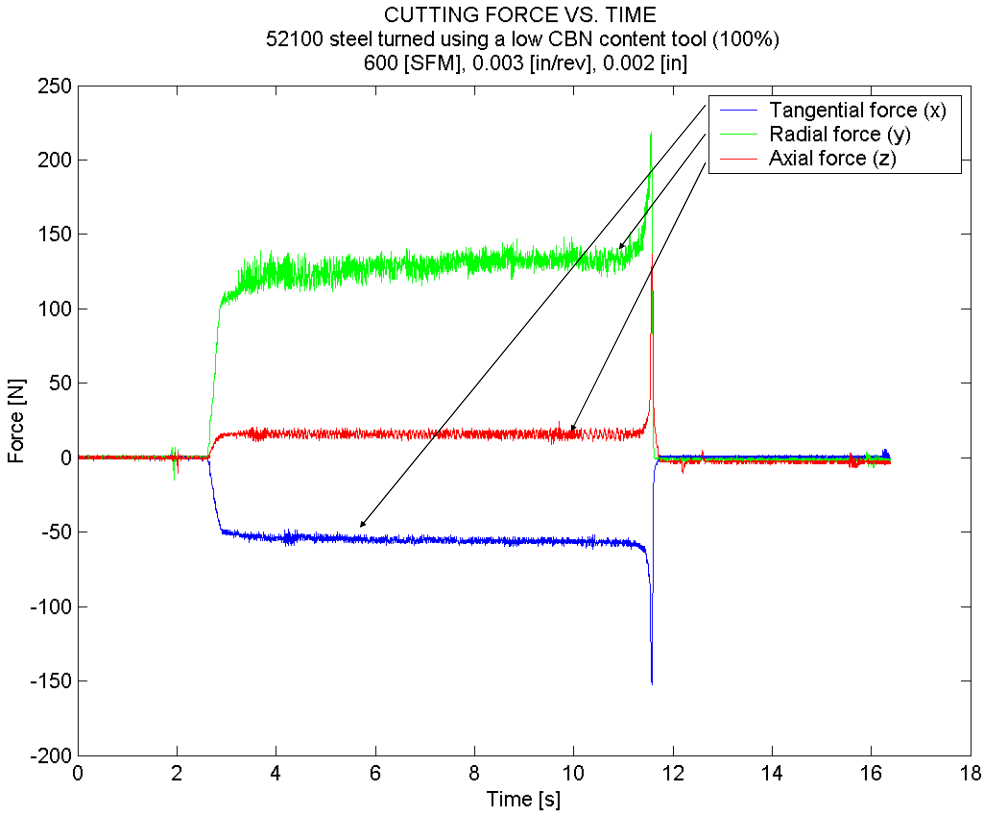

Figure 35: Example of cutting force data gathered from a fully worn cutting tool.

Micro-indentation Hardness testing

After machining, the hardness of the surface of the machined parts was measured using the Micromet 2104 micro-indentation hardness tester. Three hardness measurements were obtained from the outer (machined) surface of each part. A sample result for a specific machining condition is shown in Table 9. The remaining hardness measurements are shown in the Appendix.

Table 9: Micro-indentation hardness results.

Workpiece material:	52100
Cutting insert:	KD050
Speed:	300
Feed:	0.006

Tool life:	0%	14%	29%	43%	57%	71%	86%	100%
Measurement 1 [HRC]	63	63.1	58.6	61.6	59.6	57.5	57.6	53.9
Measurement 2 [HRC]	62.9	58.3	58.9	58.4	61.4	56.9	64.1	58.9
Measurement 3 [HRC]	64.3	59.4	62	60.3	61	59.1	61	60.4
Standard deviation	0.78	2.51	1.88	1.61	0.95	1.14	3.25	3.40
Avg	63.4	60.3	59.8	60.1	60.7	57.8	60.9	57.7

A Vickers hardness indenter was used for all of the tests. The shape of this indenter is a pyramid with faces 136^{o} apart. When the indenter is pressed into a material, it leaves an impression with similar geometry. In harder materials, this indention is smaller, in soft materials, the indention is larger. For each of the measurements in this experiment, the indention had diagonals approximately 80 μm in length. From the geometery of the indentor, this implies that the indention pierced approximately 28 μm into the surface. In is important to note that the white layer was measured to be approximately 1-15 μm deep. Therefore, if white layer was present, it only partially effected the measured hardness.

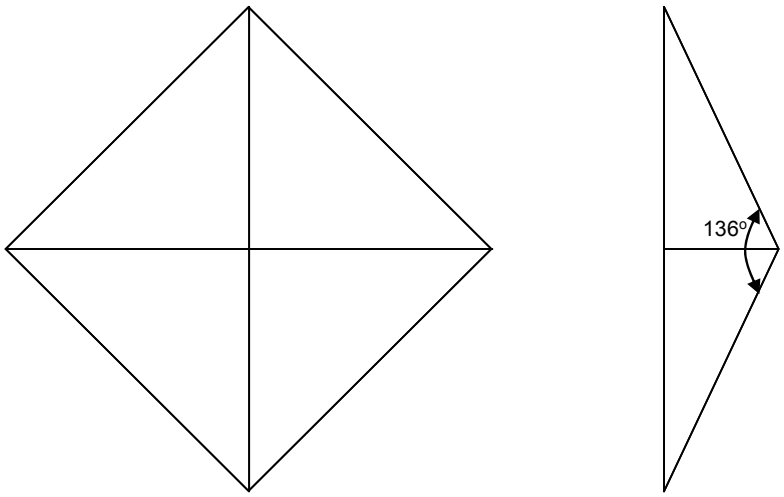

Figure 36: The shape of the Vickers hardness indenter.

Residual stress measurement

Residual stress testing using the x-ray diffractometer is in progress. Approximately 25% of the data should be collected by November 23, 2004.

Barkhausen measurements

The first step when using the Barkhausen sensor is to optimize its frequency and intensity settings so that the difference between parts with white layer is magnified. White layer is known to be 1-10 μm deep, so the highest frequency setting was used, which corresponds to a measurement depth of about 20 μm. To determine the optimum intensity (or MAGN) setting, a part known to have white layer was compared to a part without any. The readings from each part was recorded as the intensity varied through its entire range. As Figure 37 shows, there is no intensity range that showed a significant difference between the parts.

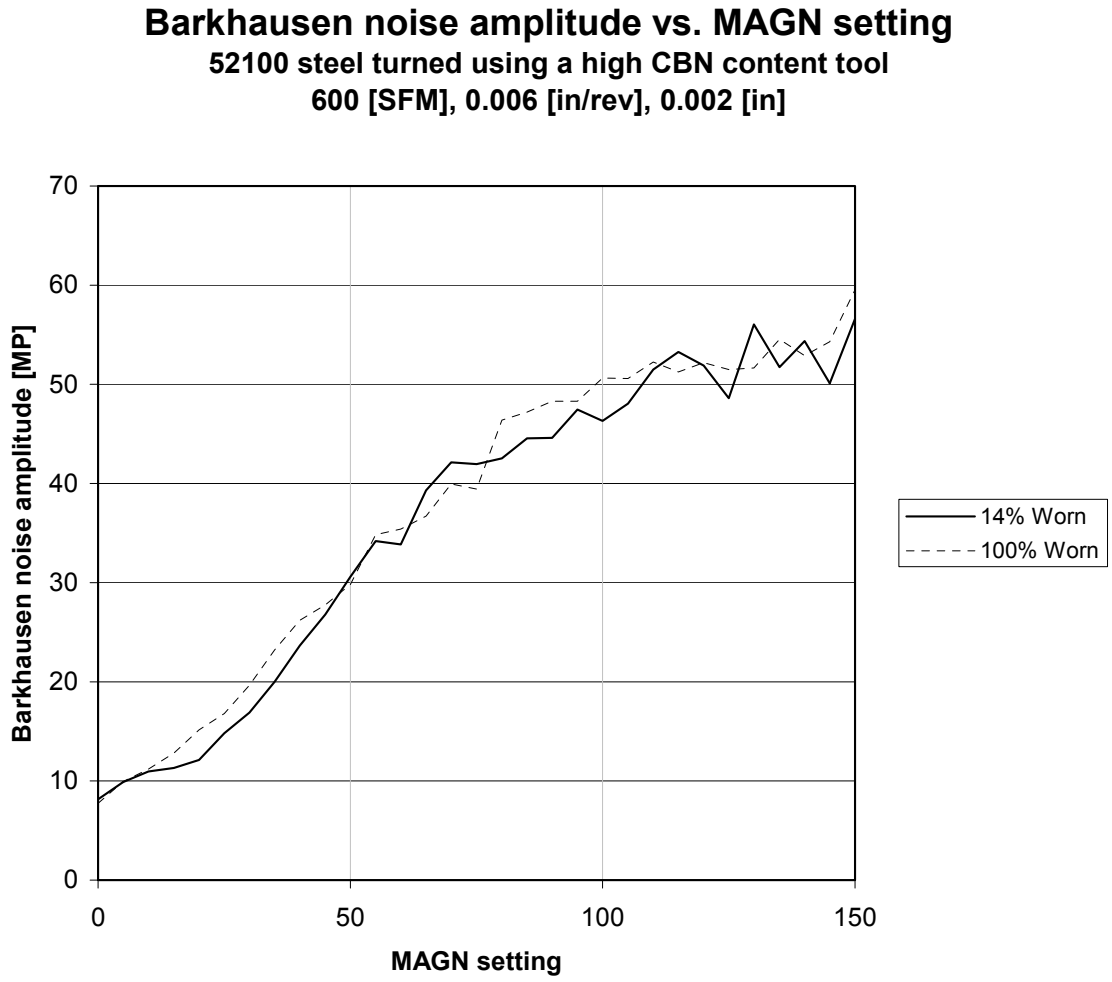

Figure 37: Barkhausen amplitude versus sensor intensity.

After measurements of the first few sample parts, no correlation between white layer and BNA was observed. For confirmation of these results, a batch of the machined samples were delivered to the company that produced the Barkhausen sensor, American Stress Technologies (AST). AST measured the samples using a different model of Barkhausen sensor, a Rollscan probe. The company also tested the residual stress of a few of the samples with an x-ray diffractometer. A comparison of the measurements are shown in Table 10 and Figure 38. Although the two independent measurements are not equal (due to using different sensors and slightly different settings), they do show the same trend.

Table 10: Comparison of my measurments against AST's measurements.

	14%	29%	43%	57%	71%	86%	100%
BNA [MPA] (by me)	67.6	54.48	66.26	56.66	51.6	58.92	55.64
BNA [MPA] (by AST)	67.31	50.35	68.46	51.06	53.84	53.89	48.3
Axial Stress [MPa]	3		263.5				292.5
Hoop Stress [MPa]	248.5		520				593.5
WL depth [um]	0	0	0	0	1.42	4.61	6.42

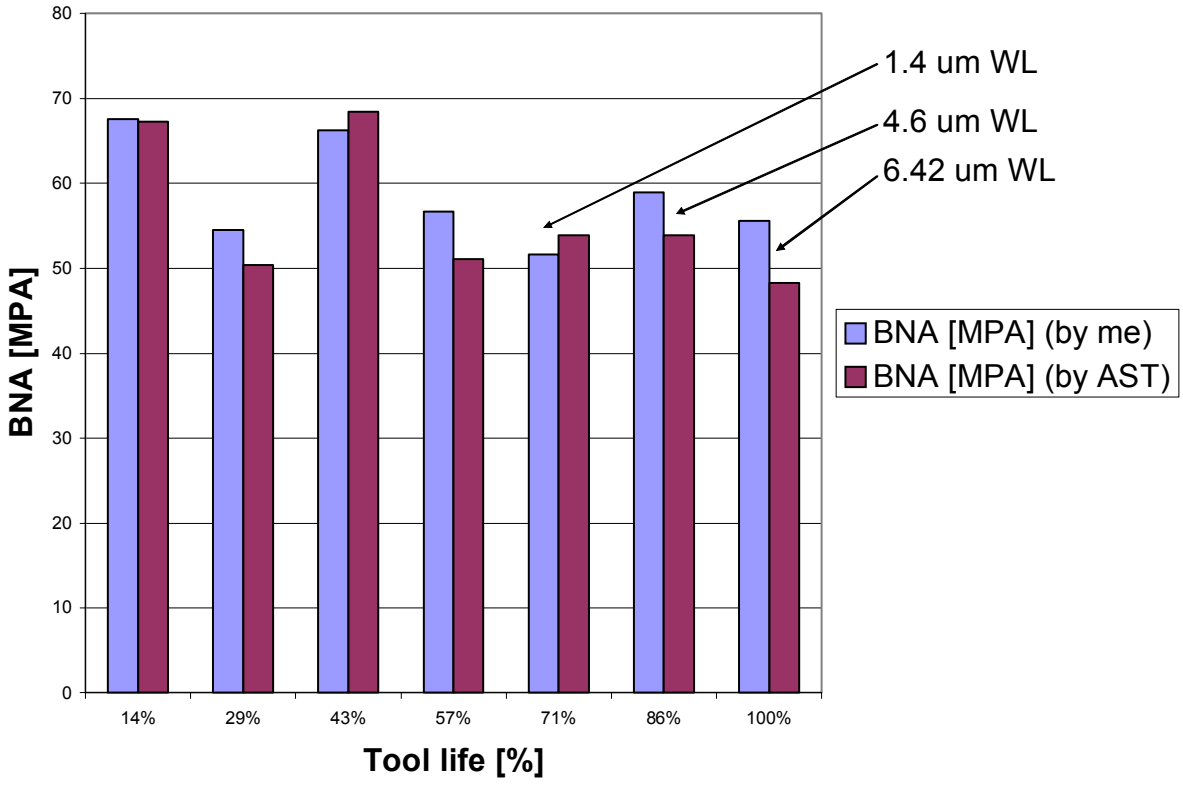

Figure 38: Comparison of my measurments against AST's measurements.

The fundamental conclusion from the Barkhausen experiments is that there was no correlation observed between the presence of white layer and the Barkhausen noise amplitude. A typical result is shown in Figure 39, where the parts machined at 71%, 86%, and 100% of the tool life showed white layer after inspection of their microstructure. Additional results from the Barkhausen sensor are listed in the Appendix.

The first observation from this plot is that there is no clear trend in the data. In this case, the BNA seemed about the same for each of the parts, scattered around 60 MP. For other machining conditions and materials, the trend-line was not necessarily horizontal, but it never showed a correlation with white layer presence. The most likely explanation for this result is that the residual stress profile varied significantly on the surface of each part, masking the effect of harder white layer.

The second important observation is that the error bars for the data points are large. In Figure 39, the error bars show the maximum and minimum of five measurements taken at different locations of the same part, as described in the experimental procedure. For example, for the part that was machined at 43% of the tool life the range is 11.2 MP, which is 16.8% of the mean. This indicates that there is substantial variation in the Barkhausen measurements, and therefore several measurements must be averaged to obtain an accurate estimate of the mean Barkhausen reading for a part.

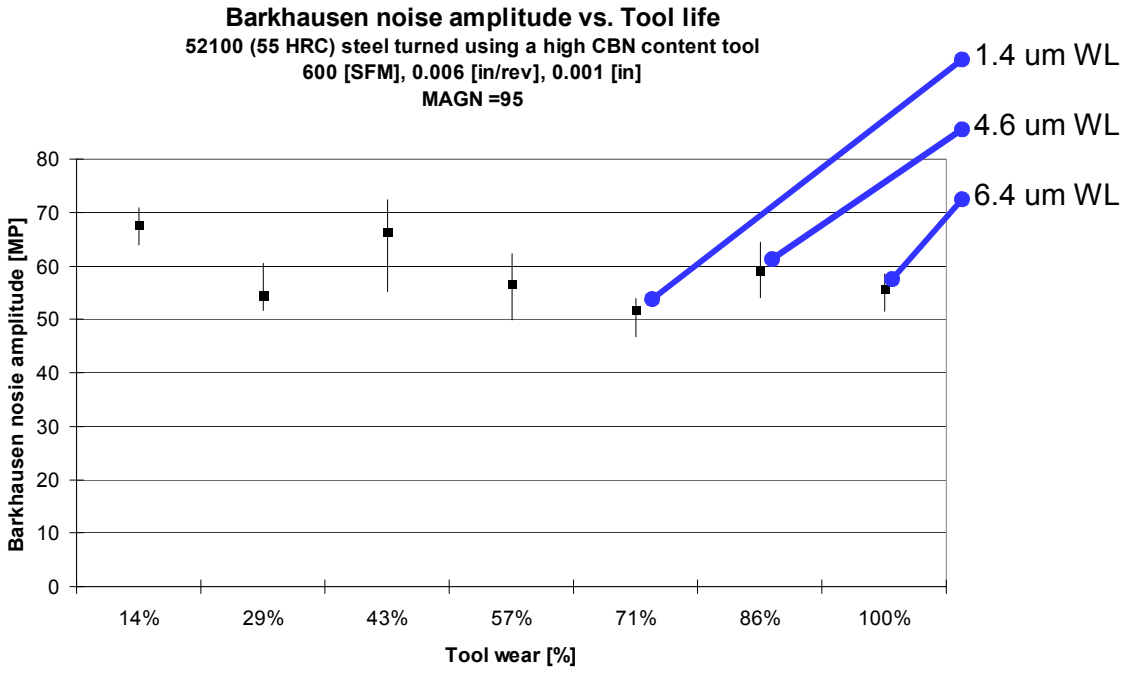

Figure 39: Example results from the Barkhausen sensor.

Electrochemisty Results

The results of the open-circuit potential measurements are summarized in Figure 40. The results show that machined parts with white layer have a different potential than those machined without the defect. Using the Tukey test for multiple comparison and a confidence of 99%, the potential for a sample with white layer is distinct from the potential for a sample without white layer. This suggests a correlation between white

layer and the electrochemical potential of a sample. Note that for the samples with white layer, its thickness on each of the samples ranged from 2.5 to 11.0 μm, with most samples having a white layer that was approximately 7 μm thick.

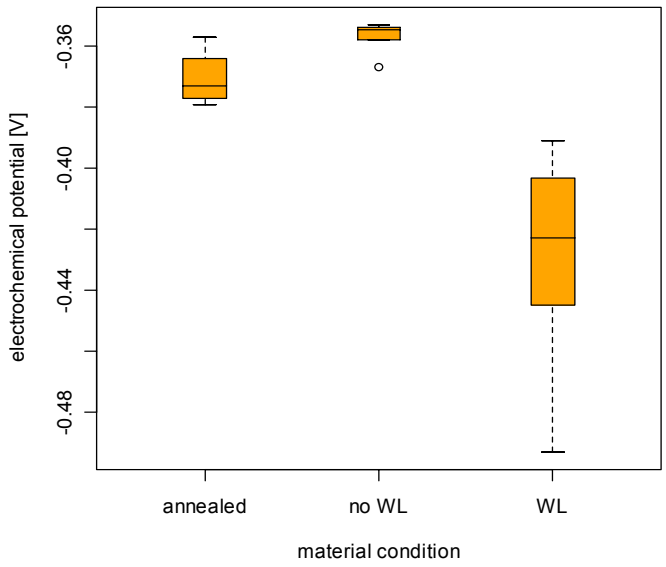

Figure 40: Electrochemical potential of samples

It is important to note that the connection between white layer and the open-circuit potential may be attributable to other factors. For example, the residual stresses in the parts without white layer could be different than the stresses in the parts with white layer. It cannot be said that the white layer is directly affecting the potential. Additional tests with white layers produced with different processes, for example using an EDM'ed surface that has white layer with minimal residual stress effects, might strengthen the relationship between the white layer defect and the open-circuit potential. Before November 23, three parts with an EDM'ed surface will be tested using the EIS technique. If the results from these parts are similar to the results for a turned surface with white layer, then this will indicate that microstructure is the primary factor influencing the impedance.

A statistically significant correlation between the machining speed and the potential was not found. This is interesting because it suggests that the difference in potential may be

independent of the process parameters that created the hard turned surface. It also suggests that the potential is independent of the white layer formation process and the surface texture. The high speed parts probably had white layer because of quenching, while the low speed parts probably had white layer due to severe plastic deformation. The two blocks also had different feed mark patterns; samples machined at high speed/low feed have more narrow feedmarks.

Results from the EIS tests give more insight into the nature of the corrosion process. These results are summarized in Figure 41, which shows the results from each of the plots together on the same Nyquist plot. Based on the model, the shape of the curves should be a semi-circle. The curves basically are the correct shape, but most of them appear flattened. This is a common phenomenon that is not completely understood (Cottis, Turgoose et al., 1999)

The EIS results suggest that a part with white layer corrodes more quickly than a part without the defect. This is apparent from the Nyquist plot, because the impedance of a part with white layer curve is less than the impedance of a part without white layer. Since the impedance (or resistance in steady-state conditions) is lower for parts without white layer, the corrosion current through them less, and therefore they corrode more slowly.

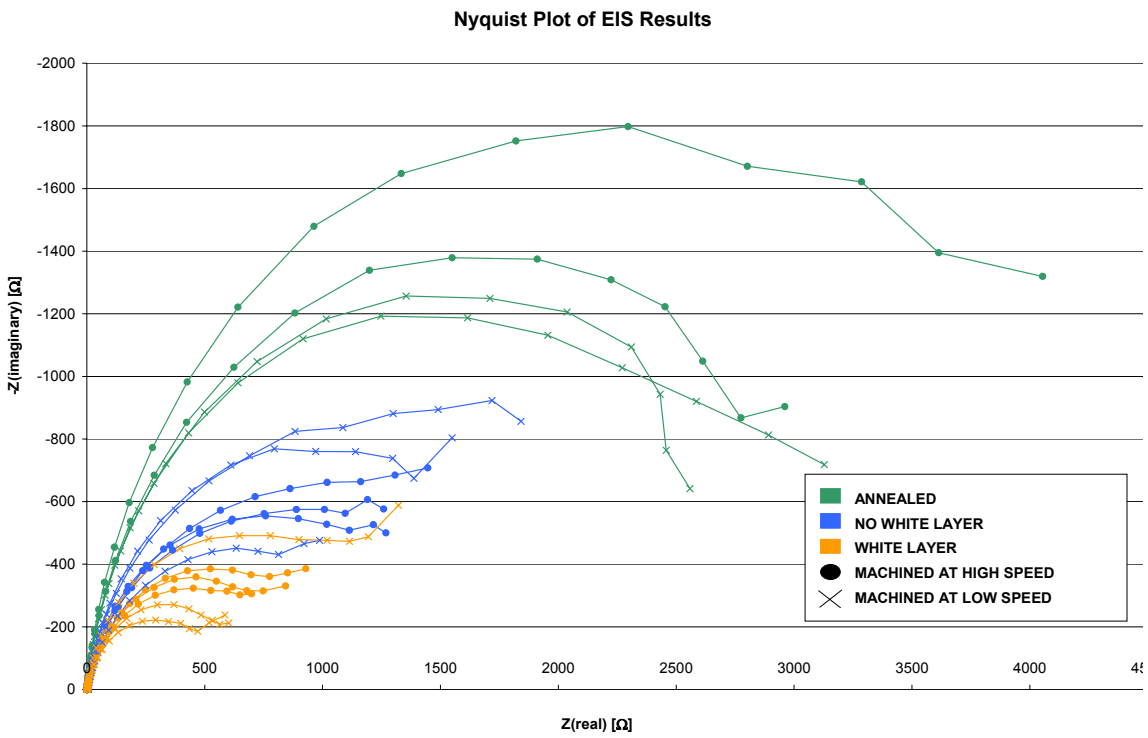

Figure 41: Nyquist plot of EIS results

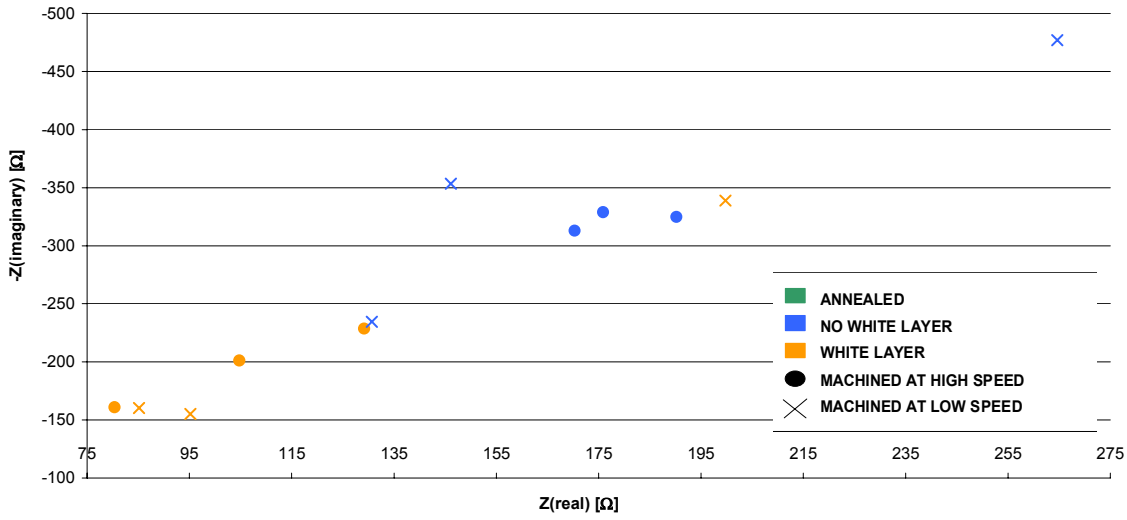

Figure 42: Results of EIS testing at f = 0.1931Hz

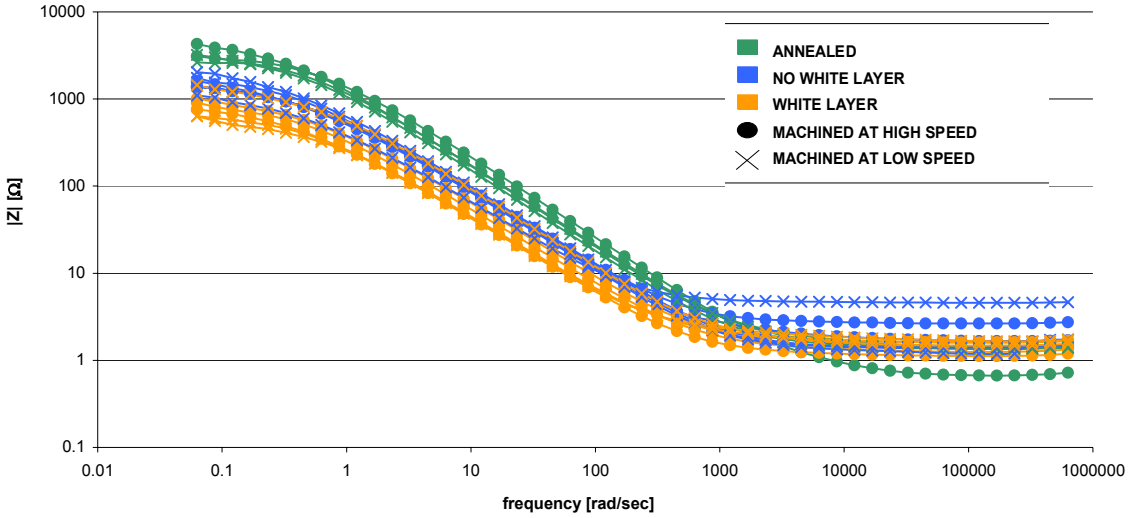

Figure 43: Bode magnitude plot of EIS results

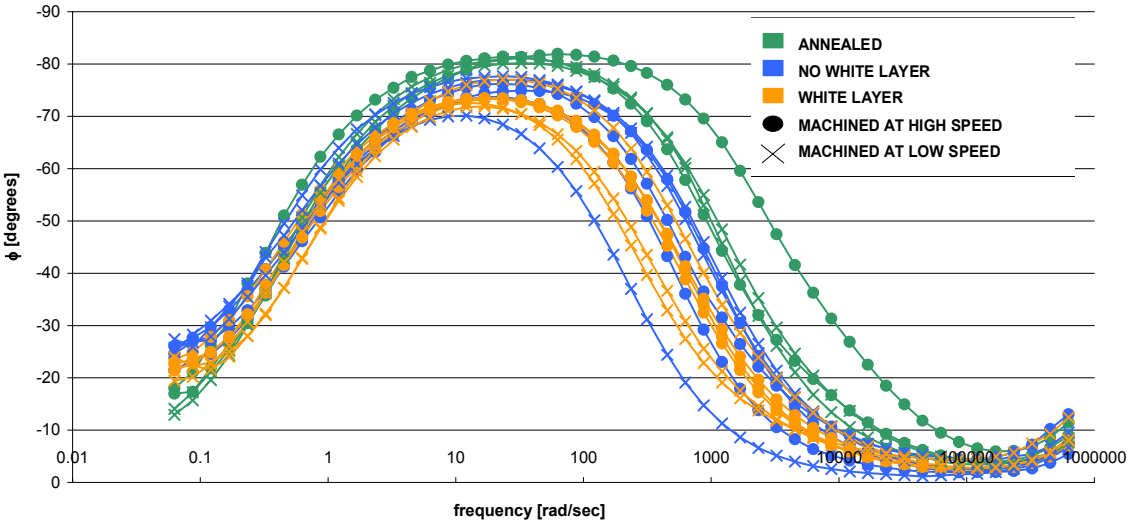

Figure 44: Bode phase plot of EIS results

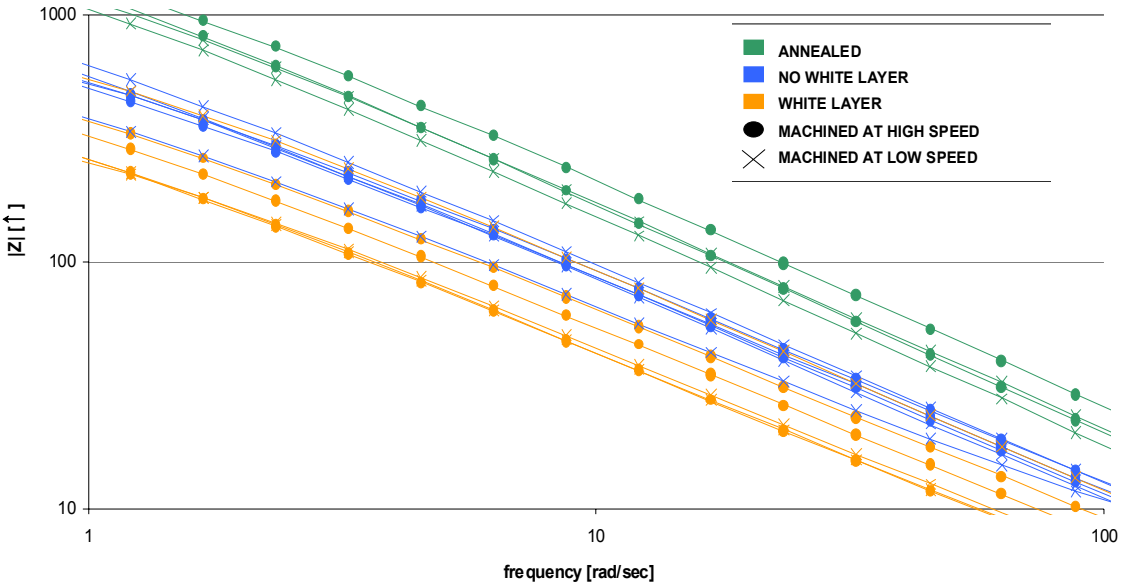

Figure 45: Bode magnitude plot of EIS results, zoomed in

CHAPTER 6

CONCLUSIONS & RECOMMENDATIONS

The primary objective of this study is to determine if either the Barkhausen sensor or the EIS method is effective as a non-destructive method for detecting white layer in hard turned parts. The goal is to recommend a method that could be adopted by industry for identifying parts with the white layer condition.

The experimental results show that output from the Barkhausen sensor is not strongly correlated with the presence of white layer. Although this sensor has been shown to be effective at detecting either residual stress or hardness individually, it is not effective at detecting the material properties of white layer. Even when the parts are made of the same type of steel and machined under the same conditions, there is no clear trend between white layer thickness and BNA.

This most likely occurred because the surface integrity of the parts varies, creating a large variance in the measurements. For example, even when white layer is present, its thickness might vary from 2 μm to 5 μm across the surface. Since white layer is harder than the bulk material, this implies that the hardness profile also varies across the surface. If the sensor is directly over an area of a part with thick white layer, it probably obtains a different reading than when it is over a region with a thin white layer. The residual stress most likely varies in a similar way, and this will be confirmed by upcoming residual stress measurements. The result is that there is a large deviation between measurements taken at different locations on a part. In some cases, this variation might be 10-15% of the mean BNA.

Furthermore, the change in hardness associated with white layer can not be detected because it is coupled with changes in the residual stress. Other studies have shown that the effect of hardness on the Barkhausen sensor is not linear and this makes it more

difficult to decouple the effects of the hardness, as the residual stress probably masks the effect of white layer. Upcoming tests using the x-ray diffractometer should indicate if the Barkhausen measurements can be explained by the residual stress.

Electrochemical impedance spectroscopy shows promising results as a method for detecting white layer. There is a clear difference between the frequency responses of a part with white layer versus one without any. At all frequencies, a sample part with white layer has lower impedance than a part without white layer. (These results are shown in a Nyquist plot in Figure 41.) An annealed part has impedance greater than both of these, which give a good agreement between increasing grain size on the surface and increasing impedance. These results are interesting because there is some debate if white layer is actually less susceptible to chemical attack by nital solutions, or if it appears white after etching because of its nanocrystalline grain structure.

The conclusions from EIS are supported by the open-circuit potential test and the linear polarization test. The open-circuit potential test shows a different potential for a part with white layer (-0.42 V) than one without white layer (-0.36 V). An annealed sample has a potential similar to a part without white layer. LPR tests on a few sample parts confirms corrosion rates for parts with white layer versus parts without any (a quantification of the corrosion rate will be prepared by November 23).

Future tests with the Barkhausen sensor should examine the reasons why the sensor is not able to detect white layer. One consideration should be if the sensor's penetration depth can be reduced so that a greater fraction is affected by white layer. The penetration depth of the sensor in the study is 20 μm, while the white layer ranges from 1-15 μm thick. A reduction in the depth could be accomplished by increasing the sensor frequency. This might explain why the sensor was not effective at detecting white layer in this study, while others have reported that it is effective at detecting grinding burn.

The effect of the residual stress profile on the Barkhausen sensor should also be examined. It is known that residual stress affects the BNA, but the effect of a residual stress profile is less well understood. If the Barkhausen results are not explained by the

surface residual stress measusurements in this study future tests could also examine the residual stress profile.

Although the EIS method is shown to be effective at distinguishing white layer, more needs to be understood before these results can be implemented by industry. Before the EIS method can be applied as a non-destructive test for white layer, it must be determined how the solution affects the part surface during the test. From the experiments in this study, it is possible to distinguish whether a part had white layer by observing its response at only one frequency (Figure 42), and this is a measurement that requires that the part be exposed to the solution for only a few seconds. It is uncertain exactly how much the solution affects the part surface over this time. Future tests might mount and etch a cross-section of a sample part after EIS testing to see if there is noticeable pitting or other damage to the surface. The integrity of the parts after EIS tests should also be verified through mechanical tests, such as fatigue tests.

The corrosion rate for parts with white layer in a 1 M NaOH solution is found to be faster than for parts without white layer. Further testing should be done to determine if other solutions could also be used to obtain a similar result. Perhaps even cutting fluid could be used. Finally, the results for EIS testing should be confirmed by testing more parts, machined other different conditions. The corrosion rate, as estimated by EIS and LPR, should be confirmed using mass loss tests.

APPENDIX A: BARKHAUSEN MEASUREMENT DATA

This Appendix contains the measurements recorded from the Barkhausen sensor along with the measured white layer thickness for each sample. Barkhausen measurements were taken on five different locations on each part, at two different sensor intensities. The plotted data are shown first, with each plot representing a set of sample parts that were machined under the same conditions and measured at a specific sensor intensity. There are two plots for each set of sample parts, one measured at low (MAGN = 35) sensor intensity and the other at high intensity (MAGN = 95). The mean of the five measurements indicated by a dot, and the error bars represent the range. If a part was observed to have white layer, then a line pointing to the data point indicates the white layer thickness. After the plots, each measurement from the Barkhausen sensor and each measurement of the white layer thickness in listed in tabular form.

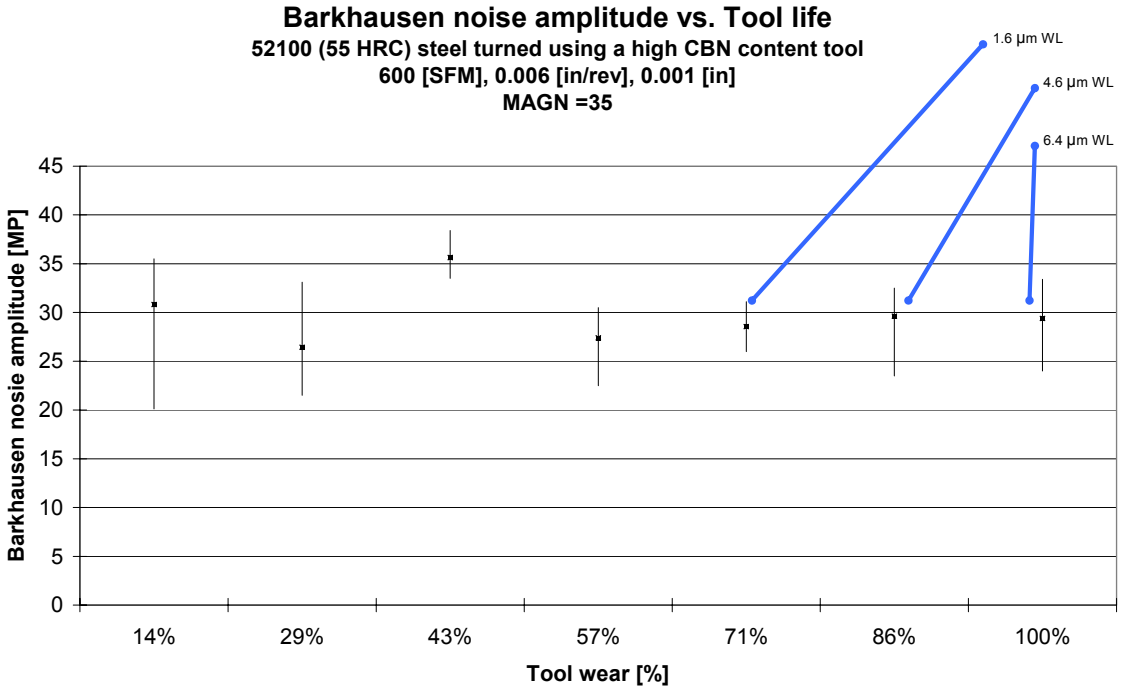
Barkhausen noise amplitude vs. Tool life
52100 (55 HRC) steel turned using a high CBN content tool
600 [SFM], 0.006 [in/rev], 0.001 [in]
MAGN =35
1.6 µm WL
4.6 µm WL
6.4 µm WL
Barkhausen nosie amplitude [MP]
0
5
10
15
20
25
30
35
40
45
14%
29%
43%
57%
71%
86%
100%
Tool wear [%]

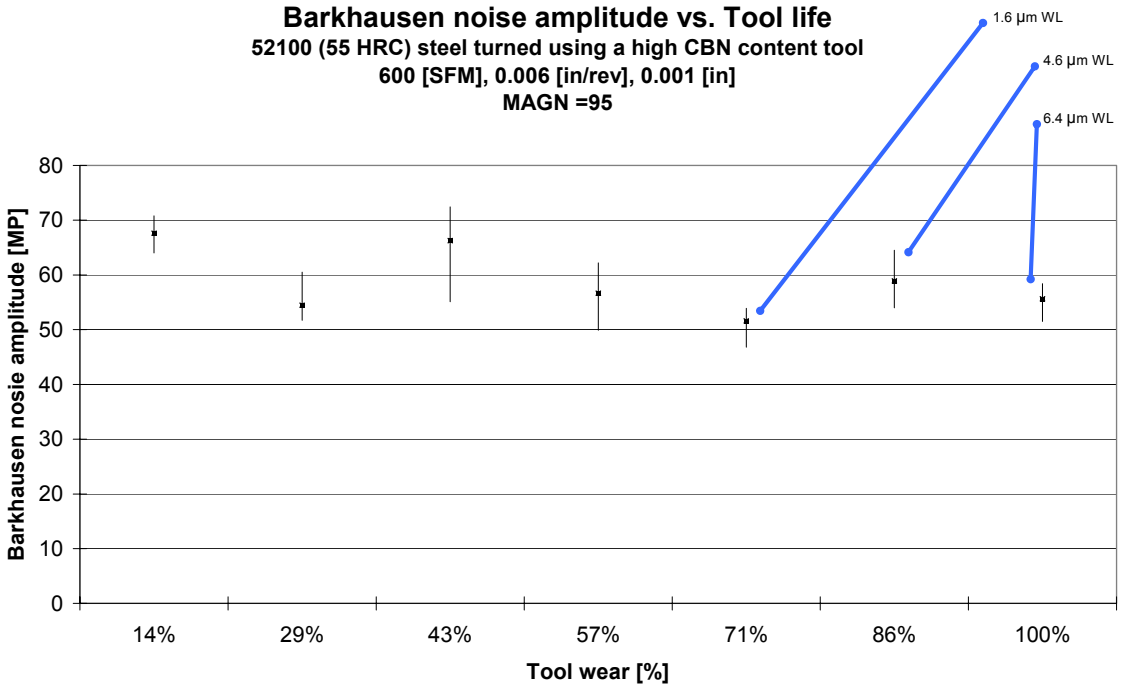
Barkhausen noise amplitude vs. Tool life
52100 (55 HRC) steel turned using a high CBN content tool
600 [SFM], 0.006 [in/rev], 0.001 [in]
MAGN =95
1.6 µm WL
4.6 µm WL
6.4 µm WL
Barkhausen nosie amplitude [MP]
0
10
20
30
40
50
60
70
80
14%
29%
43%
57%
71%
86%
100%
Tool wear [%]

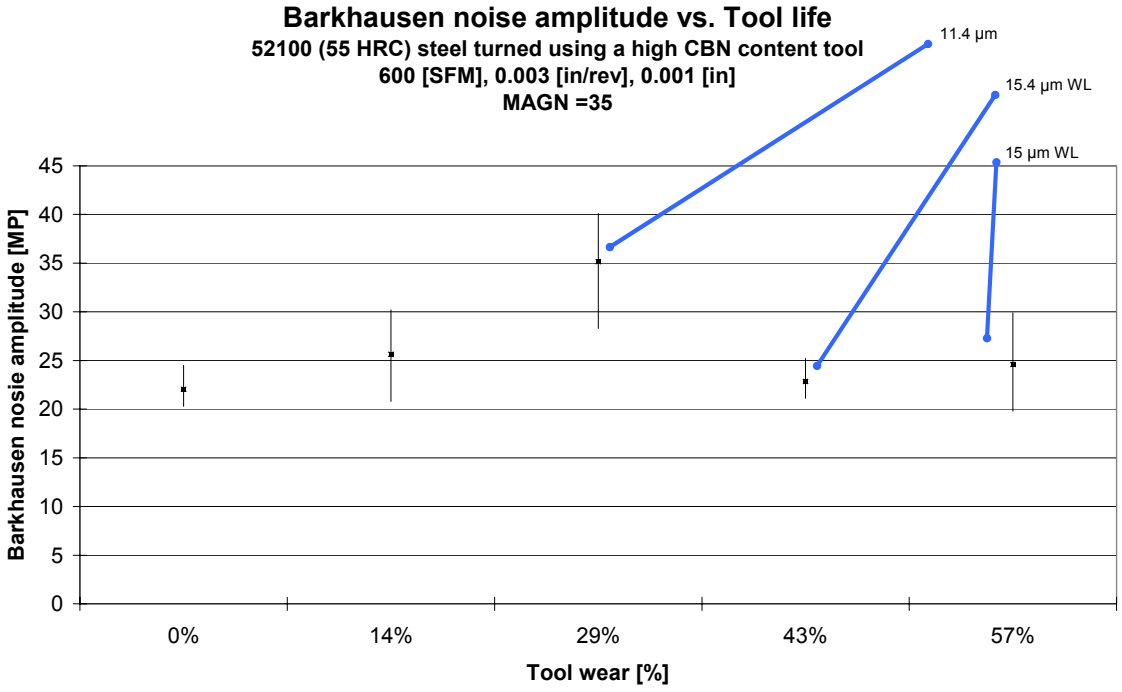
Barkhausen noise amplitude vs. Tool life
52100 (55 HRC) steel turned using a high CBN content tool
600 [SFM], 0.003 [in/rev], 0.001 [in]
MAGN =35
11.4 µm
15.4 µm WL
15 µm WL
Barkhausen nosie amplitude [MP]
45
40
35
30
25
20
15
10
5
0
0%
14%
29%
43%
57%
Tool wear [%]

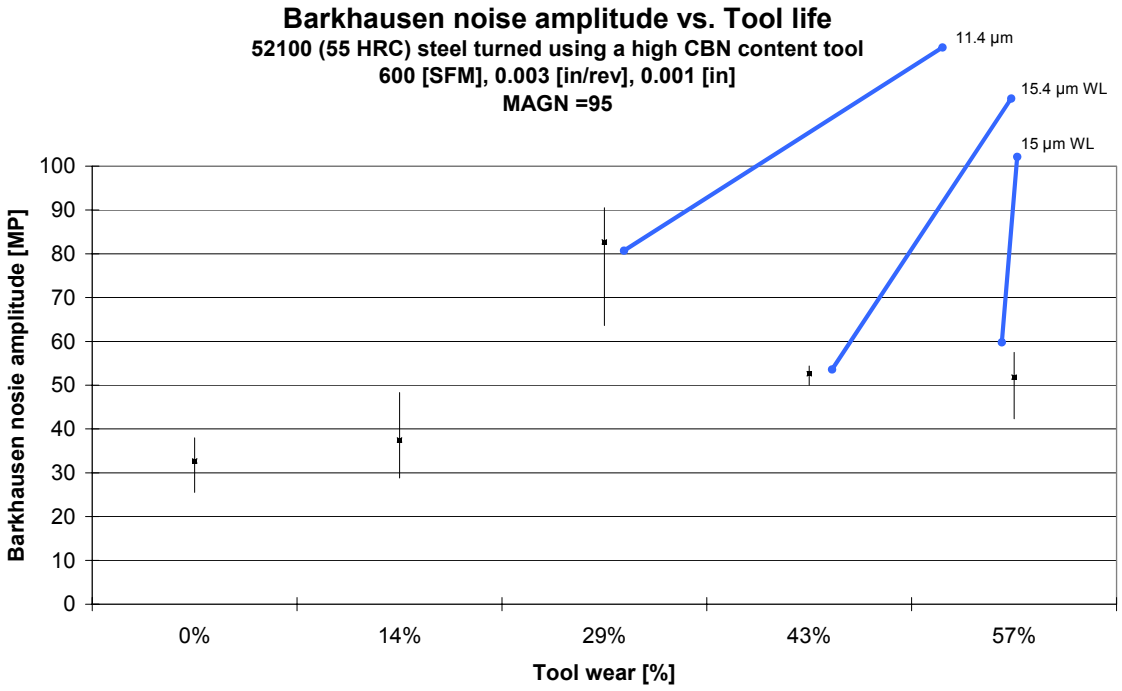
Barkhausen noise amplitude vs. Tool life
52100 (55 HRC) steel turned using a high CBN content tool
600 [SFM], 0.003 [in/rev], 0.001 [in]
MAGN =95
11.4 µm
15.4 µm WL
15 µm WL
Barkhausen nosie amplitude [MP]
100
90
80
70
60
50
40
30
20
10
0
0%
14%
29%
43%
57%
Tool wear [%]

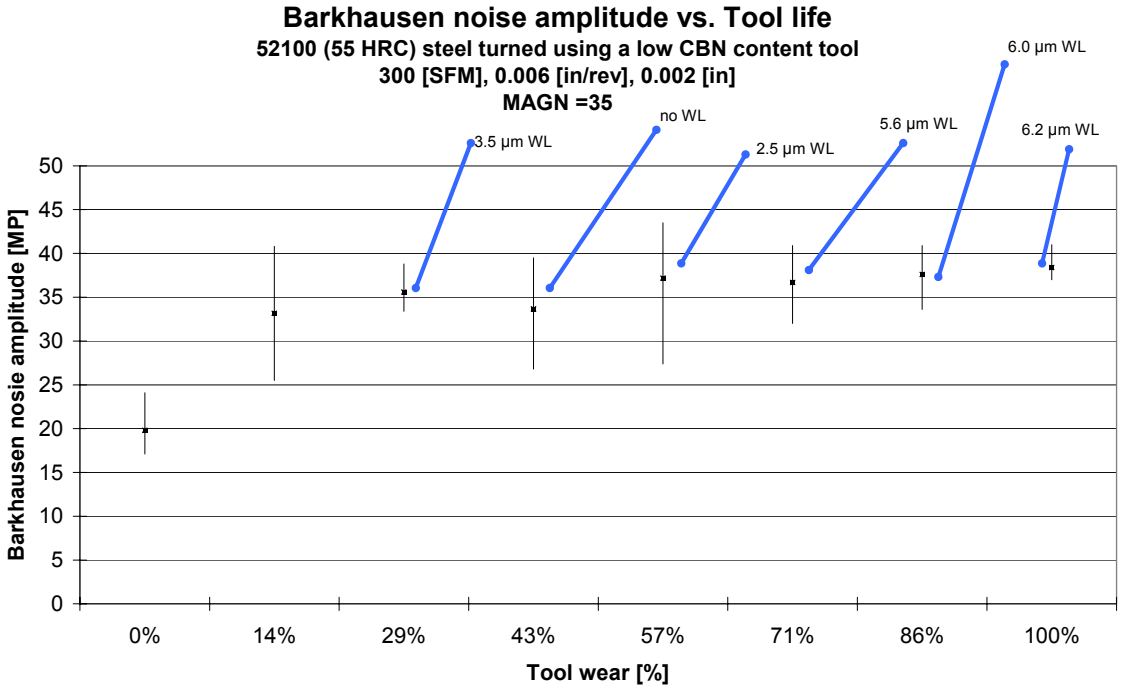
Barkhausen noise amplitude vs. Tool life
52100 (55 HRC) steel turned using a low CBN content tool
300 [SFM], 0.006 [in/rev], 0.002 [in]
MAGN =35
3.5 µm WL
no WL
2.5 µm WL
5.6 µm WL
6.0 µm WL
6.2 µm WL
Barkhausen nosie amplitude [MP]
0
5
10
15
20
25
30
35
40
45
50
0%
14%
29%
43%
57%
71%
86%
100%
Tool wear [%]

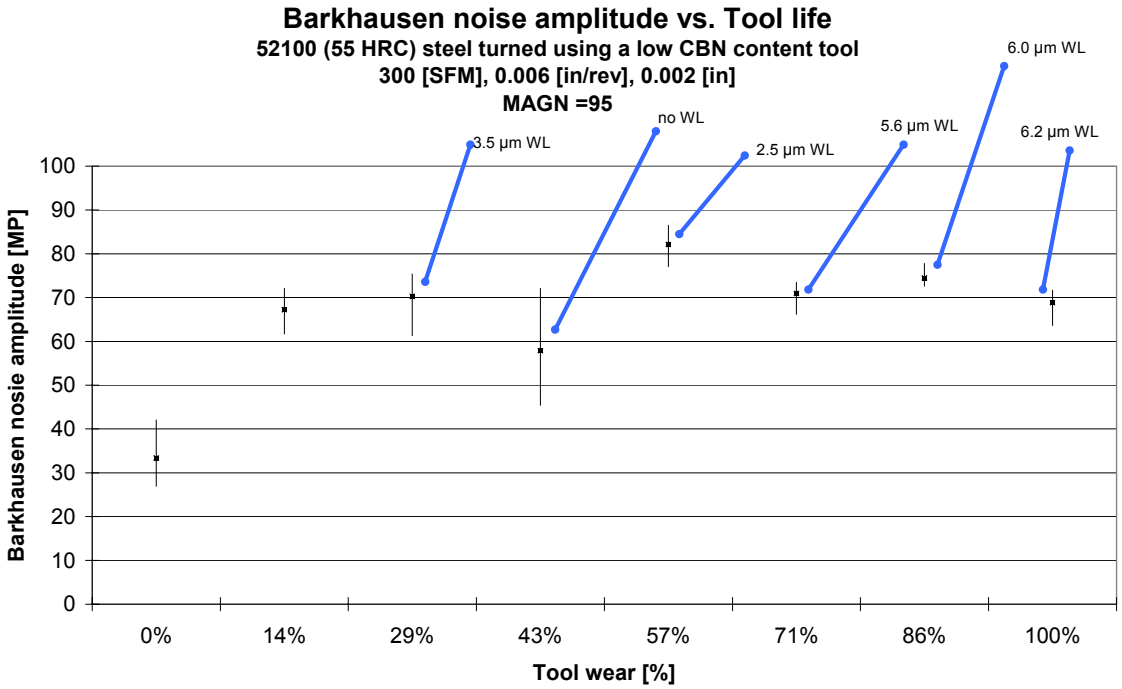
Barkhausen noise amplitude vs. Tool life
52100 (55 HRC) steel turned using a low CBN content tool
300 [SFM], 0.006 [in/rev], 0.002 [in]
MAGN =95
3.5 µm WL
no WL
2.5 µm WL
5.6 µm WL
6.0 µm WL
6.2 µm WL
Barkhausen nosie amplitude [MP]
0
10
20
30
40
50
60
70
80
90
100
0%
14%
29%
43%
57%
71%
86%
100%
Tool wear [%]

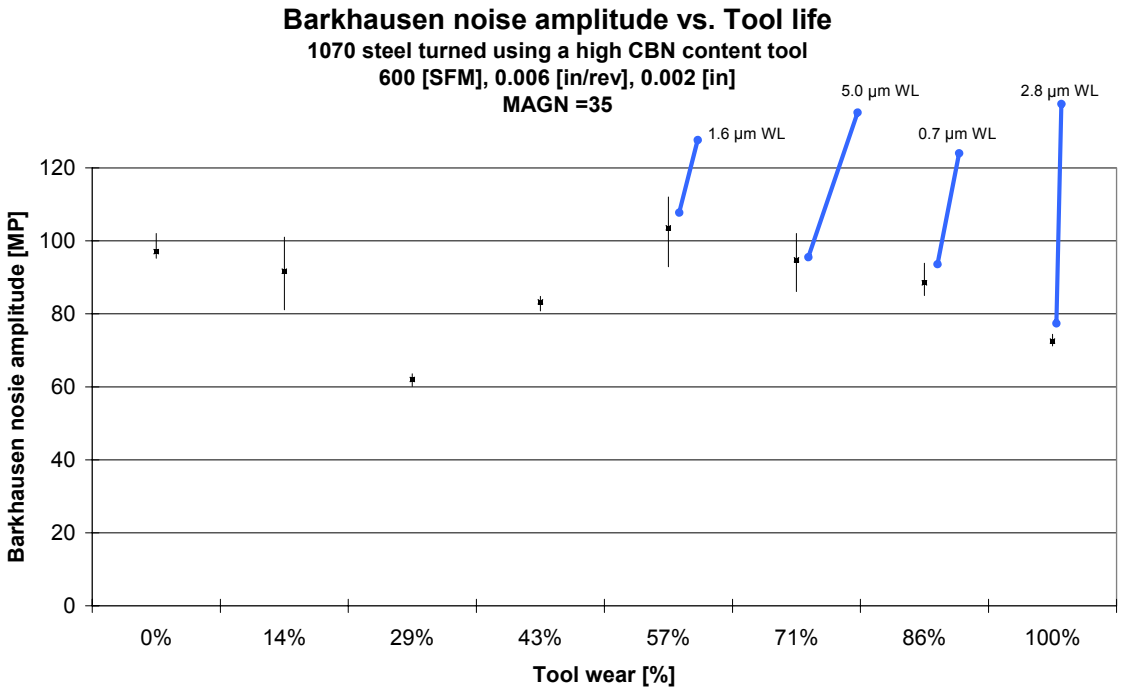
Barkhausen noise amplitude vs. Tool life
1070 steel turned using a high CBN content tool
600 [SFM], 0.006 [in/rev], 0.002 [in]
MAGN =35
1.6 µm WL
5.0 µm WL
0.7 µm WL
2.8 µm WL
Barkhausen nosie amplitude [MP]
120
100
80
60
40
20
0
0%
14%
29%
43%
57%
71%
86%
100%
Tool wear [%]

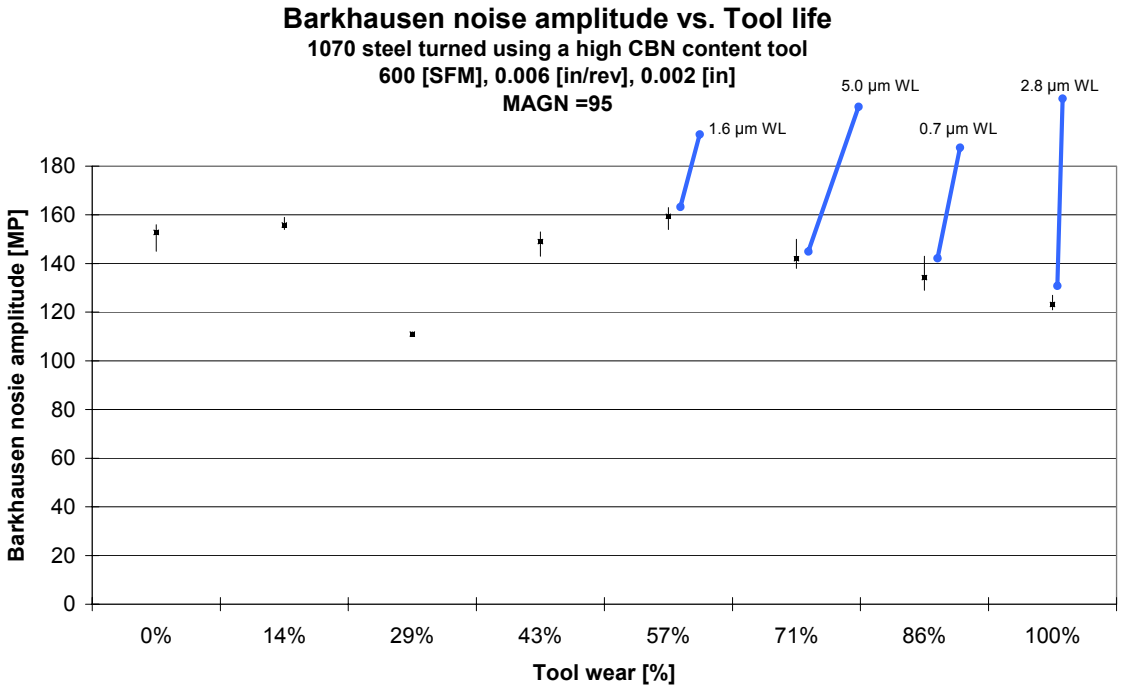
Barkhausen noise amplitude vs. Tool life
1070 steel turned using a high CBN content tool
600 [SFM], 0.006 [in/rev], 0.002 [in]
MAGN =95
1.6 µm WL
5.0 µm WL
0.7 µm WL
2.8 µm WL
Barkhausen nosie amplitude [MP]
180
160
140
120
100
80
60
40
20
0
0%
14%
29%
43%
57%
71%
86%
100%
Tool wear [%]

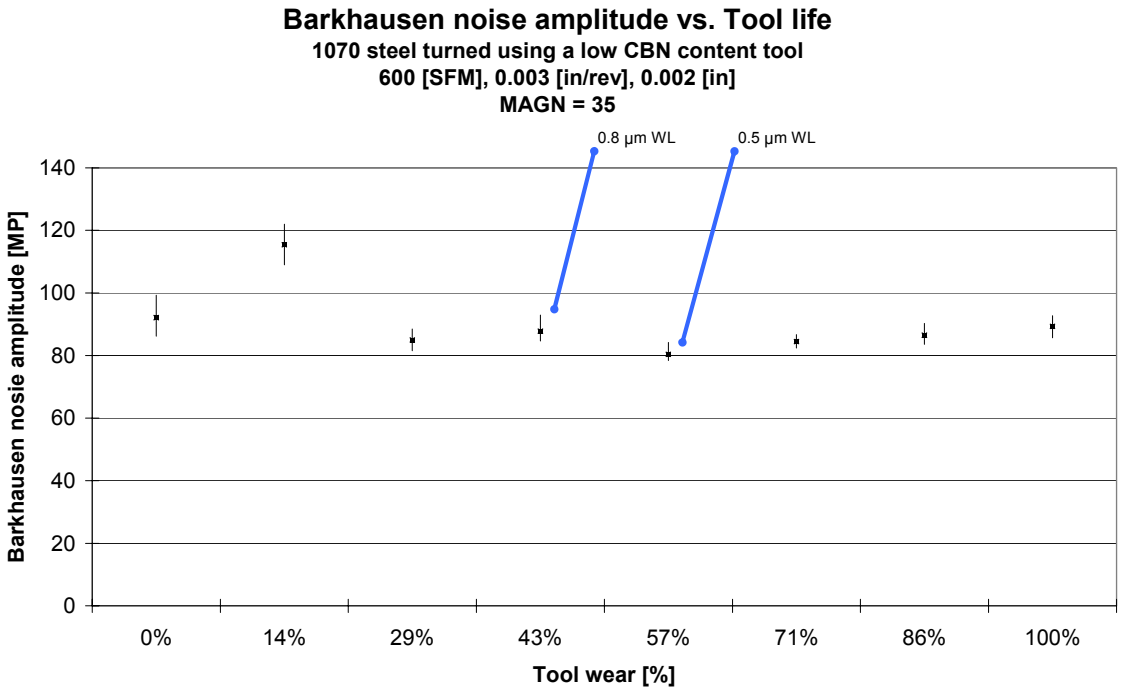
Barkhausen noise amplitude vs. Tool life
1070 steel turned using a low CBN content tool
600 [SFM], 0.003 [in/rev], 0.002 [in]
MAGN = 35
0.8 µm WL
0.5 µm WL
Barkhausen nosie amplitude [MP]
140
120
100
80
60
40
20
0
0%
14%
29%
43%
57%
71%
86%
100%
Tool wear [%]

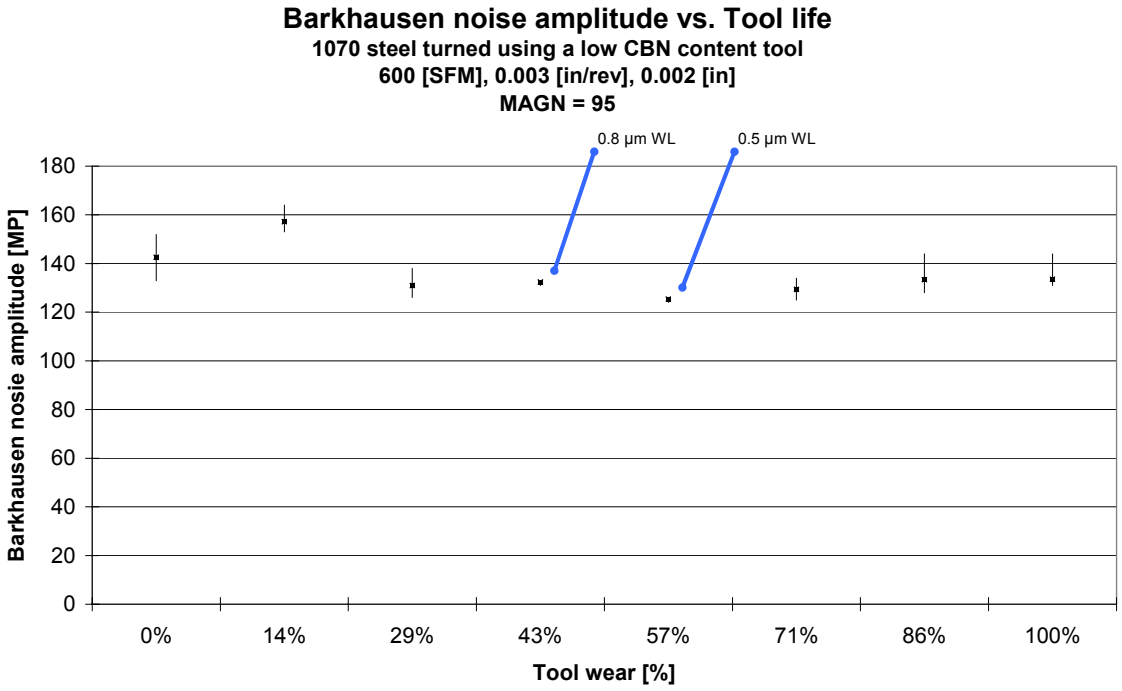
Barkhausen noise amplitude vs. Tool life
1070 steel turned using a low CBN content tool
600 [SFM], 0.003 [in/rev], 0.002 [in]
MAGN = 95
0.8 µm WL
0.5 µm WL
Barkhausen nosie amplitude [MP]
180
160
140
120
100
80
60
40
20
0
0%
14%
29%
43%
57%
71%
86%
100%
Tool wear [%]

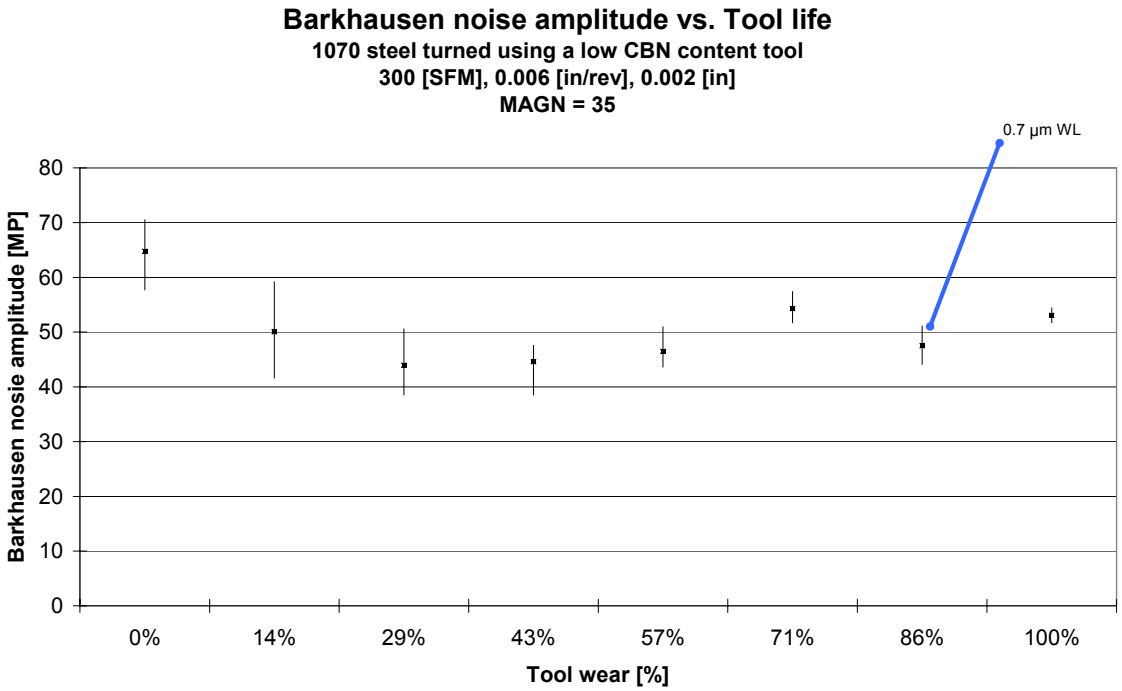
Barkhausen noise amplitude vs. Tool life
1070 steel turned using a low CBN content tool
300 [SFM], 0.006 [in/rev], 0.002 [in]
MAGN = 35
0.7 µm WL
Barkhausen nosie amplitude [MP]
0
10
20
30
40
50
60
70
80
0%
14%
29%
43%
57%
71%
86%
100%
Tool wear [%]

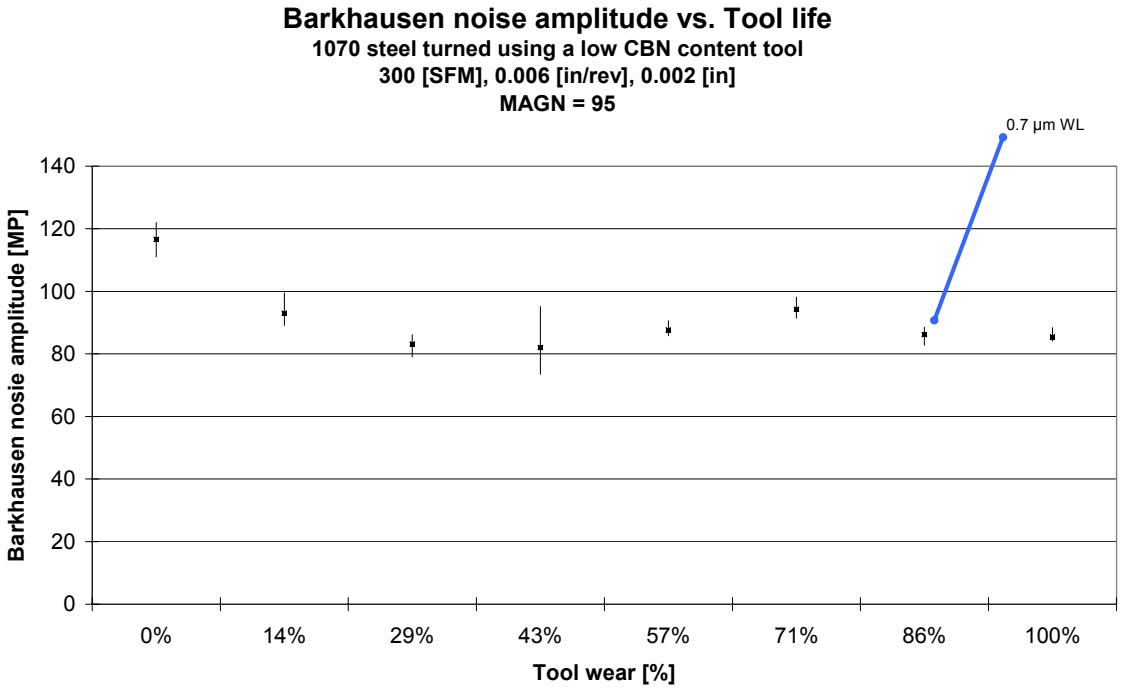
Barkhausen noise amplitude vs. Tool life
1070 steel turned using a low CBN content tool
300 [SFM], 0.006 [in/rev], 0.002 [in]
MAGN = 95
0.7 µm WL
Barkhausen nosie amplitude [MP]
0
20
40
60
80
100
120
140
0%
14%
29%
43%
57%
71%
86%
100%
Tool wear [%]

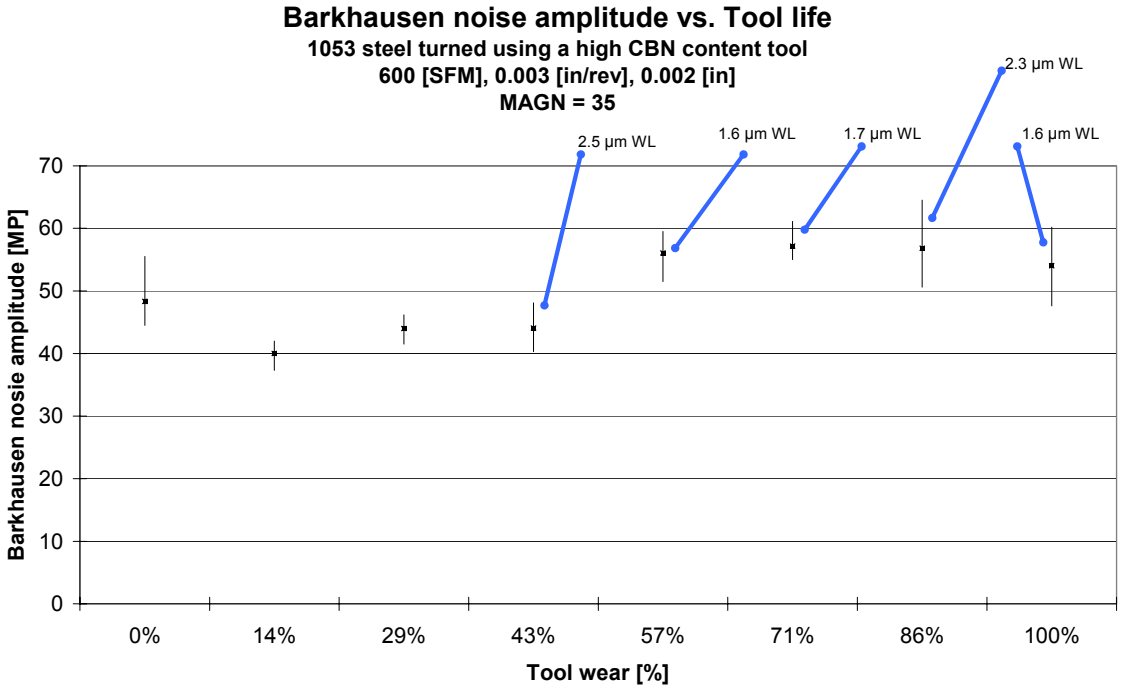
Barkhausen noise amplitude vs. Tool life
1053 steel turned using a high CBN content tool
600 [SFM], 0.003 [in/rev], 0.002 [in]
MAGN = 35
2.5 µm WL
1.6 µm WL
1.7 µm WL
2.3 µm WL
1.6 µm WL
Barkhausen nosie amplitude [MP]
70
60
50
40
30
20
10
0
0%
14%
29%
43%
57%
71%
86%
100%
Tool wear [%]

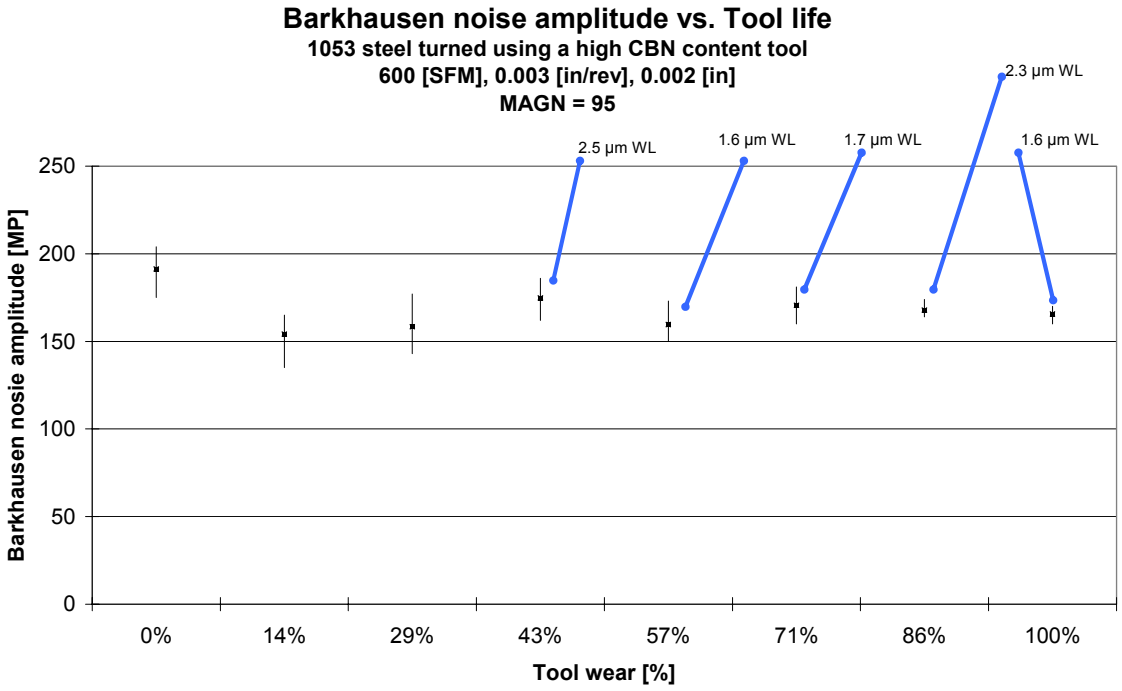
Barkhausen noise amplitude vs. Tool life
1053 steel turned using a high CBN content tool
600 [SFM], 0.003 [in/rev], 0.002 [in]
MAGN = 95
2.5 µm WL
1.6 µm WL
1.7 µm WL
2.3 µm WL
1.6 µm WL
Barkhausen nosie amplitude [MP]
250
200
150
100
50
0
0%
14%
29%
43%
57%
71%
86%
100%
Tool wear [%]

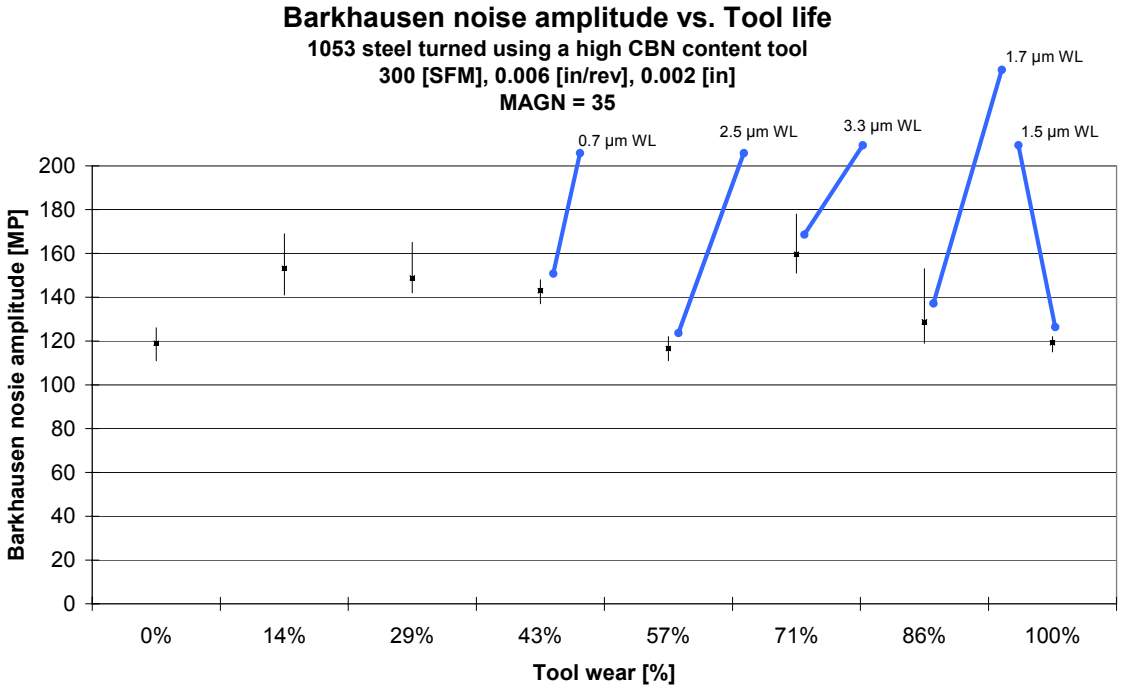
Barkhausen noise amplitude vs. Tool life
1053 steel turned using a high CBN content tool
300 [SFM], 0.006 [in/rev], 0.002 [in]
MAGN = 35
0.7 µm WL
2.5 µm WL
3.3 µm WL
1.7 µm WL
1.5 µm WL
Barkhausen nosie amplitude [MP]
200
180
160
140
120
100
80
60
40
20
0
0%
14%
29%
43%
57%
71%
86%
100%
Tool wear [%]

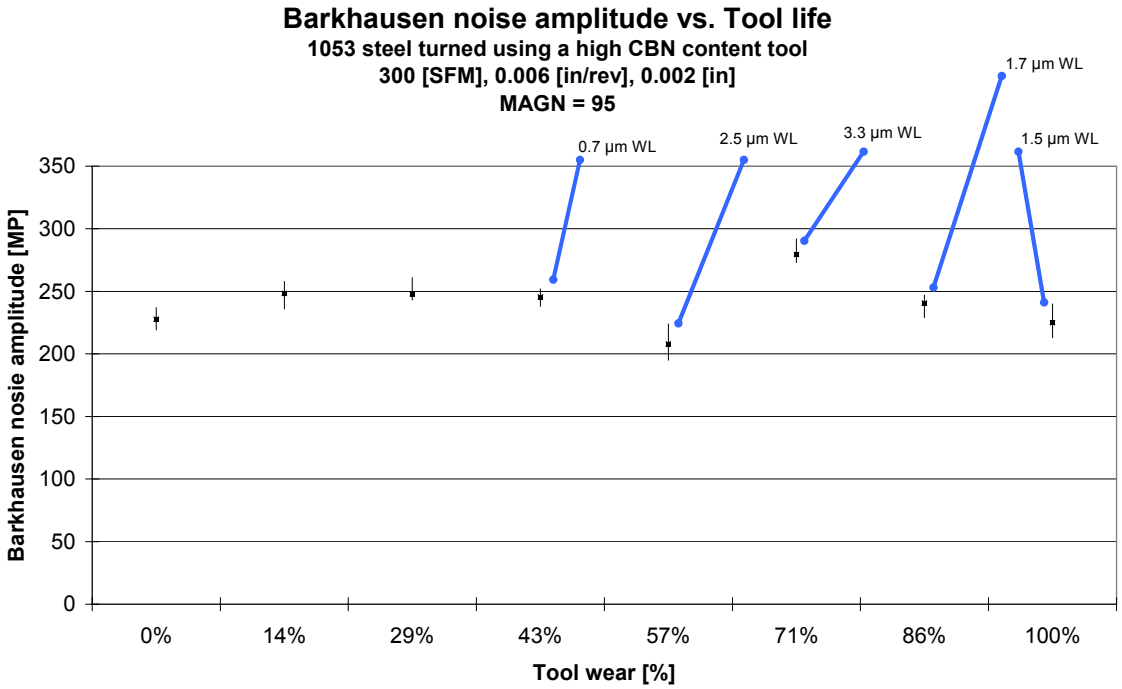
Barkhausen noise amplitude vs. Tool life
1053 steel turned using a high CBN content tool
300 [SFM], 0.006 [in/rev], 0.002 [in]
MAGN = 95
0.7 µm WL
2.5 µm WL
3.3 µm WL
1.7 µm WL
1.5 µm WL
Barkhausen nosie amplitude [MP]
350
300
250
200
150
100
50
0
0%
14%
29%
43%
57%
71%
86%
100%
Tool wear [%]

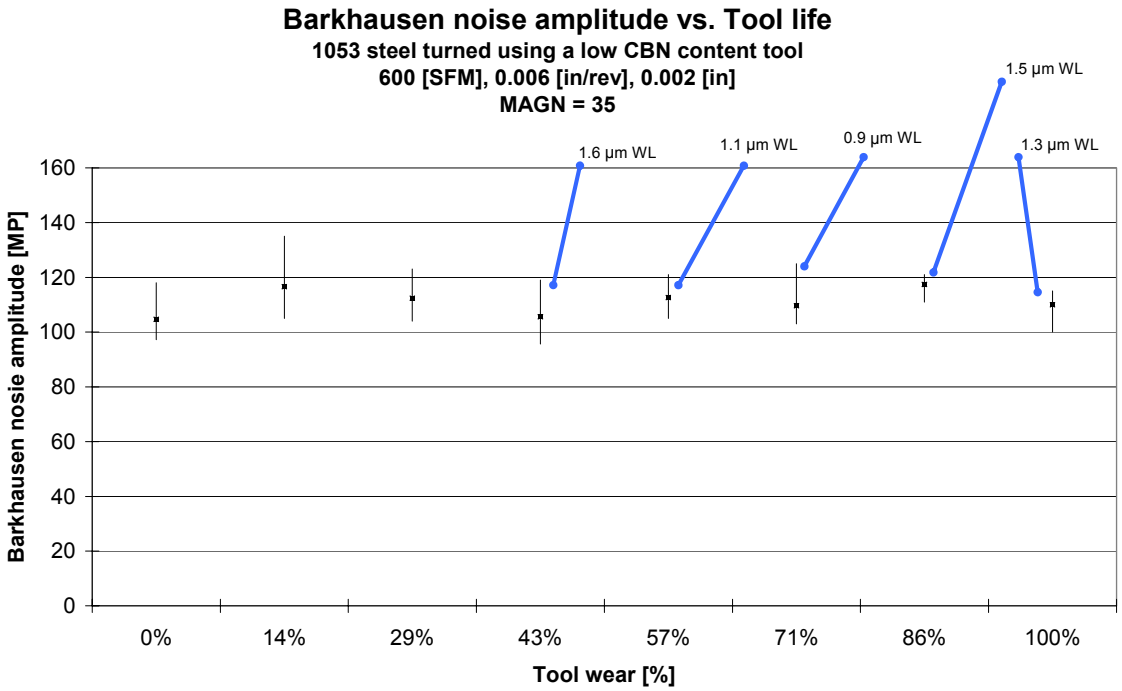
Barkhausen noise amplitude vs. Tool life
1053 steel turned using a low CBN content tool
600 [SFM], 0.006 [in/rev], 0.002 [in]
MAGN = 35
1.6 µm WL
1.1 µm WL
0.9 µm WL
1.5 µm WL
1.3 µm WL
Barkhausen nosie amplitude [MP]
160
140
120
100
80
60
40
20
0
0%
14%
29%
43%
57%
71%
86%
100%
Tool wear [%]

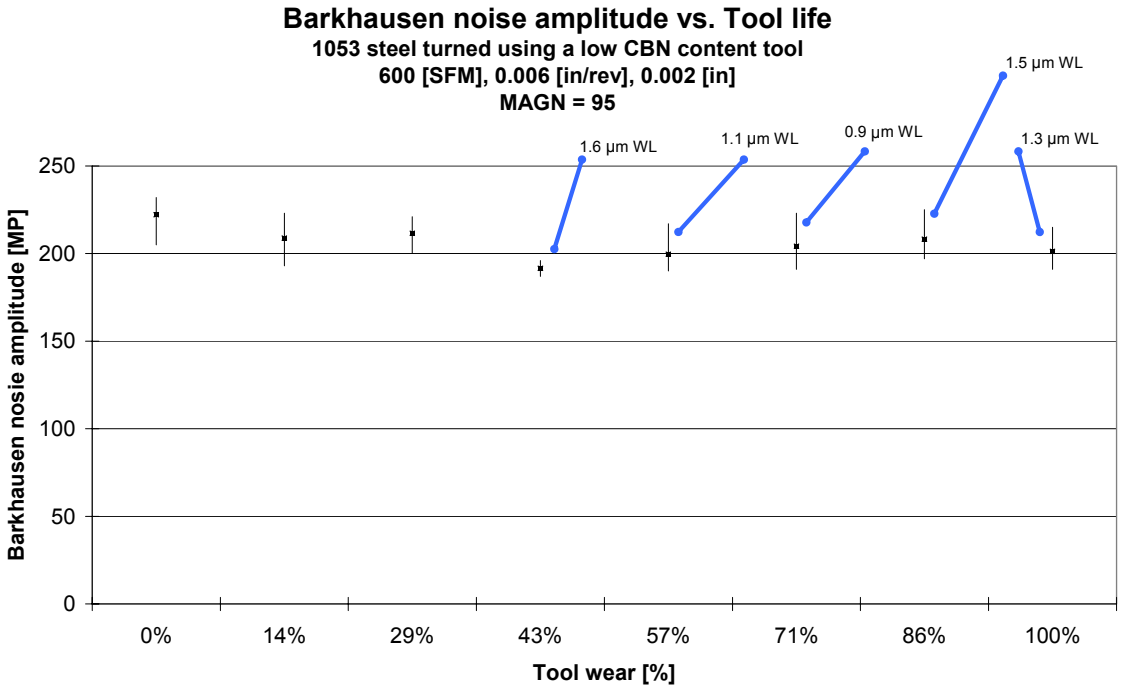
Barkhausen noise amplitude vs. Tool life
1053 steel turned using a low CBN content tool
600 [SFM], 0.006 [in/rev], 0.002 [in]
MAGN = 95
1.6 µm WL
1.1 µm WL
0.9 µm WL
1.5 µm WL
1.3 µm WL
Barkhausen nosie amplitude [MP]
250
200
150
100
50
0
0%
14%
29%
43%
57%
71%
86%
100%
Tool wear [%]

Barkhausen test measurements:

s600_f006_d001_kd120		14%	29%	43%	57%	71%	86%	100%
MAGN=35	Measurement 1	35.5	26.1	35.1	30.3	30.5	29.7	28.7
	Measurement 2	34	33.1	35.2	28	26	30.3	29.8
	Measurement 3	20.1	21.5	33.5	22.5	28	23.5	24
	Measurement 4	29.6	24.1	36	25.7	31.1	32.5	31
	Measurement 5	34.9	27.4	38.4	30.5	27.2	32.1	33.4
	High	35.5	33.1	38.4	30.5	31.1	32.5	33.4
	Low	20.1	21.5	33.5	22.5	26	23.5	24
	Avg	30.82	26.44	35.64	27.4	28.56	29.62	29.38
	Std	6.42	4.34	1.79	3.36	2.18	3.62	3.48
		14%	29%	43%	57%	71%	86%	100%
MAGN=95	Measurement 1	65.4	60.5	68	62.2	52.7	57.1	58.4
	Measurement 2	70.8	54.7	72.4	59.1	46.8	54	56.5
	Measurement 3	70.6	52.7	70.4	49.9	52.5	64.5	51.5
	Measurement 4	64	51.7	65.4	54.3	52.1	62.7	57.7
	Measurement 5	67.2	52.8	55.1	57.8	53.9	56.3	54.1
	High	70.8	60.5	72.4	62.2	53.9	64.5	58.4
	Low	64	51.7	55.1	49.9	46.8	54	51.5
	Avg	67.6	54.48	66.26	56.66	51.6	58.92	55.64
	Std	3.05	3.54	6.77	4.72	2.77	4.47	2.83

s600_f003_d001_kd120		0%	14%	29%	43%	57%
MAGN=35	Measurement 1	20.6	22.7	28.3	22.6	24.1
	Measurement 2	20.5	20.8	34.1	25.2	29.9
	Measurement 3	24.3	26.4	33.7	23.4	19.8
	Measurement 4	24.5	30.2	40.1	21.1	26
	Measurement 5	20.3	28.1	39.6	21.9	23.1
	High	24.5	30.2	40.1	25.2	29.9
	Low	20.3	20.8	28.3	21.1	19.8
	Avg	22.04	25.64	35.16	22.84	24.58
	Std	2.16	3.86	4.86	1.57	3.73
		0%	14%	29%	43%	57%
MAGN=95	Measurement 1	38	39.1	63.6	53.8	53.8
	Measurement 2	25.5	37.7	80.5	52.6	42.3
	Measurement 3	36	28.8	90.5	52.3	56.7
	Measurement 4	30.2	48.3	90.5	50	57.5
	Measurement 5	33.8	33.5	88.4	54.4	48.8
	High	38	48.3	90.5	54.4	57.5
	Low	25.5	28.8	63.6	50	42.3
	Avg	32.7	37.48	82.7	52.62	51.82
	Std	4.96	7.26	11.44	1.70	6.32

s300_f006_d002_kd050		0%	14%	29%	43%	57%	71%	86%	100%
MAGN=35	Measurement 1	17.1	40.8	33.5	33.1	27.4	40.9	37.6	38.2
	Measurement 2	18.8	37.1	33.6	39.5	38.3	37.8	36.2	41
	Measurement 3	20.6	25.5	33.4	26.8	42	32	33.6	37.4
	Measurement 4	18.5	25.9	38.8	34.3	43.5	36.4	39.7	37
	Measurement 5	24.1	36.5	38.7	34.6	34.7	36.3	40.9	38.3
	High	24.1	40.8	38.8	39.5	43.5	40.9	40.9	41
	Low	17.1	25.5	33.4	26.8	27.4	32	33.6	37
	Avg	19.82	33.16	35.6	33.66	37.18	36.68	37.6	38.38
	Std	2.70	7.01	2.88	4.55	6.45	3.21	2.88	1.56
		0%	14%	29%	43%	57%	71%	86%	100%
MAGN=95	Measurement 1	26.9	61.7	61.3	72.1	86.5	71	72.6	63.6
	Measurement 2	42.1	72.1	75.4	62.2	77.1	71.7	75.5	68.4
	Measurement 3	33.6	65.7	73.4	45.4	82.6	66.2	72.8	71.7
	Measurement 4	32.8	69.8	70.8	45.5	81	72.4	73.8	70.4
	Measurement 5	31.5	66.8	70.5	64.2	83.5	73.5	77.8	70
	High	42.1	72.1	75.4	72.1	86.5	73.5	77.8	71.7
	Low	26.9	61.7	61.3	45.4	77.1	66.2	72.6	63.6
	Avg	33.38	67.22	70.28	57.88	82.14	70.96	74.5	68.82
	Std	5.52	3.98	5.41	11.94	3.46	2.82	2.17	3.15

s600_f006_d002_kd120_1070		0%	14%	29%	43%	57%	71%	86%	100%
MAGN=35	Measurement 1	95.5	101	63.6	82.3	92.9	99.2	87.2	72
	Measurement 2	97	96.3	61.3	84.8	104	89.9	86.2	73
	Measurement 3	102	93.4	62.8	83.7	112	86.1	93.9	71.2
	Measurement 4	95.5	81.1	60.1	84.8	103	96.7	85	74.4
	Measurement 5	95.2	86.6	62.2	80.8	106	102	90.3	72
	High	102	101	63.6	84.8	112	102	93.9	74.4
	Low	95.2	81.1	60.1	80.8	92.9	86.1	85	71.2
	Avg	97.04	91.68	62	83.28	103.58	94.78	88.52	72.52
	Std	2.86	7.89	1.35	1.73	6.92	6.61	3.59	1.23
		0%	14%	29%	43%	57%	71%	86%	100%
MAGN=95	Measurement 1	156	154	110	143	159	138	132	121
	Measurement 2	154	154	110	150	160	139	129	124
	Measurement 3	145	155	112	149	163	141	143	122
	Measurement 4	153	159	111	150	154	142	131	122
	Measurement 5	156	157	112	153	161	150	136	127
	High	156	159	112	153	163	150	143	127
	Low	145	154	110	143	154	138	129	121
	Avg	152.8	155.8	111	149	159.4	142	134.2	123.2
	Std	4.55	2.17	1.00	3.67	3.36	4.74	5.54	2.39

s600_f003_d002_kd050_1070		0%	14%	29%	43%	57%	71%	86%	100%
MAGN=35	Measurement 1	86.2	122	84.6	91.4	79.2	83.4	90.3	92.7
	Measurement 2	92.9	113	81.5	85.2	78.6	84.1	84.9	90.2
	Measurement 3	92.2	111	87.4	84.7	84.2	85.7	86.9	85.7
	Measurement 4	99.3	122	88.5	84.7	78.4	82.4	86.7	87.4
	Measurement 5	90.1	109	82.9	92.9	81.6	86.7	83.6	90.6
	High	99.3	122	88.5	92.9	84.2	86.7	90.3	92.7
	Low	86.2	109	81.5	84.7	78.4	82.4	83.6	85.7
	Avg	92.14	115.4	84.98	87.78	80.4	84.46	86.48	89.32
	Std	4.78	6.19	2.95	4.03	2.48	1.74	2.53	2.77
		0%	14%	29%	43%	57%	71%	86%	100%
MAGN=95	Measurement 1	142	157	128	133	124	131	144	131
	Measurement 2	150	164	133	132	126	134	129	131
	Measurement 3	152	156	138	133	126	130	130	131
	Measurement 4	136	156	126	131	125	125	136	131
	Measurement 5	133	153	130	133	126	127	128	144
	High	152	164	138	133	126	134	144	144
	Low	133	153	126	131	124	125	128	131
	Avg	142.6	157.2	131	132.4	125.4	129.4	133.4	133.6
	Std	8.35	4.09	4.69	0.89	0.89	3.51	6.69	5.81

s300_f006_d002_kd050_1070		0%	14%	29%	43%	57%	71%	86%	100%
MAGN=35	Measurement 1	63.4	59.2	44.8	44.2	45.5	57.4	51.1	53.9
	Measurement 2	57.7	51	50.6	47.6	46.5	57.3	46.7	52.1
	Measurement 3	65.9	50.5	41.3	38.5	45.9	52.3	49	54.4
	Measurement 4	66.3	48	38.5	46.1	43.6	52.8	46.7	53.3
	Measurement 5	70.5	41.6	44.6	46.6	51	51.7	44.1	51.7
	High	70.5	59.2	50.6	47.6	51	57.4	51.1	54.4
	Low	57.7	41.6	38.5	38.5	43.6	51.7	44.1	51.7
	Avg	64.76	50.06	43.96	44.6	46.5	54.3	47.52	53.08
	Std	4.70	6.33	4.53	3.63	2.74	2.81	2.65	1.15
		0%	14%	29%	43%	57%	71%	86%	100%
MAGN=95	Measurement 1	111	95.1	85.8	95.1	90.6	98.1	84.2	84.3
	Measurement 2	114	99.5	79	85.1	85.8	93.3	87	84.1
	Measurement 3	122	89.1	85.5	73.5	86.9	94.1	88.6	86.2
	Measurement 4	118	89.1	86.2	76.1	87.5	91.4	88	88.4
	Measurement 5	118	92.4	79.5	80.5	87.7	94.5	82.8	84.5
	High	122	99.5	86.2	95.1	90.6	98.1	88.6	88.4
	Low	111	89.1	79	73.5	85.8	91.4	82.8	84.1
	Avg	116.6	93.04	83.2	82.06	87.7	94.28	86.12	85.5
	Std	4.22	4.40	3.62	8.52	1.78	2.45	2.51	1.82

s600_f003_d002_kd120_1053		0%	14%	29%	43%	57%	71%	86%	100%
MAGN=35	Measurement 1	45.7	42	46.2	43.5	59.5	57	54.9	52.9
	Measurement 2	44.5	37.3	42.5	44	57.5	55	64.5	58
	Measurement 3	45.5	39.9	41.5	44.5	55.9	61.1	50.6	51.5
	Measurement 4	50.5	39.8	43.6	40.3	51.5	57.2	52.9	60.2
	Measurement 5	55.5	41.1	46.2	48.1	56	55.5	61.2	47.6
	High	55.5	42	46.2	48.1	59.5	61.1	64.5	60.2
	Low	44.5	37.3	41.5	40.3	51.5	55	50.6	47.6
	Avg	48.34	40.02	44	44.08	56.08	57.16	56.82	54.04
	Std	4.63	1.77	2.14	2.78	2.95	2.40	5.83	5.07
		0%	14%	29%	43%	57%	71%	86%	100%
MAGN=95	Measurement 1	200	156	177	186	173	181	164	165
	Measurement 2	204	165	143	186	150	174	174	170
	Measurement 3	199	135	165	174	156	160	165	160
	Measurement 4	179	160	153	162	156	173	168	167
	Measurement 5	175	155	154	166	163	165	168	166
	High	204	165	177	186	173	181	174	170
	Low	175	135	143	162	150	160	164	160
	Avg	191.4	154.2	158.4	174.8	159.6	170.6	167.8	165.6
	Std	13.35	11.43	12.99	11.10	8.79	8.20	3.90	3.65

s300_f006_d002_kd120_1053		0%	14%	29%	43%	57%	71%	86%	100%
MAGN=35	Measurement 1	123	163	165	147	121	178	153	116
	Measurement 2	118	143	148	145	114	156	126	122
	Measurement 3	117	141	142	148	122	161	126	121
	Measurement 4	126	169	144	138	111	152	120	122
	Measurement 5	111	150	145	137	115	151	119	115
	High	126	169	165	148	122	178	153	122
	Low	111	141	142	137	111	151	119	115
	Avg	119	153.2	148.8	143	116.6	159.6	128.8	119.2
	Std	5.79	12.34	9.31	5.15	4.72	11.01	13.92	3.42
		0%	14%	29%	43%	57%	71%	86%	100%
MAGN=95	Measurement 1	237	250	248	238	215	292	240	222
	Measurement 2	231	248	244	244	224	275	246	226
	Measurement 3	231	250	243	252	210	279	247	224
	Measurement 4	221	258	261	249	196	278	241	213
	Measurement 5	219	236	244	245	195	273	229	240
	High	237	258	261	252	224	292	247	240
	Low	219	236	243	238	195	273	229	213
	Avg	227.8	248.4	248	245.6	208	279.4	240.6	225
	Std	7.56	7.92	7.52	5.32	12.47	7.44	7.16	9.75

s600_f006_d002_kd050_1053		0%	14%	29%	43%	57%	71%	86%	100%
MAGN=35	Measurement 1	118	130	122	98.2	121	110	111	115
	Measurement 2	105	135	123	119	116	106	119	109
	Measurement 3	103	107	106	95.6	115	125	115	100
	Measurement 4	97.2	105	107	107	106	104	121	113
	Measurement 5	100	106	104	108	105	103	121	113
	High	118	135	123	119	121	125	121	115
	Low	97.2	105	104	95.6	105	103	111	100
	Avg	104.64	116.6	112.4	105.56	112.6	109.6	117.4	110
	Std	8.03	14.64	9.29	9.25	6.88	9.02	4.34	6.00
		0%	14%	29%	43%	57%	71%	86%	100%
MAGN=95	Measurement 1	229	211	217	192	198	203	213	215
	Measurement 2	232	223	221	196	202	223	225	212
	Measurement 3	224	220	219	194	217	212	197	196
	Measurement 4	205	193	201	187	191	192	198	191
	Measurement 5	221	197	200	189	190	191	208	192
	High	232	223	221	196	217	223	225	215
	Low	205	193	200	187	190	191	197	191
	Avg	222.2	208.8	211.6	191.6	199.6	204.2	208.2	201.2
	Std	10.52	13.42	10.24	3.65	10.92	13.59	11.56	11.43

White layer thickness measurements:

s600_f0.006_52100_kd120	Tool wear [%]:	71%		86%		100%	
Reference	2.056	10	2.083	10	2.056	10	
Measurement 1		0.194		0.917		1.444	
Measurement 2		0.333		0.889		1.194	
Measurement 3		0.417		1.056		1.25	
Measurement 4		0.389		1.083		1.194	
Measurement 5		0.306		0.889		1.472	
Avg		0.33		0.97		1.31	
Thickness		1.59		4.64		6.38	

s600_f0.003_52100_kd120	Tool wear [%]:	29%		43%		57%	
Reference	2.04	10	2.08	10	2.08	10	
Measurement 1		2.187		3.16		3.2	
Measurement 2		2.387		3.12		3.08	
Measurement 3		2.507		3.4		3.04	
Measurement 4		2.267		3.24		3.16	
Measurement 5		2.267		3.08		3.12	
Avg		2.32		3.20		3.12	
Thickness		11.39		15.38		15.00	

s300_f0.006_52100_kd050	Tool wear [%]:	29%		43%		57%		71%		86%		100%	
Reference	0.982	10	0	0	1.007	10	0.987	10	0.993	10	0.987	10	
Measurement 1		0.32		0		0.306		0.527		0.54		0.62	
Measurement 2		0.364		0		0.215		0.5		0.587		0.58	
Measurement 3		0.369		0		0.236		0.593		0.58		0.633	
Measurement 4		0.289		0		0.236		0.58		0.627		0.66	
Measurement 5		0.373		0		0.264		0.547		0.627		0.56	
Avg		0.34		0.00		0.25		0.55		0.59		0.61	
Thickness		3.49		0.00		2.50		5.57		5.96		6.19	

s600_f0.006_1070_kd120	Tool wear [%]:	43%		57%		71%		86%		100%	
Reference	0	10	1.028	10	1.028	10	1.028	10	1.028	10	
Measurement 1		0		0.181		0.5		0.097		0.292	
Measurement 2		0		0.153		0.528		0.056		0.264	
Measurement 3		0		0.181		0.5		0.069		0.25	
Measurement 4		0		0.153		0.514		0.056		0.306	
Measurement 5		0		0.139		0.542		0.056		0.306	
Avg		0.00		0.16		0.52		0.07		0.28	
Thickness		0.00		1.57		5.03		0.65		2.76	

s600_f0.003_1070_kd050	Tool wear [%]:	43%		57%		71%		86%		100%
Reference	1.028	10	1.028	10	0	10	0	10	0	10
Measurement 1		0.097		0		0		0		0
Measurement 2		0.083		0.056		0		0		0
Measurement 3		0.069		0.069		0		0		0
Measurement 4		0.083		0.083		0		0		0
Measurement 5		0.069		0.056		0		0		0
Avg		0.08		0.05		0.00		0.00		0.00
Thickness		0.78		0.51		0.00		0.00		0.00

s300_f0.006_1070_kd050	Tool wear [%]:	86%		100%
Reference	1.028	10	0	10
Measurement 1		0.069		0
Measurement 2		0.069		0
Measurement 3		0.083		0
Measurement 4		0.083		0
Measurement 5		0.069		0
Avg		0.07		0.00
Thickness		0.73		0.00

s600_f0.003_1053_kd120	Tool wear [%]:	43%		57%		71%		86%		100%
Reference	1.042	10	1.042	10	1.208	10	1.028	10	1.028	10
Measurement 1		0.292		0.153		0.181		0.278		0.139
Measurement 2		0.25		0.181		0.222		0.264		0.153
Measurement 3		0.194		0.153		0.208		0.208		0.194
Measurement 4		0.306		0.181		0.194		0.222		0.167
Measurement 5		0.278		0.153		0.208		0.194		0.167
Avg		0.26		0.16		0.20		0.23		0.16
Thickness		2.53		1.58		1.68		2.27		1.60

s300_f0.006_1053_kd120	Tool wear [%]:	43%		57%		71%		86%		100%
Reference	1.056	10	1.042	10	1.042	10	1.056	10	1.056	10
Measurement 1		0.167		0.347		0.319		0.306		0.125
Measurement 2		0		0.472		0.347		0.361		0.181
Measurement 3		0		0.5		0.319		0.236		0.167
Measurement 4		0.111		0		0.361		0		0.139
Measurement 5		0.111		0		0.347		0		0.153
Avg		0.08		0.26		0.34		0.18		0.15
Thickness		0.74		2.53		3.25		1.71		1.45

s600_f0.006_1053_kd050	Tool wear [%]:	43%		57%		71%		86%		100%
Reference	1.042	10	1.028	10	1.042	10	1.028	10	1.028	10
Measurement 1		0.125		0.097		0.111		0.139		0.153
Measurement 2		0.167		0.125		0.083		0.181		0.111
Measurement 3		0.181		0.125		0.083		0.153		0.139
Measurement 4		0.139		0.125		0.083		0.139		0.139
Measurement 5		0.194		0.111		0.097		0.153		0.125
Avg		0.16		0.12		0.09		0.15		0.13
Thickness		1.55		1.13		0.88		1.49		1.30

APPENDIX B: CUTTING FORCE DATA

This Appendix contains the average force on the cutting tool as recorded by the piezoelectric dynamometer. The tangential force is xavg, the radial force is yavg, and the axial force is zavg.

Material	CBN-content	speed [sfm]	feed [ipr]	% of tool life	xavg [N]	yavg [N]	zavg [N]
1053	high	300	0.006	0	-54.2	74	9.1
1053	high	300	0.006	14	-65.2	99.3	11.2
1053	high	300	0.006	29	-76.9	155.4	11.4
1053	high	300	0.006	43	-82.4	179.2	15.8
1053	high	300	0.006	57	-86.2	206.2	11.9
1053	high	300	0.006	71	-90.7	209.4	9.2
1053	high	300	0.006	86	-88.2	199.7	10.1
1053	high	300	0.006	100	-93	211	14.4
1053	low	300	0.006	43	-42.4	55.6	7.9
1053	low	300	0.006	57	-48.3	71	10
1053	low	300	0.006	71	-68.5	100.7	11.4
1053	low	300	0.006	86	-48.6	69.1	10.5
1053	low	300	0.006	100	-49	69.5	11.1
1070	high	300	0.006	0	-48.3	64.8	9
1070	high	300	0.006	14	-59.7	94.6	13
1070	high	300	0.006	29	-64.2	120.9	8.8
1070	high	300	0.006	43	-66	113.3	12.1
1070	high	300	0.006	57	-76.4	150.8	15
1070	high	300	0.006	71	-88.1	184	14.2
1070	high	300	0.006	86	-69.6	124.2	11.3
1070	high	300	0.006	100	-99.9	257.8	15
1070	low	300	0.006	0	-45.3	63.6	7.9
1070	low	300	0.006	14	-49.9	66.5	11.5
1070	low	300	0.006	29	-45.8	62	10.1
1070	low	300	0.006	43	-38.8	46.8	7.3
1070	low	300	0.006	57	-45.9	64.1	10.5
1070	low	300	0.006	71	-46.2	64.1	11
1070	low	300	0.006	86	-45.9	62.4	10.8
1070	low	300	0.006	100	-45.4	61.6	10.7
1053	high	600	0.003	0	-32.7	54.7	7.7
1053	high	600	0.003	14	-45.2	90.6	6.8
1053	high	600	0.003	29	-51.7	97.1	8.3
1053	high	600	0.003	43	-48.1	94.6	7.2
1053	high	600	0.003	57	-55.6	117.6	8.5
1053	high	600	0.003	71	-59.4	135.1	10.1
1053	high	600	0.003	86	-64.4	142.3	11.3
1053	high	600	0.003	100	-68.3	147.6	12.1
1053	low	600	0.003	0	-23.9	39.4	3.1
1053	low	600	0.003	14	-26.6	44.5	7.3
1053	low	600	0.003	29	-28.1	49	7.8
1053	low	600	0.003	43	-27.2	47.1	6.3
1053	low	600	0.003	57	-29.9	58.9	8
1053	low	600	0.003	71	-30.1	58.2	8.9
1053	low	600	0.003	86	-30.5	60.6	9.2
1053	low	600	0.003	100	-40.1	75.9	10.7
1070	high	600	0.003	0	-27.9	44.9	7.6
1070	high	600	0.003	14	-39.4	77.3	10
1070	high	600	0.003	29	-51.6	118.5	14.3
1070	high	600	0.003	43	-46.2	98.9	9.9

1070	high	600	0.003	57	-49.4	100	8.7
1070	high	600	0.003	71	-51.7	149.6	15.4
1070	high	600	0.003	86	-65.3	157.7	19.8
1070	high	600	0.003	100	-50.4	138.1	9.8
1070	low	600	0.003	0	-24.9	42.2	5.2
1070	low	600	0.003	14	-27.7	48.9	7.3
1070	low	600	0.003	29	-27.3	47.1	7.2
1070	low	600	0.003	43	-28	49.2	8.4
1070	low	600	0.003	57	-27.4	46.7	6.7
1070	low	600	0.003	71	-27.4	47.4	7.4
1070	low	600	0.003	86	-27.9	49.7	7.2
1070	low	600	0.003	100	-28	50.3	8.2
1053	high	600	0.006	0	-47.4	63.2	8.1
1053	high	600	0.006	14	-54.1	74.8	11.5
1053	high	600	0.006	29	-55.1	78	11.7
1053	high	600	0.006	43	-57.5	81.8	11
1053	high	600	0.006	57	-56.4	77.3	10.5
1053	high	600	0.006	71	-69.4	113.7	15.5
1053	high	600	0.006	86	-65.4	100.9	15
1053	high	600	0.006	100	-61.7	89.6	15.2
1053	low	600	0.006	0	-42.9	64.1	9.9
1053	low	600	0.006	14	-44.9	66.2	11
1053	low	600	0.006	29	-45.3	66.5	10.7
1053	low	600	0.006	43	-45	67.1	10.5
1053	low	600	0.006	57	-45.4	68.1	10.6
1053	low	600	0.006	71	-46.4	69.7	11.1
1053	low	600	0.006	86	-46.6	70.2	10.6
1053	low	600	0.006	100	-46.2	70.7	10.7
1070	high	600	0.006	0	-47.1	60.8	8.4
1070	high	600	0.006	14	-50.4	92.4	9.6
1070	high	600	0.006	29	-55	69.7	10.3
1070	high	600	0.006	43	-69	214.1	24.4
1070	high	600	0.006	57	-75.3	166.1	20.9
1070	high	600	0.006	71	-71.9	152.3	17.6
1070	high	600	0.006	86	-70.9	134.3	15.5
1070	high	600	0.006	100	-77	133.4	15.6
1070	low	600	0.006	0	-43.2	58.1	8.9
1070	low	600	0.006	14	-43.3	58.9	9.2
1070	low	600	0.006	29	-43.6	60.3	9.4
1070	low	600	0.006	43	-43.5	62.5	9.7
1070	low	600	0.006	57	-44.4	65.9	10
1070	low	600	0.006	71	-44.8	66.9	10.3
1070	low	600	0.006	86	-45.2	68.4	10.5
1070	low	600	0.006	100	-45.4	69.3	10.7
1053	low	300	0.006	14	-48.9	69.9	10
1053	low	300	0.006	29	-48.8	69.4	10.4
52100	high	300	0.006	0	-35.3	59.6	1.7
52100	low	300	0.006	0	-42.6	66.8	7.7
52100	high	300	0.006	14	-45.3	79.3	2.3
52100	low	300	0.006	14	-67.2	119.6	17.4

52100	high	300	0.006	29	-113.1	430	17.5
52100	low	300	0.006	29	-75.6	138.3	18.3
52100	high	300	0.006	43	-117.4	534.6	27.4
52100	low	300	0.006	43	-73.9	132.1	17.7
52100	high	300	0.006	57	-141	488.8	23.9
52100	low	300	0.006	57	-109.9	362.5	42.1
52100	low	300	0.006	71	-117.1	333.9	37.3
52100	low	300	0.006	86	-119.6	368.4	36.7
52100	low	300	0.006	100	-114.7	323.6	31.5
52100	low	600	0.003	0	-26.7	51.1	9.6
52100	low	600	0.003	14	-28	59.2	9
52100	low	600	0.003	29	-32.6	68.9	10.6
52100	low	600	0.003	43	-33.5	73.2	9.9
52100	low	600	0.003	57	-39.3	78.7	8.9
52100	low	600	0.003	71	-46.9	106.6	13.3
52100	low	600	0.003	86	-52.8	125.8	16.5
52100	low	600	0.003	100	-55.2	129.2	15.8
52100	high	600	0.003	0	-11.1	20	1.2
52100	high	600	0.003	14	-39.9	89.2	5.5
52100	high	600	0.003	29	-81.7	286.4	8.6
52100	high	600	0.003	43	-99.5	395.2	16.7
52100	high	600	0.003	57	-101.1	417.9	15.5
52100	high	600	0.006	14	-31.3	46.5	3.8
52100	high	600	0.006	29	-31.9	43.1	3.8
52100	high	600	0.006	43	-44.9	102.1	9.2
52100	high	600	0.006	57	-26.7	0	2.9
52100	high	600	0.006	71	-49.8	105.2	6.6
52100	high	600	0.006	86	-61.7	155.2	11.2
52100	high	600	0.006	100	-73.8	169.3	9.4
52100	low	600	0.006	0	-36.8	55.7	4.2
52100	low	600	0.006	14	-48.9	77.8	9.4
52100	low	600	0.006	29	-52.8	79.7	11.5
52100	low	600	0.006	43	-55.9	79.4	9.7
52100	low	600	0.006	57	-59.4	94.4	10.9
52100	low	600	0.006	71	-69.4	131.7	16
52100	low	600	0.006	86	-67.4	107.3	14.4
52100	low	600	0.006	100	-79.1	224.8	24.9

APPENDIX C: HARDNESS MEASUREMENTS

This Appendix contains the hardness measurements collected from the micro-indentation hardness tester. Three measurements were collected from the machined surface of each sample part.

Workpiece material:	52100
Cutting insert:	KD120
Speed:	600
Feed:	0.006

Tool life:	14%	29%	43%	57%	71%	86%	100%
Measurement 1 [HRC]	62.5	60	64.1	62.5	61.7	60.9	61.8
Measurement 2 [HRC]	61	61.8	64.1	60.2	64.1	60.9	59.9
Measurement 3 [HRC]	61.2	61.5	62.8	59.9	59.5	59.7	59.9
Standard deviation	0.81	0.96	0.75	1.42	2.30	0.69	1.10
Avg	61.6	61.1	63.7	60.9	61.8	60.5	60.5

Workpiece material:	52100
Cutting insert:	KD120
Speed:	600
Feed:	0.003

Tool life:	0%	14%	29%	43%	57%
Measurement 1 [HRC]	61.9	61.4	61.8	71.6	65.9
Measurement 2 [HRC]	60	60.8	59.5	63	61.4
Measurement 3 [HRC]	61	61.5	61.6	61.9	67.4
Standard deviation	0.95	0.38	1.27	5.31	3.12
Avg	61.0	61.2	61.0	65.5	64.9

Workpiece material:	52100
Cutting insert:	KD050
Speed:	300
Feed:	0.006

Tool life:	0%	14%	29%	43%	57%	71%	86%	100%
Measurement 1 [HRC]	63	63.1	58.6	61.6	59.6	57.5	57.6	53.9
Measurement 2 [HRC]	62.9	58.3	58.9	58.4	61.4	56.9	64.1	58.9
Measurement 3 [HRC]	64.3	59.4	62	60.3	61	59.1	61	60.4
Standard deviation	0.78	2.51	1.88	1.61	0.95	1.14	3.25	3.40
Avg	63.4	60.3	59.8	60.1	60.7	57.8	60.9	57.7

Workpiece material:	1070
Cutting insert:	KD120
Speed:	600
Feed:	0.006

Tool life:	0%	14%	29%	43%	57%	71%	86%	100%
Measurement 1 [HRC]	59.4	61.5	62	62.1	63.8	64.5	69.4	62.2
Measurement 2 [HRC]	63.5	63.6	62.2	63.1	60.5	65	63.3	64.2
Measurement 3 [HRC]	63.4	61	64.2	63.6	64.5	62.4	64.5	59.9
Standard deviation	2.34	1.38	1.22	0.76	2.14	1.38	3.23	2.15
Avg	62.1	62.0	62.8	62.9	62.9	64.0	65.7	62.1

Workpiece material:	1070
Cutting insert:	KD120
Speed:	600
Feed:	0.003

Tool life:	0%	14%	29%	43%	57%	71%	86%	100%
Measurement 1 [HRC]	62.9	60.8	62.8	63.5	64	65.4	65	62.9
Measurement 2 [HRC]	61.4	61.6	62.7	62.2	62.2	63.4	65.1	63.9
Measurement 3 [HRC]	62.2	62.7	61.9	60.7	64.3	65.3	63.9	64.8
Standard deviation	0.75	0.95	0.49	1.40	1.14	1.13	0.67	0.95
Avg	62.2	61.7	62.5	62.1	63.5	64.7	64.7	63.9

		Tool life:	0%	14%	29%	43%	57%	71%	86%	100%
Workpiece material:	1070	Measurement 1 [HRC]	61.6	62.2	61.9	55.2	62.5	61.8	65.9	61.8
Cutting insert:	KD050	Measurement 2 [HRC]	58.3	60.8	60.5	56.3	63.3	62.3	65.2	63.5
Speed:	300	Measurement 3 [HRC]	61.4	60	60	58	61.5	62.4	65.3	63
Feed:	0.006									
		Standard deviation	1.85	1.11	0.98	1.41	0.90	0.32	0.38	0.87
		Avg	60.4	61.0	60.8	56.5	62.4	62.2	65.5	62.8

		Tool life:	0%	14%	29%	43%	57%	71%	86%	100%
Workpiece material:	1053	Measurement 1 [HRC]	62.2	59.5	62.7	58.2	58.3	61.4	59.9	61.2
Cutting insert:	KD050	Measurement 2 [HRC]	59.1	59.2	56.4	58.5	61.8	58.9	57.4	61.8
Speed:	600	Measurement 3 [HRC]	61.5	59.2	60.8	58	56.1	58.9	59.3	58.5
Feed:	0.006									
		Standard deviation	1.63	0.17	3.23	0.25	2.87	1.44	1.31	1.76
		Avg	60.9	59.3	60.0	58.2	58.7	59.7	58.9	60.5

		Tool life:	0%	14%	29%	43%	57%	71%	86%	100%
Workpiece material:	1053	Measurement 1 [HRC]	59.2	58.4	56.4	58.1	56.1	57.9	59.2	54.5
Cutting insert:	KD120	Measurement 2 [HRC]	58	59.9	54.2	55.7	54	57.4	60.6	58.3
Speed:	600	Measurement 3 [HRC]	57.5	57.6	58.6	59.4	54.8	58.6	58.9	52.8
Feed:	0.003									
		Standard deviation	0.87	1.17	2.20	1.88	1.06	0.60	0.91	2.82
		Avg	58.2	58.6	56.4	57.7	55.0	58.0	59.6	55.2

		Tool life:	0%	14%	29%	43%	57%	71%	86%	100%
Workpiece material:	1053	Measurement 1 [HRC]	55	51.5	60.4	57.7	60.6	58.6	56.1	58.5
Cutting insert:	KD120	Measurement 2 [HRC]	61.5	60.9	56.5	57.4	53.2	55.5	60.6	59.3
Speed:	300	Measurement 3 [HRC]	57.5	53.3	58.1	55.4	65.3	58.9	61.3	60.3
Feed:	0.006									
		Standard deviation	3.28	4.99	1.96	1.25	6.10	1.88	2.82	0.90
		Avg	58.0	55.2	58.3	56.8	59.7	57.7	59.3	59.4

REFERENCES

Abrao, A. M. and D. K. Aspinwall. "The Surface Integrity of Turned and Ground Hardened Bearing Steel." Wear **196**: 279-284. (1996)

American Stress Technologies, I. Stresscan 500c Operating Instructions**:** 42. (1999)

Baboian, R., Ed. Corrosion Tests and Standards: Application and Interpretation. Electrochemcial. Fredericksburg, VA, American Soceity for Testing and Materials. (1995)

Berruti, T. and M. M. Gola. "X-Ray Residual Stress Measurement on Mechanical Components with High Curvature." Experimental Mechanics **43**(1): 105-114. (2003)

Bhadeshia, H. K. D. H. Material Factors. Handbook of Residual Stress and Deformation of Steel. G. Totten, M. Howes and T. Inoue. Materials Park, OH, ASM International**:** 3-10. (2002)

Boggio, U. "The Recipe for Good Hard Turning." Manufacturing Engineering **116**(3): 95-102. (1996)

Brandon, D. G. and W. D. Kaplan. Microstructural Characterization of Materials. Chichester; New York, J. Wiley (1999).

Chou, Y. K. and C. J. Evans. "White Layers and Thermal Modeling of Hard Turned Surfaces." International Journal of Machine Tools & Manufacture **39**: 1863-1881. (1999)

Chou, Y. K., C. J. Evans, et al. "Experimental Investigation on Cubic Boron Nitride Turning of Hardened Aisi 52100 Steel." Journal of Materials Processing Technology **134**: 1-9. (2003)

Cottis, R., S. Turgoose, et al. Electrochemical Impedance and Noise. Houston, TX, NACE International (1999).

Dawson, T. G. Effects of Cutting Parameters and Tool Wear in Hard Turning. Mechanical Engineering. Atlanta, Georgia Institute of Technology**:** xiii, 113 leaves. (1999)

Dawson, T. G. and T. R. Kurfess. "An Investigation of Tool Wear and Surface Quality in Hard Turning." Transactions of the North American Manufacturing Research Institute **28**: 215-220. (2000)

Dawson, T. G. and T. R. Kurfess. "Hard Turning, Tool Life, and Surface Quality." Manufacturing Engineering **126**(4): 88-98. (2001)

Dawson, T. G. and T. R. Kurfess. Machining Hardened Steel with Ceramic-Coated and Uncoated Cbn Cutting Tools. NAMRC XXX, West Lafayette, ID, Society of Manufacturing Engineers. (2002)

Delio, T., J. Tlusty, et al. "Use of Audio Signals for Chatter Detection and Control." Journal of Engineering for Industry, Transactions of the ASME **114**(2): 146-157. (1992)

Fix, R. M., K. Tiitto, et al. "Automated Control of Camshaft Grinding Process by Barkhausen Noise." Materials Evaluation **48**(7): 904-908. (1990)

Gatelier-Rothea, C., J. Chicois, et al. "Characterization of Pure Iron and (130 Ppm) Carbon-Iron Binary Alloy by Barkhausen Noise Measurements: Study of the Influence of Stress and Microstructure." Acta Metallurgica **46**(14): 4873-4882. (1998)

Griffiths, B. J. "White Layer Formations at Machined Surfaces and Their Relationship to White Layer Formations at Worn Surfaces." American Society for Mechanical Engineers (Paper): 7. (1984)

Grover, M. P. Fundamentals of Modern Manufacturing: Materials, Processes, and Systems. Englewood Cliffs, NJ, Prentice Hall (1996).

Gupta, H., M. Zhang, et al. "Barkhausen Effect in Ground Steels." Acta Metallurgica **45**(5): 1917-1921. (1997)

Halliday, D., R. Resnick, et al. Fundamentals of Physics Extended. New York, John Wiley & Sons, Inc. (1997).

Horowitz, P. and W. Hill. The Art of Electronics. Cambridge, Cambridge University Press (1989).

Jagadish, C., L. Clapham, et al. "Influence of Uniaxial Elastic Stress on Power Spectrum and Pulse Height Distribution of Surface Barkhausen Noise in Pipeline Steel." IEEE Transactions on Magnetics **26**(3): 1160-1163. (1990)

Kalpakjian, S. and S. R. Schmid. Manufacturing Processes for Engineering Materials. Upper Saddle River, N.J., Prentice Hall (2002).

Kennametal, I. Kennametal Lathe Guide, Kennametal, Inc. (2004).

Kiran, M. B., B. Ramamoorthy, et al. "Evaluation of Surface Roughness by Vision System." International Journal of Machine Tools & Manufacture **38**(5-6): 685-690. (1998)

Krause, T. W., N. Pulfer, et al. "Magnetic Barkhausen Noise: Stress-Dependant Mechanisms in Steel." IEEE Transactions on Magnetics **32**(5): 4764-4766. (1996)

Lewin, W. Lecture Notes: Electricity and Magnetism, 8.02. Massachusetts Institute of Technology, Massachusetts Institute of Technology. (Spring 2002)

Liang, S. Y., R. L. Hecker, et al. Machining Process Monitoring and Control: The State-of-the-Art. 2002 ASME International Mechanical Engineering Congress and Exposition, New Orleans, LA, United States, American Society of Mechanical Engineers. (2002)

Lindberg, R. A. Materials and Manufacturing Technology. Boston, Allyn and Bacon [1968] (1968).

Lu, J. and Society for Experimental Mechanics (U.S.). Handbook of Measurement of Residual Stresses. Lilburn, GA Upper Saddle River, NJ, Fairmont Press; Distributed by Prentice Hall PTR (1996).

Mittal, S. and C. R. Liu. "A Method of Modeling Residual Stresses in Superfinish Hard Turning." Wear **218**(1): 21-33. (1998)

Moorthy, V., B. A. Shaw, et al. "Evaluation of Tempering Induced Changes in the Hardness Profile of Case-Carburised En36 Seel Using Magnetic Barkhausen Noise Analysis." NDT&E International **36**: 43-49. (2003)

Moshier, M. A. and B. M. Hillberry. "The Inclusion of Compressive Residual Stress Effects in Crack Growth Modelling." Fatigue Fract Engng Mater Struct **22**: 519-526. (1999)

Ogawa, K., D. Minkov, et al. "Nde of Degradation of Thermal Barrier Coating by Means of Impedance Spectroscopy." NDT&E International **32**(3): 177-185. (1999)

Ozel, T. "Modeling of Hard Part Machining; Effect of Insert Edge Preparation in Cbn Cutting Tools." Journal of Materials Processing Technology **141**: 284-293. (2003)

Parakka, A. P. and D. C. Jiles. "Barkhausen Effect in Steels and Its Dependence on Surface Condition." Journal of Applied Physics **81**(8): 5085-5086. (1997)

Prevey, P. S. X-Ray Diffraction Residual Stress Techniques. Metals Handbook. Metals Park, OH, American Society for Metals. **10:** 380-392. (1986)

Ramesh, A. Prediction of Process-Induced Microstructural Changes and Residual Stresses in Orthogonal Hard Machining**:** xxii, 315 leaves. (2002)

Rautioaho, R., P. Karjalainen, et al. "Improvement of the Barkhausen Noise Method for Stress Evaluation." Journal of Magnetism and Magnetic Materials **73**: 96-102. (1988)

Revie, R. W., H. H. Uhlig, et al. Uhlig's Corrosion Handbook. New York, Wiley (2000).

Rudd, C. Measurement of Residual Stresses. Handbook of Residual Stress and Deformation of Steel. G. Totten, M. Howes and T. Inoue. Materials Park, OH, ASM International**:** 99-117. (2002)

Schneider, J. "Ceramics and Cbn." Manufacturing Engineering **122**(1): 66-73. (1999)

Sheehy, T. "Taking the Hard out of Hard Turning." Manufacturing Engineering **118**(3): 100-106. (1997)

Shunsheruddin, A. and S. W. Kim. Adaptive Control of the Cylindrical Plunge Grinding Process. Proceedings of the Symposium on Grinding, ASME Winter Annual Meeting. (1985)

Smith, S. R. An Investigation into the Effects of Hard Turning Surface Integrity on Component Service Life. Mechanical Engineering. Atlanta, Georgia Institute of Technology. **Doctor of Philosophy**. (2001)

Thiele, J. D. An Investigation of Surface Generation Mechanisms for Finish Hard Turning of Aisi 52100 Steel**:** xx, 182 leaves. (1998)

Thiele, J. D. and S. N. Melkote. "Effect of Cutting Edge Geometry and Workpiece Hardness on Surface Generation in the Finish Hard Turning of Aisi 52100 Steel." Journal of Materials Processing Technology **94**: 216-226. (1999)

Tiitto, K. "Use of Barkhausen Effect in Testing for Residual Stresses and Material Defects." 27-36. (1987)

Tiitto, S. I. "On the Mechanism of Magnetism Transitions in Steel." IEEE Transactions on Magnetics **14**(5): 527-529. (1978)

Tlusty, J. Manufacturing Processes and Equipment. Upper Saddle River, N.J., Prentice Hall (2000).

Toribio, J. "Role of Crack-Tip Residual Stresses in Stress Corrosion Behaviour of Prestressing Steel." Construction and Building Materials **12**: 283-287. (1998)

Torres, M. A. S. and H. J. C. Voorwald. "An Evaluation of Shot Peening, Residual Stress and Stress Relaxation on the Fatigue Life of Aisi 4340 Steel." International Journal of Fatigue **24**: 877-886. (2002)

Totten, G. E., M. A. H. Howes, et al. Handbook of Residual Stress and Deformation of Steel. Materials Park, Ohio, ASM International (2002).

Yankee, H. W. Manfacturing Processes. Englewood Cliffs, N.J., Prentice-Hall (1979).

Zhu, L., X. Y. Tao, et al. "Fatigue Strength and Crack Propagation Life of in-Service High Pressure Tubular Reactor under Residual Stress." International Journal of Pressure Vessels and Piping **75**: 871-877. (1998)